THE UNIVERSITY
of EDINBURGH

Modulation of fast-spiking interneurons using two-pore channel blockers

Maximilian Whittaker B.Sc. (Hons)

A thesis presented for the degree of Doctor of Philosophy at the University of Edinburgh

Declaration

I hereby certify that this thesis and its composition are entirely my own work. No part of the work contained in this thesis has been submitted for any other degree or professional qualification.

Signed ……. Date ……..

Acknowledgements

My four years as a PhD student have been very interesting indeed. Before I thank my friends - who have made my life here in Edinburgh one of the most enjoyable episodes of my life - I will firstly and most importantly thank my primary supervisor, Michael Daw for all his help. Although Michael never joined me in the many nightclubs I frequented (although he did come to a few pubs), he instead made absolutely sure that he was there to support me in the work department. Michael was always available if I needed him, whether it involved the pair of us exchanging emails back and forth during the weekends, or even just sharing my enthusiasm for niche phenotypes within recordings, such as when I'd quickly drag him away from his office to show him a live recording of an interneuron producing the most glamourous of near-threshold oscillations! I would also like to thank my secondary supervisor Mike Shipston for all his support and guidance throughout our meetings.

Secondly, I would like to thank my friends and members of room 101 who have helped me technically throughout my PhD, and helped me overcome an array of electrophysiological problems that I encountered. These kind people are Adam Jackson, Sam Booker, Emma Perkins, Steph Barnes, Alison Todd, Sonal Kedia, and Katie 'The HEK' Marwick. Other people that have either helped me deal with molecular issues such as genotyping, or have positively impacted my working life are Christina McClure and Paul Baxter (respectively). Finally, I would like to thank Sean McKay for doing all of the above.

Without the support I had from my friends and supervisors, I would not have been as excited as I have been in the last 4 years to live and work in Edinburgh. Thank you.

Abstract

The balance between excitatory and inhibitory synaptic transmission within and across neurons in active networks is crucial for cortical function and may allow for rapid transitions between stable network states. GABAergic interneurons mediate the majority of inhibitory transmission in the cortex, and therefore contribute to the global balance of activity in neuronal networks.

Disruption in the network balance due to impaired inhibition has been implicated in several neuropsychiatric diseases (Marin 2012). Both schizophrenia and autism are two highly heritable cognitive disorders with complex genetic aetiologies but overlapping behavioural phenotypes that share common imbalances in neuronal network activity (Gao & Penzes 2015). An increasing body of evidence suggests that functional abnormalities in a particular group of cortical GABAergic interneurons expressing the calcium-binding protein parvalbumin (PV) are involved in the pathology of these disorders (Marin 2012). As deficits in this neuronal population have been linked to these disorders it could be useful to target them and increase their activity.

A conserved feature in PV cells is their unusually low input resistance compared to other neuronal populations. This feature is regulated by the expression of leak K^+ channels, believed to be mediated in part by TASK and TREK subfamily two-pore K^+ channels (Goldberg et al. 2011). The selective blockade of specific leak K^+ channels could therefore be applied to increase the activity of PV cells.

In this thesis, specific TASK-1/3 and TREK-1 channel blockers were applied in cortical mouse slices in an attempt to increase the output of PV cells. The blockade of either channel did not successfully increase the amplitude of PV

cell-evoked inhibitory postsynaptic currents (IPSCs) onto principal cells. However, while the blockade of TASK-1/3 channels failed to depolarise the membrane or alter the input resistance, the blockade of TREK-1 channels resulted in a small but significant depolarisation of the membrane potential in PV cells. Interestingly, TREK-1 channel blockade also increased action potential firing of PV cells in response to given current stimuli, suggesting that TREK-1 could be a useful target for PV cell modulation.

These results demonstrate for the first time the functional effects of using specific two-pore K^+ channel blockers in PV cells. Furthermore, these data provide electrophysiological evidence against the functional expression of TASK-1/3 in PV cells. It could therefore be interesting to further characterise the precise subtypes of leak K^+ channels responsible for their low resistivity. This would help to classify the key contributors of the background K^+ conductances present in PV cells in addition to finding suitable targets to increase their activity.

Lay Abstract

Excitatory neurons specialise in transmitting information between distinct areas of the brain, whereas inhibitory interneurons provide the fundamental means of controlling network activity, and therefore prevent hyperexcitability. Interneurons responsible for inhibition account for just a small fraction of all the neurons, and are highly diverse, yet they manage to maintain an important role in regulating the activity of the neuronal population. Consequently, imbalances between excitation and inhibition have been implicated in a number of psychiatric diseases including schizophrenia and autism.

Both schizophrenia and autism are cognitive disorders with complicated genetic origins but share several behavioural symptoms, which comprise social interaction abnormalities in addition to emotional processing deficits. While the genetics are diverse, the two disorders converge upon common deficits in the ratio between excitatory and inhibitory activity. Notably, several lines of evidence suggest that abnormalities in the function of a particular group of inhibitory interneurons known as fast-spiking interneurons are involved in these disorders. As their name suggests, fast-spiking interneurons are responsible for rapid inhibitory signalling which is important for synchronising the activity of excitatory neurons, necessary for normal cognitive function. Consistent with this finding, patients with schizophrenia or autism exhibit reductions in long-range network synchrony across the brain.

It could therefore be beneficial to amend some of the deficits associated with fast-spiking interneurons in patients with schizophrenia and autism. This project focuses on finding a specific target in fast-spiking cells that could be used to boost their activity. If successful, a drug could be given to patients with the aim of increasing the activity of fast-spiking interneurons to alleviate part of their symptoms.

Contents

Chapter 1 1

1.1 Neuropsychiatric disorders 2

1.1.1 Prevalence 2

1.1.2 Impact 3

1.1.3 Shared clinical features 4

1.1.4 Genetics and environment 4

1.1.5 Neuropathological features of schizophrenia and autism 6

1.1.6 Current treatments for schizophrenia and autism 8

1.1.7 Proposed circuit deficits in schizophrenia and autism 8

1.2 Interneurons 10

1.2.1 GABAergic transmission 10

1.2.2 Interneuron diversity 12

1.2.3 Function of interneuron subtypes 16

1.2.4 Balance between excitation and inhibition 21

1.2.5 PV interneurons 23

1.2.6 Role of PV interneurons in cortical networks 25

1.2.7 Deficits in network oscillations in neurological and psychiatric diseases 28

1.2.8 K^+ channels in schizophrenia 29

1.2.9 PV interneurons in schizophrenia 30

1.2.10 PV interneurons in autism 35

1.2.11 Specific targeting of PV interneurons as a treatment for neurological and neuropsychiatric diseases 36

1.3 Modulation of PV interneurons 37

1.3.1 Intrinsic properties of PV interneurons 38

1.3.2 Specialisations promoting fast excitation of PV cells 39
1.3.3 Specialisations promoting high frequency firing of action potentials in PV cells 41
1.3.4 Specialisations promoting fast spike propagation and synchronous transmitter release in PV cells 44
1.3.5 Targeting PV cells to increase their excitability 46
1.3.6 Two-pore-domain K^+ channel family 49
1.3.7 The modulation of PV cells via TASK and TREK 52
1.3.8 TASK-1/3 and TREK-1 pharmacology 55
1.3.9 Aims of this thesis 57

Chapter 2 58
2.1 Animals and Cell Lines 59
2.1.1 Housing and Breeding 59
2.1.2 Generation of PV/EYFP mice 59
2.1.3 Genotyping 59
2.1.4 Expressing TASK-3 in HEK cells 61
2.2 Electrophysiology 62
2.2.1 Solutions 62
2.2.2 Drugs 63
2.2.3 Preparation of acute tissue slices 64
2.2.4 Whole-cell patch clamp recordings 65
2.2.5 Thalamocortical recordings 66
2.2.6 PV cell recordings 67
2.2.7 Measuring RMP, IR and action potential firing in PV cells 68

2.2.8 Whole-cell TREK currents in PV cells 69

2.2.9 Hippocampal gamma oscillations 69

2.2.10 Data analysis 70

Chapter 3 71

3.1 Introduction 72

3.2 Modulation of PV cell output using TASK channel blockers 73

3.2.1 Thalamocortical circuit as an assay of PV cell output 74

3.2.2 Results 75

3.2.3 TASK-1/3 channel blockers have no effect on PV cell output 77

3.2.4 TASK-1/3 channel blockers have no effect on PV cell output during multiple stimulation 78

3.3 Effects of TASK channel blockers on PV cell excitability 83

3.3.1 TASK-1/3 channel blockers have no effect on RMP and input resistance in PV cells in cortex 84

3.3.2 Acidification and bupivacaine depolarises RMP and increases input resistance in PV cells 88

3.3.3 Compound 23 has no effect on RMP and input resistance in PV cells in CA1 hippocampus 90

3.3.4 TASK-1/3 channel blockers have no effect on gamma oscillation power in CA3 hippocampus 93

3.4 Analysis of efficacy of TASK channel blockers 95

3.4.1 Effects of TASK-1/3 channel blocker compound 23 on heterologously expressed TASK-3 in HEK-293 cells 95

3.5 Discussion 100

3.5.1 TASK-like conductance in PV cells mediated by K_{2P} channels other than TASK-1/3 101

3.5.2 Confirmation of efficacy of TASK-1/3 channel blockers 103

3.5.3 The effect of compound 23 failed to replicate findings in hippocampal cells and network gamma oscillations 104

3.5.4 Dynamics of the output of cortical PV cells upon multiple stimulation 105

3.5.5 DMSO appears to reduce the amplitude of PV cell-mediated feedforward IPSCs 107

3.5.6 Summary 109

Chapter 4 110

4 .1 Introduction 111

4.2 Effects of TREK-1 channel blocker amlodipine on PV cell excitability 113

4.2.1 Amlodipine depolarises RMP but has no effect on input resistance 113

4.2.2 Amlodipine does not alter the firing of PV cells in response to current steps 115

4.3 Effects of TREK-1 channel blocker spadin on PV cell excitability 120

4.3.1 Spadin depolarises RMP but has no effect on input resistance 120

4.3.2 Spadin increases the firing of PV cells in response to current steps 122

4.3.3 Spadin has no effect on PV cell output 126

4.3.4 Spadin does not affect current-voltage relationship in PV cells 128

4.4 Subcellular localisation of TREK-1 channels 130

4.4.1 Effects of locally applied tetrodotoxin (TTX) on cell excitability 131

4.5 Discussion 135

4.5.1 Effect of TREK-1 channel blockade on RMP and input resistance 135

4.5.2 Concentration and usage of blockers 137

4.5.3 The effect of spadin on the current-voltage relationship of TREK-1 138

4.5.4 Are TREK-1 channels expressed exclusively in the AIS of PV cells? 139

4.5.5 TREK-1 channel expression in astrocytes 139

4.5.6 Summary 141

Chapter 5 143

5.1 Discussion 144

5.1.1 Overall goal 144

5.1.2 Overall outcome 145

5.1.3 TASK 146

5.1.4 TREK 148

5.1.5 Other background K^+ channels 151

5.1.6 Experimental approach 152

5.1.7 Future directions for the treatment of Schizophrenia and autism 154

References 157

List of figures

Figure 1.1	Classification and developmental origins of neocortical GABAergic interneurons	14
Figure 1.2	Schematic illustrating specific subcellular innervation of different classes of GABAergic interneurons in the primary somatosensory cortex	18
Figure 1.3	GABAergic interneurons provide balance to excitatory signaling	22
Figure 1.4	Summary of alterations in cortical circuitry in patients with schizophrenia and in animal models of schizophrenia and autism	32
Figure 1.5	Specialised voltage-gated channels allow for high frequency firing of action potentials in PV cells	42
Figure 1.6	K_{2P} channels contribute to the leak K^+ background conductance	50
Figure 1.7	Relative expression of K^+ channels in PV cells	54
Figure 1.8	Chemical structures of TASK-1/3 channel blockers	56
Figure 2.1	Preparation of thalamocortical slices	65
Figure 3.1	Measuring PV cell output using the thalamocortical circuit	76
Figure 3.2	TASK-1/3 channel blocker A293 does not affect PV cell output	78
Figure 3.3	Measuring high frequency PV cell output using the thalamocortical circuit	80

Figure 3.4	TASK-1/3 channel blocker A293 does not affect PV cell output during multiple stimulation	81
Figure 3.5	More potent TASK-1/3 channel blocker compound 23 does not affect PV cell output during multiple stimulation	82
Figure 3.6	TASK-1/3 channel blocker compound 23 does not alter PV cell RMP or input resistance	85
Figure 3.7	TASK-1/3 channel blockers A293 and A1899 does not alter PV cell RMP or input resistance	86
Figure 3.8	Acidification and bupivacaine depolarises RMP and increases input resistance in PV cells	89
Figure 3.9	TASK-1/3 channel blocker compound 23 does not alter PV cell RMP or input resistance in CA1 hippocampus	92
Figure 3.10	TASK-1/3 channel blocker compound 23 does not affect gamma oscillation power in CA3 hippocampus	94
Figure 3.11	TASK-1/3 channel blocker compound 23 depolarises RMP and increases input resistance in HEK 293 cells expressing TASK-3	96
Figure 3.12	Effects of TASK-1/3 channel blocker compound 23 on the current/voltage relationship in a HEK 293 cell expressing TASK-3	99
Figure 4.1	TREK-1 channel blocker amlodipine depolarises RMP but does not alter input resistance in PV cells	114
Figure 4.2	Measuring PV cell excitability in the presence of TREK-1 channel blocker amlodipine	116
Figure 4.3	TREK-1 channel blocker amlodipine does not alter PV cell excitability	119

Figure 4.4	TREK-1 channel blocker spadin depolarises RMP but does not alter input resistance in PV cells	121
Figure 4.5	Measuring PV cell excitability in the presence of TREK-1 channel blocker spadin	123
Figure 4.6	TREK-1 channel blocker spadin increases PV cell excitability	124
Figure 4.7	TREK-1 channel blocker spadin does not alter firing threshold in PV cells	125
Figure 4.8	TREK-1 channel blocker spadin does not effect PV cell output during multiple stimulation	127
Figure 4.9	TREK-1 channel blocker spadin does not alter the current/voltage relationship in PV cells	129
Figure 4.10	Pilot puffing experiments on pyramidal cell processes	132

List of tables

Table 1.1	Summary of fast signalling properties of PV cells	47
Table 2.1	Thermocycling conditions for Cre and EYFP genotyping	60
Table 2.2	External solution composition	62
Table 2.3	Internal patch pipette solution composition	63
Table 2.4	Drugs dissolved in recording aCSF solution	64

Abbreviations

Abbreviation	Definition
$5HT_{3A}R$	$5HT_{3a}$ (5-hydroxytryptamine 3a) receptor
ACSF	Artificial cerebrospinal fluid
ADHD	Attention deficit hyperactivity disorder
AHP	Afterhyperpolarisation
AIS	Axon initial segment
AMPA	α-amino-3-hydroxy-5-methyl-4-isoxazolepropionic acid
ANOVA	Analysis of variance
APV	2-amino-5-phosphopentanoic acid
BGT-1	Betaine-GABA transporter
CA1	Cornu Ammonis 1
CA3	Cornu Ammonis 3
CB	Calbindin
CCK	Cholecystokinin
CGE	Caudal ganglionic eminence
CNQX	6-cyano-7-nitroquinoxaline-2,3-dione
CNS	Central nervous system
CNVs	Copy number variations
CR	Calretinin
DISC1	Disrupted in schizophrenia 1
DLPFC	Dorsolateral prefrontal cortex
DMSO	Dimethyl sulfoxide
DNA	Deoxyribonucleic acid
E_{Cl}	Cl^- reversal potential
EGTA	Ethylene glycol-bis(β-aminoethyl ether)-N,N,N',N'-tetraacetic acid
EEG	Electroencephalogram
EFYP	Enhanced yellow fluorescent protein
EPSC	Excitatory postsynaptic current
EPSP	Excitatory postsynaptic potential
ErbB4	Receptor tyrosine-protein kinase erbB-4
FACS	Fluorescence-activated cell sorting
FMR1	Fragile X mental retardation 1
fMRI	Functional magnetic resonance imaging
GABA	*gamma*-Aminobutyric acid
$GABA_AR$	GABA-type A receptor
GAD	Glutamate decarboxylase
GAT-1/2/3	GABA transporter 1/2/3
HEK-293	Human embryonic kidney cells 293
HEPES	4-(2-hydroxyethyl)-1-piperazineethanesulfonic acid
ING	Interneuron network gamma
IPSC	Inhibitory postsynaptic current

IPSP	Inhibitory postsynaptic potential
K_{2P}	Two-pore-domain channel
Kir	Inwardly rectifying potassium channel
Kv	Voltage-gated potassium channel
LGE	Lateral ganglionic eminence
MEG	Magnetoencephalography
MGE	Medial ganglionic eminence
mIPSC	miniature inhibitory postsynaptic potential
mRNA	Messenger ribonucleic acid
NMDA	N-methyl-D-aspartate
NPY	Neuropeptide Y
NRG1	Neuregulin 1
NRXN	Neurexin
PCR	Polymerase chain reaction
PING	Pyramidal-interneuron network gamma
POA	Preoptic area
PV	Parvalbumion
qPRR	Real-time polymerase chain reaction
RM-ANOVA	Repeated measures ANOVA
RMP	Resting membrane potential
RT-PCR	Reverse transcription PCR
SNPs	Single nucleotide polymorphisms
Sst	Somatostatin
TALK	TWIK-related alkaline-sensitive K^+ channel
TASK	TWIK-related acid-sensitive K^+ channel
TEA	Tetraethylammonium
THIK	Tandem pore domain halothane-inhibited K^+ channel
TREK	TWIK-related K^+ channel
TRESK	TWIK-related spinal cord K^+ channel
TTX	Tetrodotoxin
TWIK	Tandem of pore domains in a weak inward rectifying K^+ channel
uPAR	Plasminogen activator receptor
VB	Ventrobasal thalamus
V_m	Membrane potential

Chapter 1

Introduction

1.1 Neuropsychiatric disorders

Schizophrenia and autism are cognitive disorders characterised by disruptions in social interaction, communication, emotion processing and executive function (Cheung et al. 2010). Both schizophrenia and autism are highly prevalent neuropsychiatric disorders with complicated genetic aetiologies but overlapping behavioural phenotypes and may share common imbalances in neuronal network activity (Gao & Penzes 2015). Within the network, growing evidence suggests that a disruption of inhibitory circuits in the cortex might be responsible, in part, for the clinical features of these disorders (Lewis et al. 2012; Fatemi et al. 2010). Recent studies in humans and animal models indicate that the underlying pathology in both diseases may emerge from deficits in the development and function of interneurons – the cells that are responsible for maintaining inhibitory balance in neuronal circuits (Marín 2012). These cells not only maintain inhibition in the brain, but also provide a temporal structure for information processing believed to contribute to cognitive function (Haider et al. 2006). Aberrant interneuron function could therefore dictate common imbalances associated with schizophrenia and autism which may contribute to the development of novel therapeutic targets.

1.1.1 Prevalence

Schizophrenia affects 1% of the world's population and is often diagnosed in late adolescence or early adulthood (Owen et al. 2016). The illness is characterised by three clusters of symptoms: positive or psychotic symptoms, such as delusions, hallucinations and disorganisation of thought; negative symptoms, such as social withdrawal and apathy; and cognitive symptoms, including abnormalities in attention and working memory (Owen et al. 2016). Although positive symptoms present the most prominent manifestation in schizophrenia, disturbances in cognition are conceivably the most distinctive, leading to the conception that the very core of the disease manifests from cognitive deficits (Elvevåg & Goldberg 2000). Moreover,

cognitive tests in patients are routinely used to assist in diagnosis, as cognitive disturbances are present before the onset of psychosis (Elvevåg & Goldberg 2000).

Autism is a complex neurodevelopmental disorder affecting between 0.1-0.2% of the entire population and is characterised by severe and pervasive deficits in reciprocal socialisation, impairments in verbal and non-verbal communication in addition to repetitive or unusual behaviours (Levy et al. 2009). Autism is usually diagnosed by the age of 3 years, although prospective studies assessing at-risk infants demonstrated that a subset of clinic symptoms could manifest as early as 6-12 months (Chattopadhyaya & Di Cristo 2012). The incidence of autism has escalated dramatically over the last two decades predominantly because of the adoption of a broader diagnostic criteria in addition to increased awareness within the medical community (Levy et al. 2009). New administrative classifications of children in educational systems and the subsequent reclassifications of children from other categories to autism may explain part of this reported increase (Shattuck 2006). Consequently, autism has been classified as a heterogeneous disorder which can resemble or be comorbid with intellectual disability, obsessive compulsive disorder and attention deficit hyperactivity disorder (ADHD) (Gillberg & Billstedt 2000).

1.1.2 Impact

Schizophrenia and autism have profound consequences on both the individuals affected and society. More than 50% of individuals that are diagnosed with schizophrenia endure intermittent but long term psychiatric complications, and around 20% carry chronic symptoms and disability (Barbato 1998). Unemployment is strikingly high at 80-90% (Owen et al. 2016), and average life expectancy is reduced by up to 20 years (Chesney et al. 2014). Schizophrenia in England alone costs the economy £11.8 billion per year, with approximately a third of this figure spent directly on health and social care provided by hospitals and the community (Schizophrenia Commission 2012).

Autism affects over 700,000 people including their families in the United Kingdom and is estimated to cost £32 billion per year (McCall 2017). Despite this figure, many children and adults with autism remain secluded from society living in specialised communities. A recent report indicates that 84% of people diagnosed with autism are not in full-time employment, and two-thirds are unemployed (McCall 2017). Furthermore, the need for improved management of the general health of individuals with autism in society is evidently required, with most of the burden being placed on parents because of the communication challenges present, resulting in heightened stress within affected families.

1.1.3 Shared clinical features

The behavioural symptoms of schizophrenia and autism are intriguingly similar: Both disorders feature cognitive deficits, social interaction problems, emotional processing abnormalities and deficits in executive function (Cheung et al. 2010; Rapin & Tuchman 2008). Moreover, a subset of patients with autism experience visual and auditory hallucinations, similar to a subset of affected individuals with schizophrenia (Toal et al. 2009). Furthermore, several studies reported comorbidity between schizophrenia and autism: A study of 129 subjects with autism found that 7.8% of them had schizophrenia (Stahlberg et al. 2004), while another case-control study following 61 Danish individuals with atypical autism for 45 years found that 34% had been diagnosed with schizophrenia (Mouridsen et al. 2008).

1.1.4 Genetics and environment

Epidemiological studies indicate that schizophrenia and autism are highly heritable and arise from distinct families of genes. The contribution of different DNA variants and specific types of risk alleles have also led to the understanding that the two disorders are highly polygenic. Genome-wide association studies identified over 100 independent genetic loci comprising common alleles of small effect between schizophrenia patients and control groups, suggesting that many single nucleotide polymorphisms (SNPs) may act together to contribute to the aetiology of the disorder

(Ripke et al. 2014). Genomic studies have also identified copy number variations (CNVs) in 11 high risk genes in schizophrenia (Rees .et al. 2014). Interestingly, several of the strongly associated CNVs – such as the gene encoding the presynaptic protein neurexin 1 (NRXN1) which is essential for synapse differentiation and function - may also be involved in autism (Kirov et al. 2014) highlighting that although the genetics between the two disorders are diverse, some of the high risk genes may converge.

Genetic risk may also be highly pleiotropic in schizophrenia and autism. One gene or allele could thus influence multiple seemingly unrelated phenotypic attributes which – at the genetic level - may not have previously been categorised with known pre-existing mutations in the disease. Studies have reported significant sharing of common risk alleles between schizophrenia and a number of psychiatric disorders including ADHD, bipolar disorder, major depressive disorder and autism (Cross-Disorder Group of the Psychiatric Genomics Consortium et al. 2013), demonstrating the difficulty of categorising neurological disorders at the genetic level.

Although the convergence of individual risk genes is likely to control most of the aetiology, several environmental risk factors have been identified in schizophrenia, and to a lesser extent, autism. Meta-analytical studies have indicated that risk factors for schizophrenia include childhood trauma, immigration, drug abuse and living in urban environments (van Os et al. 2010). In autism, birth complications associated with trauma or hypoxia have been shown to have a strong association with the disorder (Modabbernia et al. 2017). Furthermore, prenatal exposure to valproate – a drug used in epilepsy - has been reported to be strongly associated with autism, thus highlighting chemical influences as a cause for the disorder (Modabbernia et al. 2017). Nonetheless, it is unlikely that environmental factors alone are enough to directly result in the development of schizophrenia or autism, however they may increase the probability when combined with risk genes.

Genetic linkage and genome-wide association studies have determined many disease-associated genes, although few have been reproducible because most genetic contributions likely involve a combination of alleles that make small influences on the overall disease pathogenesis (Harrison & Weinberger 2005; Toro et al. 2010). Furthermore, given the extreme heterogeneous nature of both conditions, most studies lack the necessary power to consistently reproduce these weak correlations (Owen et al. 2004). While there are strong candidate genes that increase the susceptibility of developing schizophrenia or autism (see sections **1.2.8** and **1.2.9**), it is evident that the vast majority of these disorders arise from the amalgamation of many genetic factors. Finally, environmental influences may also combine onto the underlying genetic pathology accelerating the onset of the diseases.

1.1.5 Neuropathological features of schizophrenia and autism

One of the most consistent neuropathological features of schizophrenia is grey matter loss. Post-mortem studies reported that brain regions showing the greatest loss of grey matter display significant reductions in spine density (Glausier & Lewis 2013). Furthermore, these areas were also associated with behavioural functions that are perturbed in the disease (Sullivan et al. 1996). One of the affected areas is the dorsolateral prefrontal cortex (DLPFC) which is crucial for working memory function, and was demonstrated to exhibit decreased activity during working memory tasks in schizophrenics (Cho et al. 2006). Spine loss has been consistently reported particularly in layer III neurons of the DLPFC (Glantz & Lewis 2000). Similarly, considerable reductions in spine density on pyramidal cells in the primary auditory cortex are present in some schizophrenic brains, which could explain the origin of auditory hallucinations perceived by a subset of individuals with the disorder (Sweet et al. 2009). Furthermore, symptoms of schizophrenia have routinely been linked to dopamine, as patients appear to show elevated levels of dopamine D2 receptors particularly in the limbic system (Kestler et al. 2001). Changes in other neurotransmitter systems, including the reduction in N-methyl-D-aspartic acid (NMDA) receptor function, which plays a key role in excitatory signalling has also been suggested to occur in schizophrenia (Krystal et al. 2003).

In autism, early brain overgrowth and circuit hyperexcitability govern the two most well-established phenotypes of the disorder. Around a quarter of children with autism exhibit an increase in brain size during the first two years of life in comparison to healthy controls (Courchesne et al. 2004). Moreover, approximately 30% of autistic children have epilepsy (Tuchman & Rapin 2002). One possible mechanistic explanation connecting the two phenotypes is elevated spine density. Several post-mortem studies revealed increases in spine density on the apical dendrites of pyramidal cells in layer II of the cortex (Hutsler & Zhang 2010). On the other hand, contradicting studies reported smaller neurons with simplified dendritic morphologies in the limbic system compared to controls, consistent with deficits in developmental maturation rather than malformation (Raymond et al. 1995). Although the discrepancy in these studies should be taken with care due to the small number of post-mortem autistic brains that have been examined in the past few decades, they also support the idea that the pathophysiology in the autistic brain is highly heterogeneous. With this in mind, functional magnetic resonance imaging studies analysing brain connectivity have consistently shown local over-connectivity in addition to long-distance under-connectivity in adult patients with autism (Wass 2011).

Finally, deficits in fast rhythmic network activity are consistently reported in schizophrenia and autism (see section **1.2.7**). This highly dynamic process enables neuronal networks to synchronise and fire in oscillations which allows for coordinated activity during normal brain function, and underlies cognitive processes such as memory and attention (Bartos et al. 2007). Strong evidence suggests that fast network oscillations are governed by the robust firing of inhibitory interneurons (Cardin et al. 2009). Hence, in addition to structural abnormalities described above, key functional mechanisms that govern network synchrony are also affected in these disorders.

1.1.6 Current treatments for schizophrenia and autism

The core symptoms of autism have not been demonstrated to respond to medication, however other drugs may be used to treat comorbid psychiatric conditions such as epilepsy (Young & Findling 2015). Antipsychotics, such as clozapine, which block the dopamine receptor D2, but also other neurotransmitter receptors including serotonin receptor $5HT_{2a}$, tend to be the most widely used amongst individuals with schizophrenia (Meltzer 1989). However, although they appear to be effective in reducing the positive symptoms of schizophrenia, they seem to have limited effects on negative symptoms and cognitive impairment (Miyamoto et al. 2012). Furthermore, antipsychotics have been reported to carry a number of severe side effects such as agranulocytosis and eosinophilia, and less severe effects including sedation, tachycardia and weight gain, which may make them undesirable to some patients (Meltzer 2013). Non-pharmacological treatment options are also currently used to treat individuals with schizophrenia and autism. These include behavioural, psychosocial and educational interventions that are routinely used from disease onset, which aim to facilitate social integration and tasks to improve cognitive skills (Pina-Camacho et al. 2016). To summarise, current treatments only alleviate several of the positive symptoms of schizophrenia, and unfortunately are prone to many unwanted side effects, whilst the development of treatments for autism have so far been unsuccessful. A new pharmacological approach is thus evidently required for the development of a more suitable method to address the cognitive and negative symptoms associated with schizophrenia; a mechanism that targets an alternative pathological pathway, and one that potentially could be used to treat symptoms associated with autism.

1.1.7 Proposed circuit deficits in schizophrenia and autism

Information transfer in the brain is heavily dependent on the functional balance between excitatory and inhibitory networks (see section **1.2.4**). This balance relies upon the maintenance of appropriate ratios of excitatory and inhibitory inputs that each individual neuron receives, which can affect the overall activity of higher order

networks. A disruption in this balance during development has been proposed to result in network hyperexcitability and epilepsy, as well as deficits in network processing, which is believed to be associated with motor and cognitive impairments (Marín 2012). Increasing evidence suggests that imbalances between excitation and inhibition in synaptic transmission within neuronal circuits may be implicated in schizophrenia and autism (Cline 2005).

Defects in inhibitory neurotransmission have now been associated with multiple neuropsychiatric diseases (see sections **1.2.8** and **1.2.9**). Post-mortem studies indicate a reduction in the number of interneurons in the prefrontal cortex of individuals with schizophrenia leading to the proposition that a decline in inhibitory inputs onto pyramidal cells may contribute to the pathophysiology of the disease (Benes et al. 2001). Although interneuron loss might be the case in some patients with the disorder, deficits occurring preferentially at the level of inhibitory synapses are now more widely accepted (Woo et al. 1998). With autism, as post-mortem brain tissue examinations are still relatively sparse, much less is known about the human pathology, however, several studies demonstrate a reduction in inhibitory signalling and therefore a disruption in the excitatory-inhibitory balance that manifests in cortical circuits (Fatemi et al. 2002).

These findings indicate that while the genetics are diverse, both disorders may converge on similar pathophysiological processes. An emerging hypothesis suggests that modifications in the excitatory to inhibitory ratio of cortical activity could be responsible for the cognitive and social deficits observed in patients with schizophrenia and autism. Post-mortem studies consistently describe a reduction in the expression of molecular markers that govern the inhibitory system (see sections **1.2.8** and **1.2.9**). Furthermore, as interneurons are essential for the establishment and maintenance of synchronised, rhythmic network activity, – a phenotype that is consistently aberrant during working memory tasks in schizophrenics – these cells may form part of the underlying aetiology. Thus, the ability to modulate the activity

of inhibitory interneurons could therefore contribute to the development of more efficacious therapeutic interventions.

1.2 Interneurons

Excitation and inhibition are the fundamental means of signalling within the mammalian brain (Isaacson & Scanziani 2011). Cortical networks are comprised of glutamatergic excitatory neurons and GABAergic inhibitory interneurons that play a critical role in gating signal flow and sculpting network activity (Tremblay et al. 2016). Although GABAergic interneurons represent a minority of the entire neuronal population, they are however much more diverse in terms of their morphological, biochemical and biophysical properties, as well as in their connectivity with other cells (Markram et al. 2004). By releasing GABA which acts as a primary inhibitory neurotransmitter in the CNS, interneurons maintain the stability of cortical networks by temporally controlling principal cell firing, modulating dynamic range, balancing excitation with inhibition, and generating network synchrony (Haider & McCormick 2009). Malfunctions of these neurons has been associated with the establishment of schizophrenia and autism (Marín 2012).

1.2.1 GABAergic transmission

Two major neurotransmitters induce ionotropic inhibitory responses: GABA and glycine (Ito 2016). GABA is the major inhibitory transmitter in the cerebrum, while glycine is more abundant in the spinal cord and brain stem (Van den Pol & Gorcs 1988). GABA is synthesized by two different isoforms of glutamic acid decarboxylase (GAD), GAD65 and GAD67, both of which are present in most interneurons. GAD67 is distributed throughout the cell body where it synthesises cytoplasmic GABA, while GAD65 is specifically targeted to nerve endings where it synthesises GABA destined for vesicular release (Soghomonian & Martin 1998). GABA is released from presynaptic nerve terminals of GABAergic interneurons and

triggers the activation of three different types of GABA receptors, each of which has been identified based on their pharmacology and electrophysiology. $GABA_A$ and $GABA_C$ receptors are ligand-gated ion channels that control the flow of Cl^- and HCO^-_3 ions across the cell membrane (Jentsch et al. 2002). Both channels are predominantly expressed at the postsynapse where they mediate fast inhibitory transmission. $GABA_A$ receptors are pentameric transmembrane receptors composed of a group of subunits from eight different classes (α1-6, β1-3, γ1-3, δ, ε, θ, π, and ρ1-3), most often assembling with a 2α:2β:γ stoichiometry (Laurie et al. 1992). $GABA_B$ receptors however belong to a family of heptahelical metabotropic G-protein receptors that are linked via G-proteins to inwardly-rectifying K^+ channels and Ca^{2+} channels (Kaupmann et al. 1998). These receptors are mostly located at non-synaptic sites and presynaptic terminals where their effects tend to have a delayed onset and favour a longer duration (Kulik et al. 2003).

Low extracellular concentrations of GABA are required between synaptic release to prevent tonic GABA receptor activation. Extracellular concentrations of GABA are maintained by four specific high-affinity, Na^+/Cl^- dependent transporters encoded by the genes GAT-1, GAT-2, GAT-3 and BGT-1, of which GAT-1 and GAT-3 are expressed in the cerebral cortex. At birth, GATs are expressed at relatively low levels in rodents before progressively reaching adult levels during the first postnatal month, where they function to quickly remove GABA from the synaptic cleft, thus terminating the effect of the neurotransmitter (Conti et al. 2004). In the adult brain, the effects of GABA are mainly inhibitory due to the hyperpolarised nature of the Cl^- reversal potential (E_{Cl}). E_{Cl} depends on the Cl^- concentration gradient across the membrane, which is regulated by the opposite action of Cl^- cotransporters NKCC1 and KCC2, required in Cl^- uptake and extrusion, respectively. During the first postnatal week, KCC2 is upregulated, leading to a reduction in the concentration of intracellular Cl^-, shifting E_{Cl} to a negative value (Rivera et al. 1999). Upon GABAergic stimulation, Cl^- channels open allowing Cl^- influx, which hyperpolarises the membrane.

During neuronal maturation, the time course of GABAergic currents speed up due to changes in $GABA_A$ receptor subunit composition. In late embryonic stages of development, predominant expression of α3, α5 and β3 subunits generate IPSCs with slow decay. Throughout postnatal development, the transcription of these three genes decreases, while expression of α1, α4 and δ subunits gradually increase. This developmental change in subunit expression is paralleled by a reduction in the decay time constant of GABAergic IPSCs (τ_{IPSC}). Interestingly, τ_{EPSC} only marginally decreases during development, whereas τ_{IPSC} reduces almost 10-fold (Okaty et al. 2009). It has been demonstrated that τ_{IPSC} is inversely related to the ratio of α1 to α5 subunits and takes approximately 3 postnatal weeks until IPSCs acquire their mature properties (Dunning et al. 1999). Importantly, it highlights that as the brain matures, $GABA_A$ receptor mediated inhibitory currents become more temporally precise.

1.2.2 Interneuron diversity

Inhibitory interneurons represent a minority of all cortical neurons constituting approximately 10-15% (Meyer et al. 2011). While excitatory glutamatergic neurons of the cortex and olfactory bulb are produced locally by progenitor cells in the developing pallium, GABAergic interneurons originate in the subpallium, at the base of the telencephalon (Ma et al. 2013). Studies over the past decade have determined that nearly all neocortical interneurons in the brain originate from four main sources in the subpallium: the medial, lateral and caudal ganglionic eminences (MGE, LGE and CGE, respectively), and the preoptic area (POA) (Gelman & Marín 2010). Although glutamatergic neurons migrate radially to adopt their analogous laminar position in the cortex, interneurons first move to the pallium and subsequently spread tangentially to occupy the entire cortex. Finally, they spread out radially and integrate specific layers of the cortex (Marín 2013). A large body of evidence suggests that different classes of interneurons (explained in further detail below) originate from specific regions in the subpallium and are controlled by various transcription factors throughout migration during development (DeBoer & Anderson 2016).

GABAergic interneurons are a highly diverse cell population in terms of morphology, molecular expression and electrophysiology (Tremblay et al. 2016). Anatomically, they display a variety of somatic, dendritic, and axonal morphologies, in addition to specific subcellular domains targeted by their axons. Electrophysiologically, an array of firing patterns has been described, a consequence of the interplay between ion channel composition and membrane cable properties. Thus, the active and passive membrane biophysical properties will differ among interneuron subtypes. In addition, synapses of specific subtypes are coordinated with GABA receptors differing in subunit composition, resulting in distinct kinetics of the GABAergic response (Dunning et al. 1999). Interneurons also express receptors for different neuromodulators such as acetylcholine, serotonin, noradrenaline, and dopamine, which can have dramatic effects on the function of neocortical circuits, leading to dynamic changes associated with different brain states (Tremblay et al. 2016). Finally, interneurons differ in their expression of molecules that include calcium-binding proteins and neuropeptides. All these characteristics highlight the vast number of interneuron subtypes present in the brain, and most have substantial consequences on cellular and network computations. Although they represent a small proportion of all cortical neurons, their differences in subcellular targeting, connectivity, synaptic kinetics, and intrinsic membrane properties enable them to control the activity of principal cells with high spatiotemporal specificity and precision (Fig 1.1 & 1.2).

Classification of interneurons has been relatively successful in the hippocampal CA1 region. Morphological features including somatic location and dendritic and axonal innervation fields are used to reliably map out different populations of interneurons within CA1, which subsequently match nicely to functional and molecular properties based on these morphological criteria (Klausberger & Somogyi 2008). The success of this classification system depends predominantly on the simplified laminar layout of the hippocampus, where a given interneuron subtype can easily be identified based on its cellular and axonal location. In contrast, in the neocortex, the amalgamation of different cell types in most cortical layers has made a similar attempt very difficult. An effort to therefore systematically classify neocortical interneurons based on

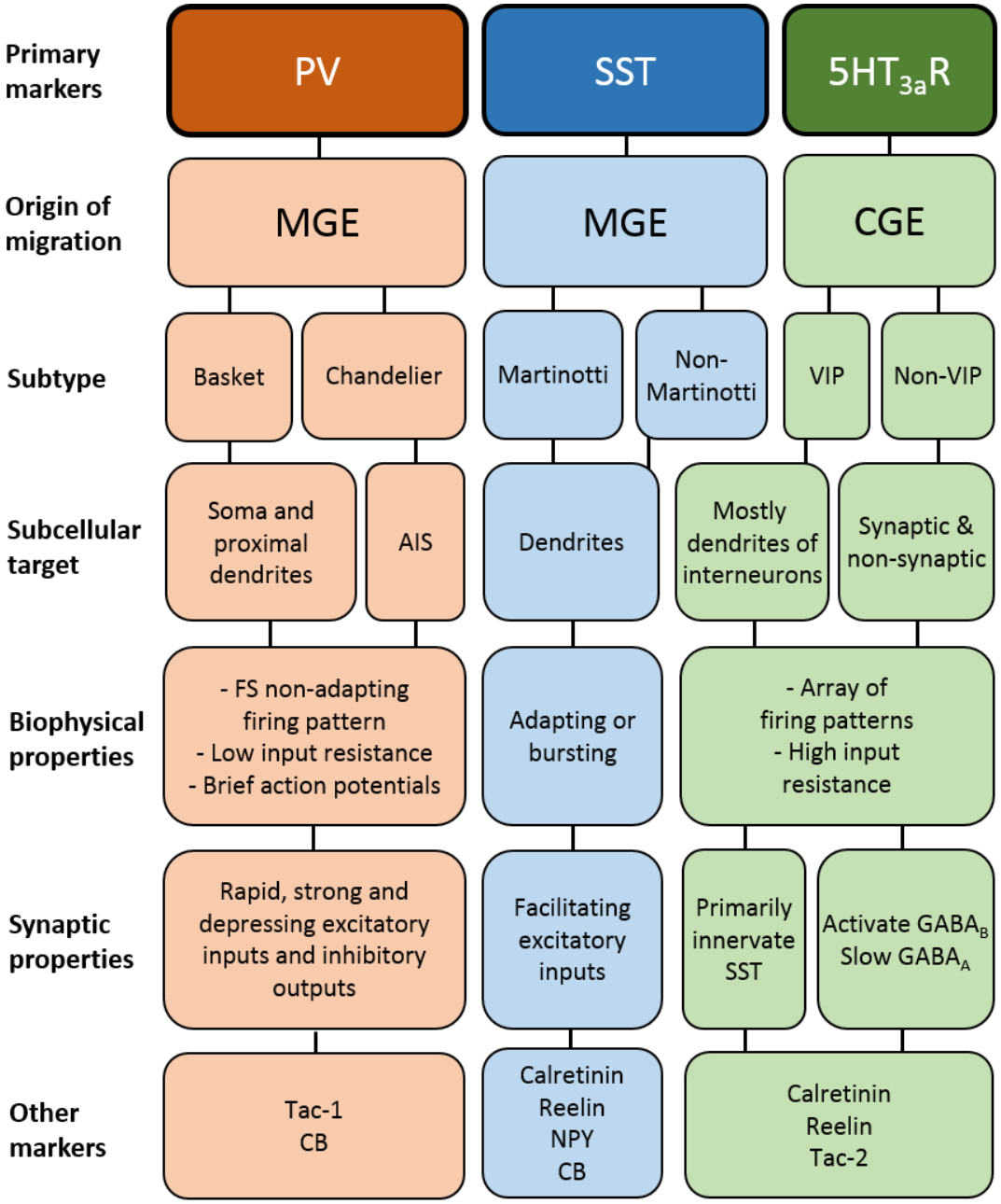

Figure 1.1 Classification and developmental origins of neocortical GABAergic interneurons Most neocortical interneurons originate from the medial or caudal ganglionic eminences (MGE or CGE). Almost all neocortical interneurons can be classified by the expression of three non-overlapping markers: Ca^{2+}-binding protein parvalbumin (PV), the neuropeptide somatostatin (SST), or the ionotropic serotonin $5HT_{3a}$ receptor ($5HT_{3a}R$). Each molecular group can be subdivided further to reveal distinct biophysical and synaptic properties and subcellular targeting specificity. Several other important characteristics including morphological and anatomical properties have been omitted from this diagram. Figure adapted from Tremblay et al. 2016.

morphological characteristics alone demonstrated that there are too many ambiguities, resulting in overlapping subgroups (Defelipe et al. 2013).

More recently, the expression of certain molecular markers has provided an initial platform to begin characterising specific interneuron subtypes in the cortex. Advances in molecular genetics have made it possible to express fluorescent proteins or enzymes such as Cre recombinase, which, when under the control of a promoter encoding a marker gene, allows for identification of specific groups of interneurons (Taniguchi et al. 2011). Three major distinct and largely non-overlapping subgroups of interneurons, which account for nearly 100% of GAD67 mRNA-expressing neurons in the neocortex have been identified (Fig 1.1). These cells either express the Ca^{2+}-binding protein parvalbumin (PV), the neuropeptide somatostatin (SST), or the ionotropic serotonin $5HT_{3a}$ receptor ($5HT_{3a}R$). Furthermore, the developmental origins of these cortical interneuron groups can be defined by their molecular markers. PV and SST interneurons originate in the MGE of the subpallium from progenitors expressing Nkx2.1 amongst other transcription factors, whereas $5HT_{3a}R$ interneurons are derived from the CGE (DeBoer & Anderson 2016). Importantly, interneurons belonging to each of these groups show a preference in functionally relevant properties that are either exclusive or not as distinguished in other groups, as well as in gene expression patterns (Zeisel et al. 2015).

The PV and $5HT_{3a}R$ interneuron groups can each be separated into two more, clearly disparate subgroups. The PV group accounts for approximately 40% of GABAergic neurons and includes fast-spiking basket cells and chandelier cells (Xu et al. 2010). Basket cells, which form most of the PV group make perisomatic “basket” terminals on principal cells and interneurons. Chandelier, or axo-axonic cells however, target the axon initial segment (AIS) of principal cells. The $5HT_{3a}R$ group can be segregated into two subgroups based on whether the cells express vasointestinal peptide (VIP), a neuropeptide that is not expressed in PV or SST interneurons (Lee et al. 2010). The SST group, which predominatly target dendrites of principal cells, include Martinotti cells, which have axonal projections that reach into layer I, as well

as a subset of neurons that specifically target layer IV. In addition to the three main molecular markers and along with VIP, other markers are frequently used to label cortical interneurons. These include the glycoprotein reelin, the Ca^{2+}-binding proteins calbindin (CB) and calretinin (CR), the neuropeptides cholecystokinin (CCK) and neuropeptide Y (NPY), and several neurotransmitter precursor proteins (Tac-1 and Tac-2) (Tremblay et al. 2016). In comparison to the first four, these additional markers are not expressed in non-overlapping groups.

1.2.3 Function of interneuron subtypes

While glutamatergic synapses from principal cells are limited to the dendritic tree of postsynaptic neurons, GABAergic synapses made from interneurons are dispersed along the entire axis of both excitatory and inhibitory cell types (Megías et al. 2001; Glickfeld et al. 2009). Thus, excitatory and inhibitory inputs coexist on the peripheral dendritic tree, whereas the proximal areas receive only inhibition (Pouille et al. 2013). Furthermore, depending on the driving force, synaptic inputs can produce either a depolarising or hyperpolarising response, or simply no change in the membrane potential of postsynaptic cell. The activation of postsynaptic $GABA_A$ receptors, where the membrane potential is often very close to the reversal potential may only generate very small or no hyperpolarising responses, however still in these cases, the net effect will be inhibitory. This is because the net synaptic conductance is increased, thus lowering the input resistance of the postsynaptic cell, resulting in the shunting of excitatory inputs. As a result, GABAergic synaptic inhibition can decrease the excitability of the postsynaptic cell in two ways: by eliciting a hyperpolarising current which is thought to have a subtractive effect on neuronal output, or by increasing the conductance of the cell, which is considered to produce a divisive effect (Chance et al. 2002). This divisive effect is known as gain modulation, and is essential for network balance, as it modulates the input-output function of a neuron - by changing the slope of its firing rate curve (Chance et al. 2002). Models suggest that inhibition produces a divisive effect on postsynaptic potentials if the change in conductance is large and located near the soma, whereas a subtractive effect will be produced if conductances are small and distally located

(Silver 2010). For these reasons, GABAergic interneurons are understood to be key components in regulating the dynamics of recurrent excitatory circuits at distinct spatial and temporal scales.

The employment of qualitatively different interneuron subtypes to the same network, albeit in small numbers, provides a substantial expansion of computational possibilities (Roux & Buzsáki 2015). Essentially every compartment of the somatodendritic surface of cortical principal cells is under the specific control of a particular class (Fig 1.2), each determining the nature of inhibition produced and its net effect on the output of the postsynaptic cell (Markram et al. 2004). This is particularly important because many principal cells exhibit elaborate dendritic fields differentially associated with distinct excitatory inputs and intrinsic active properties. The functional capacity of principal cells can therefore be multiplied using mostly local interneuron wiring which act to modulate the gain and dynamic range of cortical circuits (Roux & Buzsáki 2015). The differences in interneuron subtypes and how they integrate into circuits with specific computational impacts are discussed below.

Basket cells within the PV group primarily target the somata and proximal dendrites of principal cells in addition to other PV cells (Fig 1.2), which places them in a unique position to powerfully influence the output of their targets. Consequently, these interneurons are believed to be critical for the precise timing of pyramidal cell firing, coordinating their synchrony though gamma oscillations (Buzsáki & Wang 2012). Chandelier cells however, exclusively target pyramidal cells at the AIS, and have recently been suggested to induce a depolarising rather than a hyperpolarising postsynaptic response due to an unusually depolarised E_{Cl} at the AIS, due to the absence of the Cl^- extrusion transporter KCC2 (Szabadics et al. 2006). Despite these important differences, both cell types within the PV group typically have multipolar morphology and share very similar electrophysiological features. They fire high-frequency non-accommodating trains of action potentials comprised of fast and deep afterhyperpolarisation potentials (AHP), and with very little spike-frequency

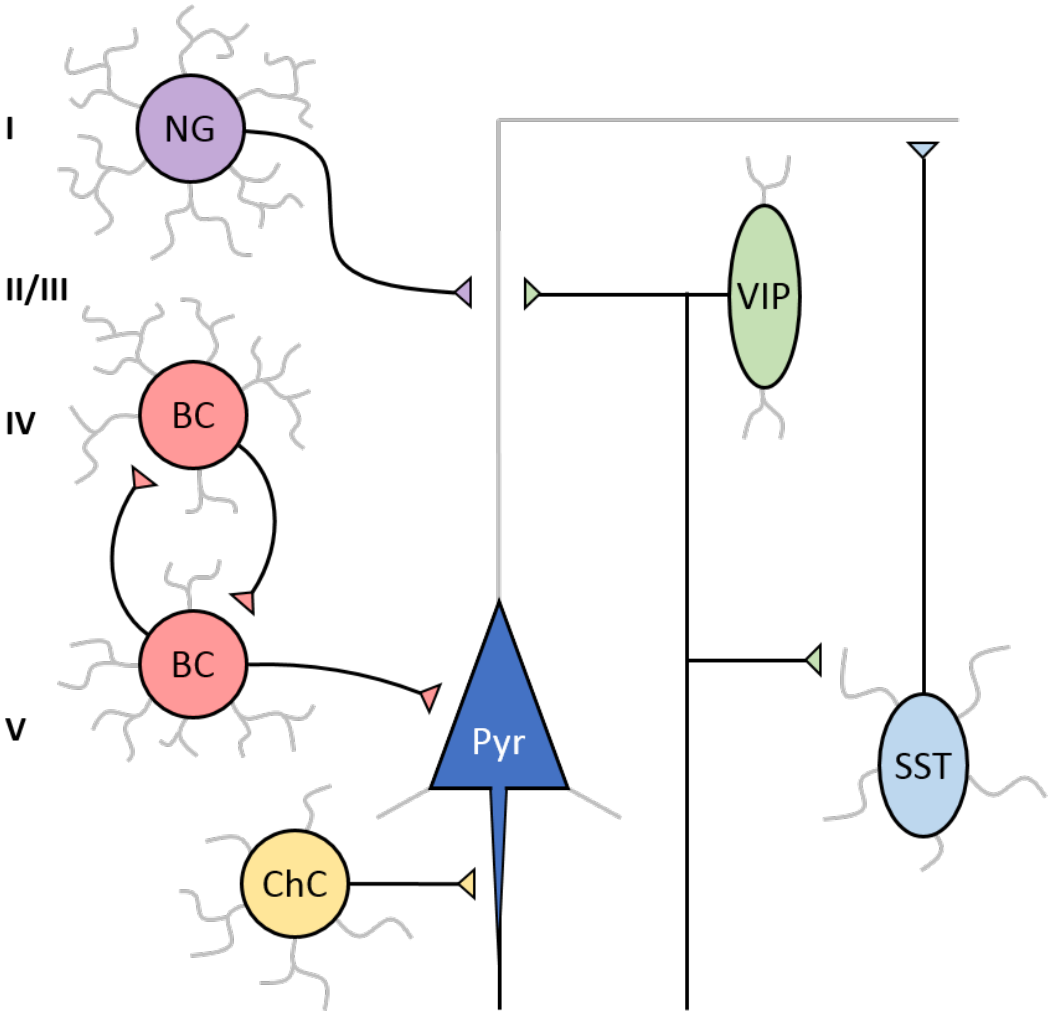

Figure 1.2 Schematic illustrating specific subcellular innervation of different classes of GABAergic interneurons in the primary somatosensory cortex Axons and dendrites are depicted by black and grey lines, respectively. PV basket cells (BC) primarily target the soma and proximal dendrites of pyramidal cells (Pyr) and other interneurons, predominantly other PV cells. PV cells maintain mostly locally projecting axons but can project across multiple layers depending on their laminar location. PV cell axons show extensive arborisation (not shown) enabling them to inhibit the vast majority of local cells, while their dendrites often span across cortical layers enabling them to sample input from a large population of neurons. PV chandelier cells (ChC) specialise in targeting the AIS of pyramidal cells. SST cells predominantly target the dendrites of pyramidal cells and other interneurons while Martinotti cells (which make up most of the group) almost always project a significant portion of their axon into layer I where they target dendritic tufts of pyramidal cells. The $5HT_{3a}R$ group includes VIP cells which primarily target other interneurons, mainly SST cells, usually at their dendrites. They therefore specialise in disinhibitory control. Also in this group are neurogliaform cells (NG), which unlike other interneuron subtypes can regulate non-synaptic, spatially non-specific input to surrounding cells. Roman numerals indicate cortical layer.

adaptation (Erisir et al. 1999). This enables fast and precise signalling onto target neurons, allowing them to participate in numerous functions including controlling feedforward inhibition (see section **1.2.4**) of many cortical circuits, which is important in establishing a strict window for temporal summation of excitatory inputs in principal cells (Hu et al. 2014).

In contrast to PV cells, the SST group are dendritic targeting (Fig 1.2), and therefore have different functional dynamics as they specifically control the kinetic properties of distal processes (Tremblay et al. 2016). Most PV interneurons have strongly or moderately depressing excitatory inputs, whereas SST cells, regardless of subtype, are strongly facilitating (Kapfer et al. 2007). This key feature is likely of considerable physiological interest, as it allows for a very few number of excitatory inputs to drive EPSP summation and induce SST cell firing. While PV interneurons require synchronous firing of many presynaptic cells to make them discharge, the facilitation of inputs onto SST cells allows for even a single excitatory cell to recruit them (Kapfer et al. 2007), and therefore SST cells are reliably recruited to perform important functions such as providing feedback inhibition (see section **1.2.4**). Martinotti cells, which make up the majority of the SST group, are typically bitufted or multipolar in morphology, and are found throughout layers II-VI but are more abundant in layer V (Wang et al. 2004). Their axons usually extend into layer I where they spread out horizontally into neighbouring columns and make synapses on dendritic tufts of pyramidal cells, as well as many types of interneurons (Pfeffer et al. 2013). Given the facilitating dynamics of their inputs and their axonal arborisation, the inhibition mediated by these cells escalates as a function of rate and duration of presynaptic firing, which subsequently spreads into distal areas where they can influence neighbouring columns.

The $5HT_{3a}R$ group are more heterogeneous than the PV and SST groups, despite them all expressing functional $5HT_{3a}$ and nicotinic receptors (Lee et al. 2010). They primarily populate supragranular cortical layers, where they represent the largest interneuron population. VIP cells, which constitute approximately 40% of all the

cells in the $5HT_{3a}R$ group, are found mostly in layers II/III, and have a vertically oriented, bipolar-like, translaminar dendritic morphology. Their axons, also being vertically extended, often span many or even all cortical layers in a narrow columnar fashion (Fig 1.2). This suggests that this subtype not only integrates a large range of inputs spanning over long distances, but also provides feedforward and feedback inhibition across all cortical layers. These cells exhibit an array of firing patterns that can be irregular, bursting, and adapting. Perhaps the most important intrinsic electrophysiological feature of VIP cells is their high input resistance, which is higher than most cortical neurons, and makes them particularly sensitive to excitatory inputs. For example, although thalamic stimulation generates relatively weak excitatory synaptic currents onto deep layer III VIP cells, their high input resistance enables substantially larger depolarising inputs (Lee et al. 2010). Importantly, VIP cells have been reported to target many other interneuron groups, particularly SST interneurons (Fig 1.2), and therefore specialise in disinhibitory control (Pi et al. 2013). Furthermore, their ability to respond to long range input allows for translaminar inhibition across multiple cortical layers (Xu & Callaway 2009).

Non-VIP cells account for the remaining 60% of the $5HT_{3a}R$ group (Rudy et al. 2011). They are usually reelin positive and make up more than 90% of all the neurons in layer I. They include neurogliaform cells which have small multipolar dendritic arbors, and although predominant in layer I, are also located in other layers (Hestrin & Armstrong 1996). These cells typically display a late-spiking firing pattern characterised by a slow depolarisation ramp preceding firing at threshold. During larger suprathreshold depolarisations, the cells fire adapting firing trains (Kawaguchi & Kubota 1997). Neurogliaform cells are unique because they elicit slow, long-lasting IPSPs on pyramidal cells and other interneurons, via a combination of slow $GABA_A$ and $GABA_B$ receptor activation. In addition to this, their highly dense axonal plexuses and high release-site densities, many of which are not associated with synapses contribute to volume transmission of GABA (Oláh et al. 2009). Unlike other interneuron types that specifically synapse onto particular compartments of postsynaptic neurons, neurogliaform cells, in part, regulate non-

synaptic, spatially non-specific input to surrounding cells and therefore dampen down the neural activity in a local area (Tamás et al. 2003).

1.2.4 Balance between excitation and inhibition

Neurons in the cerebral cortex form dense mosaics of excitatory and inhibitory connections that illustrate both convergence and divergence (Haider et al. 2006). Crucially, the response of any specific neuron is determined by the impact of thousands of synaptic inputs (Binzegger et al. 2004). The balance between excitation and inhibition is therefore essential for cortical function. Within a given local cortical network, neurons gather inputs from other nearby neurons which form recurrent excitatory, as well as feedforward and feedback inhibitory circuits (Markram et al. 2004). Considering the great diversity of interneurons in terms of their connectivity and functional properties, cortical excitation can be robustly controlled to form a dynamic equilibrium between excitation and inhibition (Shu et al. 2003). This dynamic control of excitation that governs cortical network activity is accomplished through feedback and feedforward inhibition (Isaacson & Scanziani 2011). This provides a way for interneurons to mediate precise gating of information through specific signalling pathways, and limits the time window for the summation of excitatory inputs. They accomplish these goals by controlling both spatially and temporally the measure of excitatory and inhibitory inputs that specific neurons receive (Vogels & Abbott 2009), which is often dependent on the brain state (T. Klausberger et al. 2003).

Both feedforward and feedback inhibitory circuits can produce rapid sequences of excitation and inhibition (Fig 1.3). In the feedforward scenario, afferent inputs contact both principal cells and interneurons, resulting in the onset of excitation recorded in principal cells preceding the onset of inhibition by a monosynaptic delay (Gabernet et al. 2005). In principal cells of the somatosensory barrel cortex, for example, whisker deflections induce excitation followed rapidly by inhibition (Swadlow 2002). Similarly, in the auditory cortex, brief tones lead to an increase in

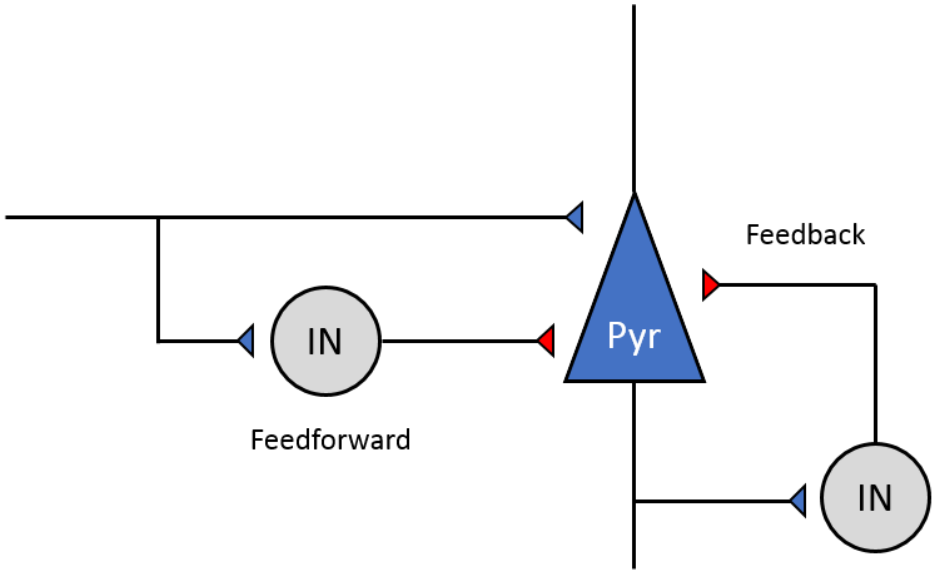

Figure 1.3 GABAergic interneurons provide balance to excitatory signaling
Schematic illustrating feedforward and feedback inhibition in a cortical microcircuit. In feedforward inhibition (left), a distant neuron excites an interneuron (coloured grey) which in turn inhibits a principal cell (coloured blue). The disynaptic GABAergic signal received by the principal cell arrives within a couple of milliseconds after the monosynaptic excitatory response. In feedback inhibition (right), the interneuron receives excitation from the same excitatory cell that it is going to inhibit in return. Excitatory and inhibitory synapses are coloured blue and red, respectively.

synaptic excitation that is accompanied by a surge in inhibition within a couple of milliseconds (Wehr & Zador 2003). Feedback circuits where local principal cells are followed by the recruitment of interneurons which 'feedback' on the principal cells also provide stability as it prevents runaway excitation. These rapid discrepancies in the ratio between excitation and inhibition can have fundamental consequences in tuning cortical neurons to individual stimuli and in temporally shaping their activity patterns.

Finally, the counterbalance of excitatory and inhibitory conductances within the brain is maintained at comparable values across different cortical layers (Zhang et al. 2011). As cortical transmission is largely enforced by GABAergic and glutamatergic ionotropic receptors that produce fast synaptic conductances, the possibility of

shifting the ratio between synaptic excitation and inhibition allows for the membrane potential in neurons to be effectively altered. Interneurons therefore contribute to the global balance of activity which is essential to maintain the stability of cortical networks. It is believed that this balance is fundamental for the maintenance of cortical network rhythms responsible for higher order cognitive functions (Haider et al. 2006).

1.2.5 PV interneurons

Out of the extensive diversity of GABAergic interneurons in the cerebral cortex (Markram et al. 2004), PV cells are the largest interneuron population in the neocortex (Rudy et al. 2011). The activity of basket and chandelier cells – which comprise most of the PV group - is important in regulating the membrane potential at proximal regions of postsynaptic neurons, since PV cells primarily synapse onto the somata, AIS and proximal dendrites (Hu et al. 2014). The proximity of their perisomatic inputs to the site of action potential generation puts them in a favourable position to robustly inhibit the activity of target neurons.

PV basket cells have diverse axonal and dendritic arborisation territories (Staiger et al. 2015). In layer IV of the somatosensory cortex for example, PV basket cells maintain mostly locally projecting axons, while in other layers they can project across multiple layers, which include PV cells in layer V. Since these cells target the perisomatic region of principal cells, local cells will inhibit mostly local populations, while translaminar cells enable interlaminar interactions via inhibition. Furthermore, some supragranular and infragranular - but not layer IV – PV basket cells contain axons that extend across several columns, suggesting that they can influence neighbouring columns in addition to their own column.

The morphological properties of PV cell axons differ from most other types of interneuron. PV cell axons in rats show extensive arborisation, where an individual PV cell can have a cumulative axonal length of 20 and 50 mm in the frontal cortex

and hippocampal CA1 region, respectively (Karube et al. 2004; Sik et al. 1995). It has been reported that their axon arbors in the cortex can make 3,000-5,000 *en passant* terminals onto postsynaptic targets, enabling them to inhibit the vast majority of nearby cells (Karube et al. 2004). Each PV cell innervates target principal cells with 5-15 boutons, and is therefore considered to contact 200-1000 principal cells. Consequently, PV cells produce a massively divergent inhibitory output, utilising their strategically placed perisomatic terminals to form a blanket of inhibition in territories covered by their axons.

PV cell dendrites are also intriguing as they often span across cortical layers, which enable them to sample input from a large population of neurons (Gulyá et al. 1999). Their somata and dendrites are densely covered with synapses, making them extremely receptive to picking up local activity from individual neurons as well as neuronal ensembles. It is estimated that in CA1 or CA3, a single PV cell can have between 16,000 to 35,000 synapses, 94% of which are excitatory and 6% inhibitory (Gulyá et al. 1999; Tukker et al. 2013). A large fraction of inhibitory synapses are made from other PV terminals, but inhibitory inputs from SST and VIP interneurons are also present (Hioki et al. 2013). PV cells therefore receive convergent excitatory synaptic input from principal cells, and inhibitory input predominantly from other PV cells. Interestingly, a large proportion of PV cell dendrites are gap junction-coupled with dendrites from adjacent PV cells. These are constructed from membrane-inserted connexin 36 proteins, and are present in approximately 80% of PV cells (Ma et al. 2011). PV cells are therefore highly interconnected both synaptically and electrically, which may help widen the spatial range of detection of principal neuron activity. Thus, excitatory input synapses onto one PV cell could still influence the activity of an unconnected PV cell, via electrical coupling of adjacent PV cells (Galarreta & Hestrin 2001). As a result, gap junctions have been suggested to boost the efficacy of distal inputs (Vervaeke et al. 2012), in addition to supporting synchrony between PV cells. This may also function in reinforcing the population of inhibition in the cortical microcircuit.

PV basket cells can fire repetitively at up to 400 Hz, faster than any other cell in the brain (Kawaguchi 2001). Action potential frequency however is much lower *in vivo* because of functionally powerful autapses, which provide feedback inhibition that reduces excitability (Bacci et al. 2003). It has become apparent that PV basket cells respond to excitatory stimulation with remarkable speed and with exquisite temporal precision. During sharp-wave ripples or theta rhythms *in vivo*, basket cells are recruited by inputs from principal cells with short latency and minimal jitter (Klausberger et al. 2003). These neurons set narrow time windows for temporal summation in principal neurons through fast feedforward and feedback inhibition. It is becoming clear that this neuronal population is extremely important in tasks requiring rapid and temporally precise modes of inhibitory signalling; from cellular functions such as coincidence detecting to network-wide maintenance of network oscillations.

1.2.6 Role of PV interneurons in cortical networks

A fundamental characteristic of cortical activity is the rhythmic and synchronous oscillation of the membrane potential of neuronal populations. Fast oscillations at gamma frequencies (30-80 Hz) have been hypothesised to be essential for information processing in cortical neurons by increasing the reliability of both spike probability and timing (Buzsáki & Schomburg 2015). These fast oscillations occur under a range of behavioural states, either spontaneously or in response to sensory stimuli, and are believed to be involved in coordinating large numbers of neurons, distributing information within and across different areas of the brain. As target neurons are depolarised more efficiently when excitatory inputs are actively synchronised instead of distributed in time, oscillations allow neurons to contribute to the depolarisation of cell assemblies for efficient transmission of downstream targets (Azouz & Gray 2000). Information processed in distinct cortical areas can therefore be consolidated through gamma oscillations, which may underlie cognitive processes related to temporal binding, where two distinct groups of neurons recruit a third group to which they both project, thereby ‘binding’ them into functionally coherent assemblies (Engel et al. 2001).

Inhibition mediated by PV basket cells has not only been demonstrated to be directly involved in the generation of these fast oscillations, but also in synchronising participating neurons as well as maintaining their coherence in space (Cardin et al. 2009; Cobb et al. 1995). Several important properties of PV basket cells appear to be essential in the generation of synchronised oscillations. Firstly, these cells synapse onto the perisomatic region of their target cells, which minimizes the effects of dendritic filtering and the time required for signal propagation, placing them in a strategic position to control action potential generation (Miles et al. 1996). Secondly, they form reciprocal synaptic connections onto each other (Gibson et al. 1999), a functional property that has been shown to be valuable for the robustness of oscillations in models (Bartos et al. 2007). These reciprocal connections produce a shunting rather than a hyperpolarising effect on neighbouring PV cells, which shortens the interspike interval for low levels of drive but prolongs it at high levels (Vida et al. 2006). Lastly, PV basket cells are electrically coupled via gap junctions, enabling large populations to be synchronised with millisecond precision (Galarreta & Hestrin 1999). It has been suggested that both electrical and synaptic coupling act synergistically to reinforce the degree and precision of neuronal synchronisation. The relative timing of gap junction potentials and IPSPs derived from the same presynaptic cell has been shown to be invariant, resulting in the generation of precisely sculpted, biphasic postsynaptic potentials which accurately lays down the timing of postsynaptic action potentials (Tamás et al. 2000).

Two alternative models for circuit mechanisms implicated in gamma oscillations have been proposed: pyramidal-interneuron network gamma (PING) and interneuron network gamma (ING) (Tiesinga & Sejnowski 2009). The PING model hypothesises that the excitatory cells generate the gamma oscillations, where reciprocal connectivity between pyramidal cells and interneurons are important. In this model, pyramidal cells conduct phasic excitation to interneurons on each cycle, timing the firing of interneurons to a specific phase of the gamma cycle. Furthermore, the pace of the oscillation is set by the decay time constant of inhibition of pyramidal cells. The ING model however highlights the significance of the strength and timing of GABAergic synaptic connectivity, in addition to the importance of electrical

coupling between PV basket cells and their intrinsic membrane properties (Whittington et al. 1995). Given the right conditions, the synaptically-coupled PV basket cells generate fast synchronous oscillations of the network, resulting in the entrainment of pyramidal cells (Van Vreeswijk et al. 1994). Regardless of whichever model is correct, the fact that individual basket cells contact a very large proportion of neighbouring pyramidal cells – and vice versa – adds to the concept that both PV basket cells and pyramidal cell types are essential for gamma oscillations to occur.

The interaction between excitation and inhibition in response to sensory stimuli displayed in gamma oscillations is tightly balanced. Two groups of neurons that synchronously oscillate in phase may act synergistically to recruit downstream neurons by exciting them simultaneously. However, even the slightest alteration in phase or frequency of the oscillations between the two groups may dramatically alter this synchrony and the ensuing recruitment of target neurons (Fell et al. 2001; Schoffelen et al. 2005). Despite the changes in frequency of this information, the neuronal network has been shown to maintain the magnitude of inhibition proportional to excitation during each oscillation cycle (Atallah & Scanziani 2009). Moreover, oscillations depict a time lag between the excitatory and inhibitory components, where the inhibitory phase is delayed by 1-2 ms relative to the excitatory phase (Atallah & Scanziani 2009). The outcome of this action favours excitation early in the oscillation cycle while shifting the balance towards inhibition later. This progression of events results in relatively narrow time windows for neuronal firing, which is exhibited in the tightly phase-locked firing patterns of pyramidal cells relative to oscillations (Poo & Isaacson 2009). This time window which is approximately 10-30 ms in the cortex is also in the same range as the membrane integration time for pyramidal cells during spontaneous activation *in vivo* (Léger et al. 2005). Moreover, this narrow temporal window governs the capability of how the network responds to the timing of synaptic inputs (Azouz 2005). The transmission of information during gamma oscillations is therefore a highly dynamic process that relies on precise timings of oscillations, and further emphasises the role that PV basket cells play in carrying out sophisticated neuronal operations underlying cognition and behaviour.

1.2.7 Deficits in network oscillations in neurological and psychiatric diseases

The formation of functional networks through synchronised gamma oscillations is heavily dependent upon excitatory and inhibitory dynamics that create transient connections between neuronal ensembles by modulating the degree of neuronal responsiveness (Haider & McCormick 2009). In addition to the role of neuronal synchrony in temporal coding, integration of neuronal assemblies and top-down modulation of sensory stimuli, there is growing evidence indicating aberrant neural synchrony as a pathophysiological mechanism in neuropsychiatric disorders (Spencer et al. 2003; Marín 2012). Impaired synchronisation of oscillatory activity has been suggested to result in cognitive deficits linked to working memory, attention, and perceptual organisation (Marín 2012).

A large body of electroencephalographic (EEG) and magnetoencephalographic (MEG) studies now indicate deficits in gamma-band oscillations during cognitive tasks in patients with schizophrenia. Recent MEG studies have reported impairments in the performances of visual tasks accompanied by widespread deficits in the power of gamma oscillations (Grützner et al. 2013). Similar results were found using EEG recordings of auditory and visual steady-state responses to repetitive stimulation where reductions in the power of the stimulus-locked response in the beta and gamma frequency range, but not in the lower frequencies were uncovered (Krishnan et al. 2005; Kwon et al. 1999). In addition to analyses of spectral power, the synchronicity of gamma oscillations has also been found to be reduced during cognitive tasks in patients with schizophrenia (Spencer et al. 2003; Uhlhaas et al. 2006). This is important because it is now being considered that functional networks underlying perception and attention rely on coordination across widely distributed cortical regions by the phase-locking of oscillatory activity (Fries 2005). As a consequence, reductions in long-range phase synchronisation may lead to dysconnectivity across neuronal ensembles thus resulting in abnormal functional integration of processes within the brain (Stephan et al. 2009).

Similar to work in schizophrenia, pathophysiological mechanisms associated with cognitive dysfunctions in autism are believed to converge, in part, on deficits in temporal coordination of distributed neuronal activity (Uhlhaas & Singer 2007). Both disorders for example are characterised by shortfalls in perceptual integration during auditory and visual perception (Happé & Frith 2006; Uhlhaas & Silverstein 2005). In analogy to the findings in schizophrenia, subjects with autism display a marked reduction in auditory steady-state gamma-band power in response to repetitive stimulation (Wilson et al. 2007). In addition, deficits in task-related gamma-band power were identified in autistic individuals during visual perceptual integration (Milne et al. 2009).

1.2.8 K^+ channels in schizophrenia

The fast rhythmic activity governed by the coordinated firing of PV cells largely relies on the rapid properties of voltage-gated K^+ channels specific to this cell-type. In order for this highly dynamic process to occur, each PV cell undergoes rapid repolarisation of their action potential before it can robustly fire again. Voltage-gated Kv3.1 and Kv3.2 channels which are kinetically optimised for high-frequency action potential generation (see section **1.3.3**) have been shown to be highly expressed in PV cells to give them their fast-spiking phenotype (Rudy & McBain 2001). Post-mortem tissue from individuals with schizophrenia revealed reduced expression levels of the Kv3.1 channel protein in the prefrontal cortex (Yanagi et al. 2014). Furthermore, a loss of the fast-spiking electrophysiological phenotype as well as impairment in neuronal synchrony have been reported in Kv3.1 knockout mice (Joho et al. 1999; Porcello et al. 2002), suggesting that deficits in this channel could underlie some of the pathophysiology found in schizophrenia. Alterations in cortical EEG patterns as well as an increased susceptibility to epileptic seizures consistent with deficits in cortical inhibitory mechanisms were also reported in Kv3.2 knockout mice (Lau et al. 2000). This highlights the functional importance of a key ionic channel responsible for maintaining rapid firing kinetics within PV cells, and how they are essential for the generation of fast network synchrony.

Other K^+ channels have also been suggested to be involved in neuropsychiatric disorders. Mutations in the small-conductance Ca^{2+}-activated K^+ channels type 3 (KCNN3) gene has been reported in subjects with schizophrenia. This channel functions to regulate neuronal excitability in the CNS. Case-control studies revealed expanded polyglutamine (CAG) repeats in the second CAG triplet of the KCNN3 gene in individuals with schizophrenia from two separate human populations (Tsai et al. 1999; Dror et al. 1999). The dysfunction of KCNN3 channels could therefore modify the ability of a cell to regulate the slow component of afterhyperpolarisations (AHPs). Finally, Ca^{2+}-activated BK channels may also be involved in schizophrenia as antipsychotics used to treat the disorder have been reported to alter the Ca^{2+}-activated conductance in neurons (Zhang et al. 2006).

1.2.9 PV interneurons in schizophrenia

GABAergic circuits have been shown to possess a variety of abnormalities in adults with schizophrenia (Fig 1.4). One of the most consistent observations found from independently performed studies is that only certain interneuron subtypes seem to be affected. A marked reduction in the levels of GAD67 and PV mRNA exclusively in PV cells have been reported in layers III-V of the prefrontal cortex from post-mortem schizophrenic brains (Akbarian et al. 1995; Hashimoto et al. 2003). In addition, GAD67 mRNA levels are left unaltered in other interneurons between subjects with schizophrenia and healthy controls (Hashimoto et al. 2003), suggesting that the pathology is restricted to the PV cell population. Levels of the GAD67 protein itself has also been reported to be lower in PV cells, indicating a downstream reduction in the functional enzyme required for GABA synthesis within this cell type (Guidotti et al. 2000; Curley et al. 2011). In patients with schizophrenia, the expression of the $\alpha 1$ subunit of the $GABA_A$ receptor (see section **1.3.4**) is reduced in cortical pyramidal cells at postsynaptic sites made by PV basket cells (Glausier & Lewis 2011). This could indicate fewer inputs from basket cell axons onto pyramidal cells, further supported by a decline in the density of PV-immunoreactive boutons (putative basket cell axon terminals) in layers III-IV of the prefrontal cortex in schizophrenia (Lewis et al. 2001). Another study demonstrated that genetic knockdown of GAD67 in PV

cells during development leads to a decline in PV basket cell axonal arborisation and synapse formation (Chattopadhyaya et al. 2007). Thus, diminished levels of GAD67 mRNA in PV cells in schizophrenia, if prompted early in life, could give rise to fewer PV basket cell synapses, and therefore a reduction in synapses requiring the α1 subunit in postsynaptic cells (Fig 1.4).

Furthermore, the expression of α2 is upregulated in pyramidal cells at postsynaptic inputs from chandelier cells (Volk et al. 2002), while the expression of GAT-1 is downregulated in chandelier cell terminals (Pierri et al. 1999). It is possible that these are compensatory mechanisms carried out by chandelier cells in the attempt to rectify weakening perisomatic inhibitory signalling from basket cells. Increasing the content of $GABA_A$ receptors with α2 subunit may amplify the effect of GABA on these synapses, while simultaneously reducing GAT-1 expression slows down GABA re-uptake and increases the time during which the transmitter is present in the synaptic cleft to maximise its effect (Fig 1.4).

The observation that NMDA receptor antagonists reproduce behaviours reminiscent of schizophrenia in mice led to the assumption that NMDA receptor hypofunction may implement an essential role in the disease (Rotaru et al. 2012). Genetically modified mice with reduced NMDA receptor expression are reported to have cognitive, negative and positive symptoms linked to the disorder in humans (Mohn et al. 1999). Moreover, administration of NMDA receptor antagonists produces elevated cortical activity (Breier et al. 1997), indicating that NMDA receptor hypofunction may principally occur in interneurons. There is also evidence that NMDA antagonists reduce the activity of GABAergic interneurons in the prefrontal cortex of rats (Homayoun & Moghaddam 2007). Because PV expression is reduced in the brains of individuals with schizophrenia, and PV cells are believed to be critical for the generation of gamma oscillatory activity, it has been hypothesised that NMDA receptor hypofunction specifically in PV cells is a core feature of the disease. Indeed, NDMA receptor antagonists have been reported to downregulate PV expression (Behrens et al. 2007; Kinney et al. 2006).

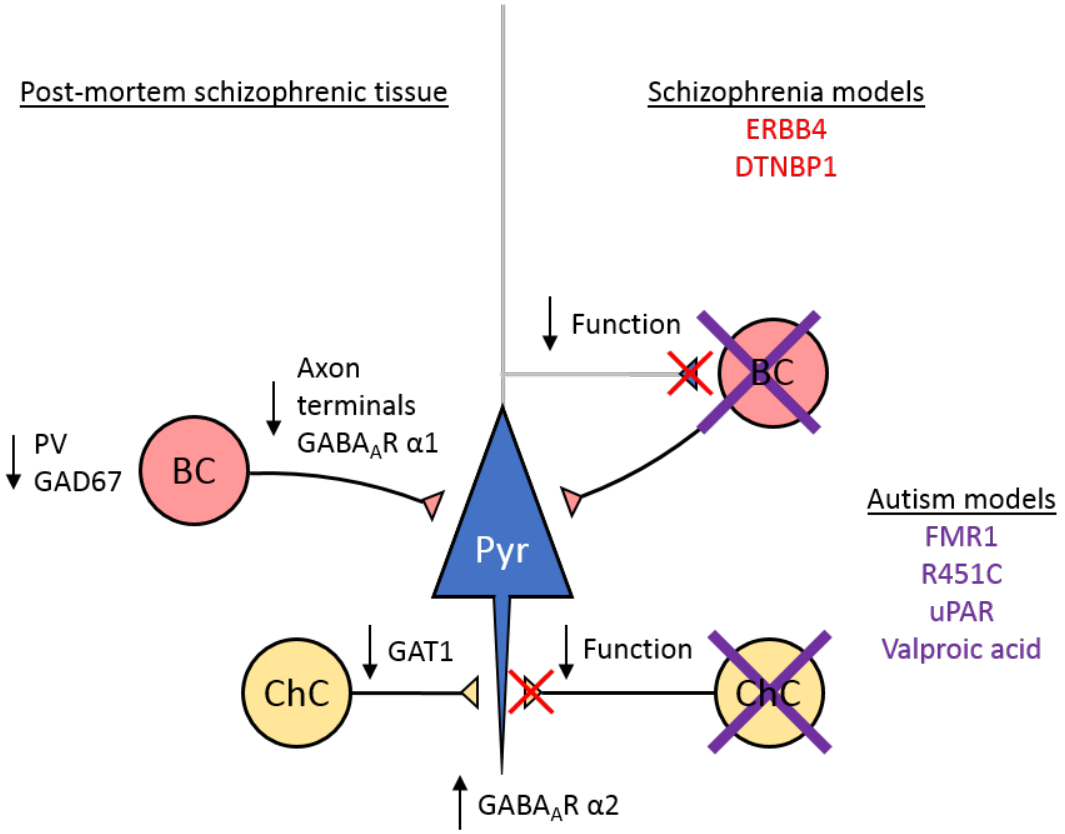

Figure 1.4 Summary of alterations in cortical circuitry in patients with schizophrenia and in animal models of schizophrenia and autism Left, GABAergic network pathology in layer III DLPFC observed from post-mortem tissue of patients with schizophrenia. Abnormalities include reduced expression of GAD67 and PV mRNAs in PV cells, reduced expression of postsynaptic GABA α1 receptor subunits which may correspond to a reduction in the number of basket cell (BC) inputs onto pyramidal cells. Other alterations that could be interpreted as possible compensatory mechanisms include a reduction in GAT1 protein in the presynaptic terminals of chandelier cells (ChC) paralleled by an increase in GABA α2 receptor subunit expression in the AIS of postsynaptic pyramidal cells (Pyr). Both disorders display significant reductions in mRNA expression of the GABA-synthesising enzyme, GAD67. Right, structural and functional network pathology observed from animal models of schizophrenia (red) and autism (purple). Mutant ERBB4 and DTNBP1 mice exhibit behavioural symptoms associated with schizophrenia show a reduction in mIPSC frequency in pyramidal cells and a decline in the number of axo-axonal synapses from chandelier cells onto pyramidal cells as well as a reduction in the formation of glutamatergic synapses onto PV cells (red crosses). Genetic mouse models for autism (FMR1, R451C, uPAR) and environmental insult (valproic acid) consistently show severe reductions in the number of PV cells (purple crosses).

It should be considered however that there is also evidence to argue against NMDA receptor hypofunction in adult PV cells as a causal factor in schizophrenia. In the healthy forebrain, NMDA receptor expression in PV cells compared to NMDA receptor expression in pyramidal cells and other interneurons is already low in the first place (Wang & Gao 2009), and NMDA receptors in PV cells might actually be less prone to activation than those on pyramidal cells (Hull et al. 2009). Similarly, PV cell-mediated disynaptic inhibition onto pyramidal cells in the somatosensory cortex – which is critical for regulating the coincidence detection window in principal neurons – is NMDA receptor-independent (Wang & Gao 2009). This suggests that dysfunctional NMDA receptors in PV cells might not necessarily underlie the cause for schizophrenia, as other cell types that depend more heavily on NMDA receptors would be more susceptible to NMDA receptor-mediated impairments. Nonetheless, since NMDA receptor expression is higher during development than in adulthood (Wang & Gao 2009), it is still possible that NMDA receptor hypofunction in PV cells during development, rather than in adulthood, could be responsible, in part, in the progression of the disease. The selective ablation of NMDA receptors in a fraction of interneurons including PV cells in the mouse forebrain was shown to induce deficits attributable to schizophrenia in humans only if the ablation is carried out during early postnatal development but not in adulthood (Belforte et al. 2010). Hence, deficient NMDA receptor function during development may lead to impaired PV cell activity and consequently result in the reduction in GAD67 and PV expression.

Deficits in the maturation of PV cells have been linked to susceptibility genes in the development of schizophrenia. Neuregulin 1 (NRG1) and its receptor tyrosine kinase, ErbB4, are associated with an increased risk of schizophrenia as well as abnormities in interneuron development (Stefánsson et al. 2003). NRG1 is important in a variety of roles during neuronal development, including regulation of neuronal migration, synaptogenesis and neurotransmission (Harrison & Law 2006). Recent studies have found that ErbB4 is expressed exclusively in interneurons, particularly in PV cells, where the NRG1 protein stimulates GABA release, inhibiting pyramidal cells in the prefrontal cortex (Wen et al. 2010). NRG1/ErbB4 signalling cell-

autonomously promotes the formation of axo-axonal synapses from chandelier cells onto pyramidal cells as well as the formation of glutamatergic synapses onto PV cells (Fazzari et al. 2010). Moreover, the conditional deletion of ERBB4 in PV cells resulted in a reduction in the frequency of miniature inhibitory currents (mIPSC) in pyramidal cells which was paralleled by a reduction in the number of inhibitory synapses onto pyramidal cells (Fig 1.4) (Fazzari et al. 2010). It can therefore be presumed that disruption of NRG1 function can have a considerable effect on the balance between excitatory and inhibitory input in the network. More evidence suggests that ErbB4 exerts its effects on PV cells: the ablation of ErbB4 receptors specifically in PV cells in mice exhibit schizophrenia-like phenotypes similar to those observed in NRG1 or ErbB4 null mutants (Wen et al. 2010). Another susceptibility gene, DISC1, which displays behavioural abnormalities when mutated in mice, has also been linked to the development of PV cells. Dominant-negative DISC1 mice were shown to have a reduced density of PV cells in the prefrontal cortex (Hikida et al. 2007). Furthermore, the genetic knockout of dysbindin (DTNBP1) – a possible binding partner of DISC1 – revealed similar deficits in PV cell function to those found in conditional ERBB4 mutant mice (Fig 1.4) (Ji et al. 2009).

In addition to perturbed maturation of PV cells, there is also evidence to suggest that molecular pathways associated with schizophrenia regulate the migration of interneurons during development. NRG1/ErbB4 signalling has been shown to support the migration of immature cortical GABAergic interneurons (Flames et al. 2004). Similarly, DISC1 is necessary for the tangential migration of MGE-derived cortical GABAergic interneurons, which is impaired following knockdown of the gene during early development (Steinecke et al. 2012). Abnormal interneuron migration is consistent with the increased density of interneurons found in the superficial white matter of the orbitofrontal cortex in schizophrenic brains (Joshi et al. 2012). Thus, the possibility that MGE-derived interneurons including PV cells becoming inadequately connected to cortical networks during development, in addition to receiving reduced excitatory inputs could all contribute to the development of schizophrenia.

1.2.10 PV interneurons in autism

Deficits in GABAergic signalling have also been described in autism (Gao & Penzes 2015). Many studies point to an imbalance between excitation and inhibition in autism, providing evidence for impairments in both excitatory and inhibitory synaptic transmission (Gao & Penzes 2015). Evidence for alterations in GABAergic circuits also originate from post-mortem examinations showing significantly reduced expression of GAD65 and GAD67 (Fatemi et al. 2002) together with reduced expression of $GABA_A$ and $GABA_B$ receptors (Fatemi et al. 2010) in the cortex and cerebellum of autistic patients. These alterations may branch from widespread transformations in GABA innervation and release, which may reduce the threshold for developing seizures, given the strong correlation of autism with network hyperexcitability and its high comorbidity with epilepsy (Brooks-Kayal 2010). In support of this hypothesis, a recent study showed a decline in the absolute number of PV cells in the prefrontal cortex of subject brains with autism (Zikopoulos & Barbas 2013). As PV cells provide robust perisomatic contacts onto pyramidal cells - which is fundamentally required in maintaining network balance - a decline in their number could explain the aberrant GABAergic signalling and predisposition for epilepsy in autism. Collectively, these matters demonstrate that heterogeneous changes in glutamatergic and GABAergic circuitry in the autistic brain can converge upon an overall increase in the ratio between excitation and inhibition.

Alterations of PV cells is one of the most noticeable features in animal models of autism (Fig 1.4). Prenatal exposure to valproic acid - an animal model of autism - resulted in a large reduction in the number of PV cells in the neocortex of mice (Gogolla et al. 2009). Similarly, mice designed to carry a mutation of the urokinse plasminogen activator receptor (uPAR) gene, which has been found to be mutated in the cerebral cortex of post-mortem brains with autism (Campbell et al. 2008), showed a 50% decline in neocortical GABAergic interneurons including a near-complete loss of PV cells (Powell et al. 2003). These mice also exhibited spontaneous seizures and behaviours associated with autism (Powell et al. 2003).

It is possible that these effects result from pathophysiological mechanisms upstream of GABAergic signalling, however, there is evidence that indicates causal roles of GABAergic mechanisms in nonsyndromic autism. For example, mutations in genes coding for cell adhesion molecules of the neurexin-neuroligin families which are expressed at glutamatergic and GABAergic synapses are often found in autism (Chih et al. 2005). Mice with a point mutation in neuroligin 3 (R451C) developed impaired social behaviours (Tabuchi et al. 2007), while over half of PV cell numbers were abolished (Gogolla et al. 2009). Finally, genes associated with syndromic autism have been linked to alterations in PV cells. Mice lacking the Fragile X mental retardation 1 (FMR1) gene exhibited autistic-like behaviours (Spencer et al. 2005), and displayed significant reductions in PV cell density in addition to alterations in their lamina distribution in the somatosensory cortex, whereas other interneurons were unaffected (Selby et al. 2007).

1.2.11 Specific targeting of PV interneurons as a treatment for neurological and neuropsychiatric diseases

The full sequence of developmental processes that are disrupted in both schizophrenia and autism is far from being completely understood. However, it is clear from growing evidence that disruptions in the GABAergic circuitry particularly in PV cells play a fundamental role in these disorders. PV cells are essential in establishing the opening and closing of critical periods in multiple brain regions (Fagiolini et al. 2004; Le Magueresse & Monyer 2013), which in humans takes place during early postnatal development - when the initial symptoms of autism are also detected (Le Magueresse & Monyer 2013). One could assume that deficits in PV cell function impairs plasticity, leading to improperly developed cortical wiring during a very confined period of early postnatal maturation. The abnormal function of PV cells may also manifest at later stages of postnatal development affecting their ability to drive gamma oscillations, consistent with altered gamma oscillations found in the cortex of subjects with schizophrenia.

Throughout development and into adulthood, PV cells are crucial in mediating rapid feedforward and feedback inhibition, temporal sculpting of information transfer in neuronal networks, maintaining the balance between excitation and inhibition, as well as contributing to fast network oscillations. GABA-mediated plasticity of cortical networks throughout the developmental period could therefore be used to develop new therapies aimed at selectively targeting specific cell types in the attempt to rectify part of the network dysfunctions. Many mutations that provoke and lead to neurodevelopmental disorders disrupt genes that are also expressed in adult brain. Therefore, in addition to structural and functional effects on the developing brain, it is conceivable that modified gene function in adulthood may be partly responsible for associated cognitive phenotypes. With this in mind, several studies using animal models of neurodevelopmental disorders demonstrated that reversing the disrupted molecular deficits can restore proper cognitive function even if treatments are started in adulthood. (Ehninger et al. 2008). These studies validate the idea that treatment specifically in adults may successfully amend some of the disrupted molecular and cellular mechanisms resulting in noticeable improvements in cognitive function.

New pharmacological strategies could be implemented either during development, before cortical circuits lose their developmental plasticity, or even in adult patients suffering from neurological disorders. Thus, in patients with schizophrenia and autism where there are deficits in the function of PV cells, it could be beneficial to develop a drug that selectively targets PV cells to increase their activity. This could then be administered to patients during development or in adulthood, with the goal of either correcting part of the aberrant wiring from an early postnatal stage, or to alleviate part of the symptoms later in the adult brain.

1.3 Modulation of PV interneurons

Given the deficits in PV cells associated with neurodevelopmental disorders, the ability to selectively modulate PV cells and increase their excitability in the network

could be extremely useful in patients. There are undoubtedly many approaches that could be explored in order to restore normal PV cell function at the cellular level as well as within the network circuitry which is heavily reliant on the proper function of PV cell inputs. Studies looking into the pathophysiological mechanisms of schizophrenia and autism indicate a number of distinct malfunctions present in PV cells: reductions in GAD67 and PV mRNA thought to be essential for their proper function may result in reduced activity; a decline in the number of synapses between PV cells and pyramidal cells potentially gives rise to poor synaptic transmission; and reductions in the number of PV cells themselves, which again reduces the overall synaptic contacts between PV cell and pyramidal cells (Fig 1.4). An attempt to increase the number of PV cells or PV cell synapses in patients would be extremely difficult as the former would require the manipulation of complex machinery to induce cell proliferation, while the specific targeting of distal processes to induce synaptogenesis would be exceptionally challenging due to the number of intricate mechanisms that would need to be considered. Accordingly, an easier approach would be to target PV cells in their entirety and exploit their electrophysiological properties to increase their excitability. A drug could be applied to target key attributes unique in PV cells to make them more excitable and fire with a higher probability, without directly altering other cell populations. Increasing the excitability of PV cells could also compensate for the reduction in cell number and synaptic inputs.

1.3.1 Intrinsic properties of PV interneurons

In order to manipulate PV cells and increase their excitability, it is necessary to understand the functional features that make them so fast and efficient in the first place. PV basket cells have developed numerous molecular and cellular properties to ensure that they generate fast, strong, reliable, and temporally precise inhibition onto their target cells. The speed and precision of PV cell firing relies upon a combination of biophysical and molecular specialisations covering the entire cell; from excitatory synapses PV cells receive in their dendrites, to distinctive attributes that span their

axon and presynaptic terminals. These intrinsic features are highlighted in three main categories below (and summarised in table 1.3):

1.3.2 Specialisations promoting fast excitation of PV cells

The first key feature of PV cells incorporates characteristics favouring fast excitability. Large amplitude AMPA receptor-mediated postsynaptic conductances with fast time courses ensure rapid and reliable excitation of PV cells, whilst narrowing EPSP summation to near-synchronous inputs, enabling fast coincidence detection sensitive to spatially distributed inputs (Hull et al. 2009; Hu et al. 2010). PV cells express specialised AMPA receptors containing GluA1 or GluA4 subunits that have fast deactivation kinetics, which contribute to the rapid time course of excitatory inputs (Geiger et al. 1997). PV cells functionally express AMPA receptors composed of GluA2-lacking subunits allowing for high Ca^{2+} permeability and fast gating, resulting in larger and faster excitatory inputs compared to other neurons (Geiger et al. 1995). It has been demonstrated that thalamic excitation of putative PV cells displaying fast-spiking phenotypes produces AMPA-mediated EPSCs with a fourfold larger underlying quantal amplitude compared with inputs onto non-PV regular-spiking cells (Hull et al. 2009). Since GluA2-lacking AMPA receptors are known to have single channel conductances that are several-fold larger than GluA2-containing AMPA receptors (Swanson et al. 1997), the presence of these receptors may provide an explanation for the large quantal amplitude, although alterations in the number of postsynaptic receptors between PV cells and other neurons may also play a role.

An important characteristic designed to speed up the time course of EPSPs is the phenomenon that PV cells possess a low membrane resistance (Doischer et al. 2008). This is driven by a developmentally regulated expression of leak K^+ channels mediated by $K_{ir}2$ subfamily inward rectifier K^+ channels and TASK subfamily two-pore K^+ channels, the latter reaching mature levels by the end of the third postnatal week (Goldberg et al. 2011; Okaty et al. 2009). This accelerates the membrane time

constant and therefore sharpens EPSPs, which in turn narrows the time window for integration of inputs (described in further detail in the next paragraph). Consequently, TASK-1/3 double knockout mice were found to have an approximately twofold increase in membrane resistance, approaching values similar to that observed in pyramidal cells, as well as a similar increase in the membrane time constant (Goldberg et al. 2011). The input resistance is further reduced by the presence of gap-junctional coupling between PV cells (Galarreta & Hestrin 1999). PV cells in connexin 36 knockout mice were reported to have a 25% reduction in resting leak conductance in layer IV of the barrel cortex (Deans et al. 2001). Similarly, mefloquine, which blocks connexion 36 channels, increases PV cell input resistance by 15% in the same cortical region in rats (Cruikshank et al. 2004). Another observation routinely demonstrated in acute brain slices recordings is the high frequency of spontaneous synaptic activity onto PV cells, which may reduce the input resistance at rest via a shunting mechanism. Studies have demonstrated that blocking glutamatergic neurotransmission results in an input resistance increase of over 40%, suggesting that continuous synaptic activity contributes to the conductance at rest (Cruikshank et al. 2004). Furthermore, somatodendritic recordings reveal that cable properties across the axis of PV basket cells are nonuniform, where the membrane resistance is lowest in the soma and proximal dendrites, intermediate in the distal dendrites, and highest in the axon (Nörenberg et al. 2010). Computational analysis demonstrate that these unique properties accelerate the time course of EPSPs at the soma in response to fast inputs, while enhancing the efficacy of slow distal inputs (Nörenberg et al. 2010).

Specialisations in the active dendritic properties in PV cells facilitate the generation of fast, temporally independent EPSPs (Hu et al. 2010). This is thought to be important in the detection of temporally coincident inputs, whilst promoting fast, reliable and temporally precise conversion of EPSPs to action potentials. Basket cell dendrites possess low densities of voltage-gated Na^+ channels but are enriched with specialised voltage-gated K^+ channels belonging to the Kv3 subfamily – particularly Kv3.1 and Kv3.2 - which accelerates EPSP kinetics (Hu et al. 2010). This shortens the time period for temporal summation allowing basket cells to detect the

synchronous activity of converging, spatially distributed excitatory inputs. During EPSP action potential conversion, the high expression of dendritic K^+ channels ensures precise 1:1 coupling between EPSP and action potential, repressing the generation of action potential bursts by large excitatory inputs. Furthermore, these channels maintain a constant action potential initiation threshold during repetitive stimulation. These characteristics are likely to be important *in vivo* during network activity including sequential activation of feedforward and feedback inputs on basket cells. K^+ channels therefore shape the electrical properties of PV cells at the level of input as well as during EPSP action potential conversion.

1.3.3 Specialisations promoting high frequency firing of action potentials in PV cells

The second key group of features are conveyed in specialised intrinsic properties that enable PV cells to generate spikes with short latency, and the capability to discharge brief action potentials repetitively at high frequencies with minimal adaptation during sustained stimulation (Erisir et al. 1999). The diverse action potential waveforms of cortical neurons are regulated by the interplay between voltage-gated Na^+ and K^+ channels in addition to morphological properties as well as channel distribution along the somatodendritic axis (Mainen & Sejnowski 1996). Previous studies have suggested that differences in firing patterns are largely determined by the expression of distinct K^+ channels. In this manner, PV cells in the cortex and hippocampus have been shown to express K^+ channels that activate and deactivate with remarkable speed, but inactivate very slowly (Du et al. 1996). These properties allow for rapid fluctuations in the membrane potential in PV cells necessary for their fast-spiking phenotype.

High levels of Kv3 channels, which activate at more depolarised potentials than most other voltage-gated K^+ channels in other cells, but with fast deactivation rates, ensure rapid repolarisation of the membrane without compromising spike initiation or height (Rudy & McBain 2001). Kv3 channels reinforce the generation of deep and fast

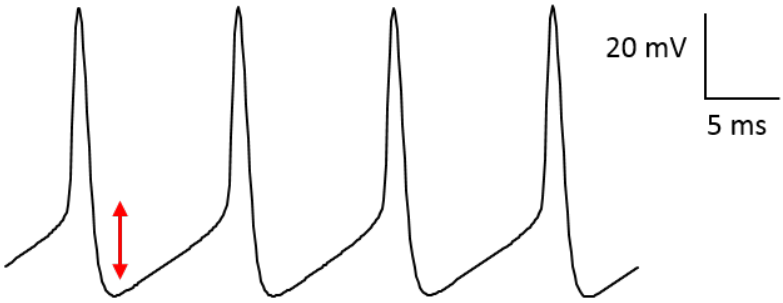

Figure 1.5 Specialised voltage-gated channels allow for high frequency firing of action potentials in PV cells High expression of Kv3.1 and Kv3.2 channels with fast deactivation kinetics generate short half-width action potentials with deep AHPs (indicated by red arrow) enabling rapid repolarisation of the membrane. This facilitates the recovery of voltage-gated Na^+ channels from inactivation, ensuring the initiation of the next action potential in quick succession.

AHPs which facilitates the recovery of voltage-gated Na^+ channels from inactivation (Fig 1.5) (Rudy et al. 1999). The large AHP produced by the activation of Kv3 channels also functions to rapidly terminate the outward K^+ current, which, due to their fast deactivation rate does not extend the refractory period, thereby keeping the inter-spike interval short (Rudy et al. 1999). Kv3 channels also shorten the half-width of action potentials (Du et al. 1996), which reduces the amount of Na^+ channel inactivation that occurs, yielding a population of Na^+ channels that are primed and ready to go for the next action potential. Low concentrations of tetraethylammonium (TEA) and 4-aminopyridine (4-AP), which block Kv3 channels results in the near-abolishment of the fast AHP, the reduction in the maximum rate of spike repolarisation, increased spike broadening, and the decline in maximal firing frequency (Erisir et al. 1999; Du et al. 1996). It should be noted that other known K^+ channels including Kv1, KCNQ2 and BK Ca^{2+}-activating channels are also blocked with low concentrations of TEA, however the application of various toxins known to block these other channels were shown to have little effect on the action potential waveform (Erisir et al. 1999). These electrophysiological properties are therefore essential for sustained high frequency firing of action potentials as large and rapid

repolarisations of the membrane ensures that it is ready for the next depolarisation to take place.

High frequency action potentials are further maintained in PV cells through the expression of specialised voltage-gated Na^+ channels comprising slower inactivation and faster recovery (Martina & Jonas 1997). A decrease in the overlap between inactivation and activation in PV cells may prevent an increase in the slow depolarising potential during repetitive firing seen in principal neurons, which in a subset of cells may lead to their intrinsic bursting phenotype. The recovery of Na^+ channels from inactivation is quicker in PV cells compared to principal neurons, thus enabling a constant supply of Na^+ channel availability during spike trains, thereby preventing spike frequency adaptation and spike threshold accommodation (Martina & Jonas 1997). Na^+ channels may therefore enable the generation of spike trains that retain the precise temporal structure of synaptic input. Their fast recovery could also allow PV cells to fire doublets that may synchronise neuronal ensembles that are spatially distributed (Traub et al. 1996).

Subthreshold-operating Kv1 channels specifically localised in the AIS exert a considerable influence on the excitability of PV basket cells by regulating near-threshold responsiveness (Goldberg et al. 2008). The low activation threshold and slower gating of these channels suppresses the generation of spikes to long current pulses. In contrast, large EPSPs fast enough to bypass Kv1 channel activation successfully result in action potential initiation with short delay (Goldberg et al. 2008). Thus, Kv1 channels filter slowly rising depolarisation events, making them fire in response to large-amplitude or synchronous inputs, with rapid kinetics. GABAergic interneurons have previously been subdivided into delay-type, where cells fire after a delay of variable duration; continuous fast-spiking; and stuttering types, based predominantly on firing patterns in slice recordings (Ascoli et al. 2008; Gupta et al. 2007). Interestingly, Kv1 channel blockade eliminates the characteristic delay to first spike observed with near-threshold current injections, converting PV cells with delay-type firing patterns to continuous fast spiking patterns suggesting

that these channels are responsible for the delayed spiking phenotype in a subset of PV cells.

1.3.4 Specialisations promoting fast spike propagation and synchronous transmitter release in PV cells

The third key feature that ensures PV cells are built for speed and precision incorporate specialisations that enable fast and reliable spike propagation in their axon and terminals. PV basket cell axons contain unusually high densities of voltage-gated Na^+ and K^+ channels in their axon, which allow for the transmission of high-frequency action potentials with increased conduction velocity and with minimal delay (Hu & Jonas 2014). Their high expression of Na^+ channels and prominent expression of Kv3 channels compensate for unfavourable morphological properties of PV axons - small diameter, extensive branching, high density of boutons (Hu et al. 2014). Na^+ channels in PV cell axons preferentially contain $Na_v1.1$ and $Na_v1.6$ subunits, although the contribution of other subunits is also present (Ogiwara et al. 2007; Lorincz & Nusser 2008). Loss-of-function mutations in the SCN1A gene encoding $Na_v1.1$ in mice – which is found exclusively in GABAergic interneurons - results in the development of epileptic seizures within the first postnatal month (Ogiwara et al. 2007), further supporting the importance of Na^+ channels in PV cell function.

PV basket cells have been shown to exhibit a distinct distribution of Na^+ channels: their density increases from the soma to the proximal axon in a stepwise fashion, followed by a further gradual increase into the distal axon, where the Na^+ conductance density has been reported to be around 600 pS μm^{-2} (Hu & Jonas 2014). Thus, PV cells confer a weakly excitable somatodendritic domain and a highly excitable axonal domain connected by a steep transition zone. It has been speculated that approximately 99% of all Na^+ channels are located in the PV cell axon (Hu et al. 2014). Hence, the means of excitability in PV cells is essentially axonal, which again highlights the rationale of expressing such a high density of Na^+ channels in the

axonal membrane. Although experiments and simulations indicate that the density of Na^+ channel expression is greater than the critical value required for action potential propagation reliability (calculated to be around 200 pS μm^{-2}), it has been suggested that this 'supercritical' value ultimately increases action potential propagation speed and maximum frequency (Hu & Jonas 2014).

In addition to expression in other regions, Kv3 channels have also been shown to be expressed in PV cell terminals, suggesting additional roles that these rapidly activating/deactivating channels play in neurotransmitter release. As well as keeping action potentials brief, synaptically localised Kv3 channels limit Ca^{2+} influx into the presynaptic terminal and decrease the release probability (Goldberg et al. 2005). Blocking Kv3 channels with low concentrations of TEA enhanced PV-cell spike-evoked GABA release onto neocortical pyramidal cells nearly twofold, and reduced the paired pulse ratio (PPR) (Goldberg et al. 2005). Furthermore, the large effects of TEA were absent in Kv3 knockout mice, spike-evoked GABA release was larger, and the PPR was reduced compared to wildtype mice (Goldberg et al. 2005). Thus, it is likely that Kv3 channels in PV cells keep action potentials brief, thus limiting Ca^{2+} influx and hence release probability, resulting in fast and synchronous transmitter release (Hu & Jonas 2014).

PV cells have special adaptations facilitating fast, reliable, efficient and temporally precise transmitter release. Whereas several types of synapses use combinations of P/Q-, N-, and R-type Ca^{2+} channels for transmitter release, PV cells rely exclusively on P/Q-type Ca^{2+} channels (Zaitsev & Povysheva 2007), which comprise faster kinetics (Li et al. 2007), and maintain tight nanodomain coupling between Ca^{2+} influx and transmitter release (Bucurenciu et al. 2008). The fast gating of P/Q-type channels results in minimal synaptic delay and enhanced temporal precision of transmitter release while their tight coupling with release sensors of exocytosis additionally boosts the efficacy of release. Furthermore, only a small number of Ca^{2+} channels are required for GABA release (Bucurenciu et al. 2010), which may help prevent the broadening of presynaptic action potentials, resulting in fast and

temporally precise transmitter release. Moreover, a subset of cortical and hippocampal PV cells employ synaptotagmin 2 as a release sensor instead of synaptotagmin 1, which is predominantly used in principal neurons (Sommeijer & Levelt 2012; Kerr et al. 2008). Synaptotagmin 2 displays the fastest Ca^{2+}-binding kinetics across the synaptotagmin family which further highlights specialised mechanisms that result in rapid PV cell signalling (Xu et al. 2007).

Finally, in addition to functional specialisations that exist within PV basket cells, the GABAergic synapses that they create with principal cells and other PV basket cells are also important in maintaining rapid signalling as well as network synchrony. Synapses made from PV basket cells onto the somata of pyramidal cells have been shown to have a much higher density $GABA_A$ receptors containing the α1 subunit compared to synapses from non-PV cells (Klausberger et al. 2002). Furthermore, synapses interconnecting PV basket cells also contain high densities of α1 subunit-containing receptors (Klausberger et al. 2002). These synapses exhibit faster IPSC decay kinetics which not only contributes to fast and precise signalling at the cellular level, but also in the regulation of fast postsynaptic conductance changes required for the generation of oscillatory activity in the network (Bartos et al. 2002; Galarreta & Hestrin 2002).

1.3.5 Targeting PV cells to increase their excitability

The proper function of PV cells in the healthy brain clearly relies upon a multitude of properties enabling the execution of fast, efficient, and temporally precise GABAergic transmission (Table 1.1), as previously discussed. These comprise functional specialisations along the entire somatodendritic axis including both input and output synapses that serve to maximise the speed of PV cell signalling. With the aim of increasing their excitability, a suitable target is therefore required to induce a functional change in PV cells to enable them to fire with higher probability. Given the intrinsic properties that enable PV cells to fire so quickly in the first place (Table 1.1), there would be little reason to specifically target them as they are already

Property	Functional consequence	Molecular mechanism
Fast and brief EPSCs	Rapid EPSP time course; coincidence detection	GluA1 and GluA4 AMPA receptor subunits, TASK-like channels (low input resistance)
Fast IPSCs	Rapid EPSP time course; High-frequency network oscillations	$GABA_A$ receptor with α1-containing subunits
High density of Na^+ channels in axon (fast recovery from inactivation)	Rapid and reliable action potential propagation; fast-spiking action potential phenotype	$Na_v1.1$ $Na_v1.6$
Perisomatic K^+ channels (fast deactivation, high activation threshold)	Brief action potentials; fast-spiking action potential phenotype	Kv3.1 and Kv3.2
Dendritic K^+ channels (fast deactivation, high activation threshold)	Sublinear summation; sensitivity to distributed inputs	Kv3.1 and Kv3.2
K^+ channels in AIS (low activation threshold, slow gating)	Filters out slow events suppressing firing	Kv1
Fast presynaptic Ca^{2+} channels	Speed and temporal precision of GABA release	P/Q-type
Tight coupling between presynaptic Ca^{2+} channels and release sensors	Speed and temporal precision of GABA release	Not known
Fast release sensors	Speed and temporal precision of GABA release	Synaptotagmin 2

Table 1.1 Summary of fast signalling properties of PV cells Table adapted from Hu et al. 2014.

functioning at full capacity. For example, it would be impractical to increase the output of voltage-gated Na^+ or K^+ channels in PV cells. Firstly, both channel populations already inactivate very slowly during sustained stimulation. Secondly, Na^+ channels are already designed to rapidly recover from inactivation, and K^+ channels have fast deactivation kinetics. Finally, a 'supercritical' density of Na^+ channels in the axon ensures rapid and reliable action potential propagation. Hence, increasing the number or function of these channels would not be an effective method of increasing the overall excitability of PV cells as they are already operating at a high capability.

Teasing out properties that could impede the overall excitability of PV cells would instead be a better approach to increase the basal firing of PV cells and boost their excitability. Given that PV cells express leak K^+ channels mediated by $K_{ir}2$ subfamily inward rectifier K^+ channels and TASK subfamily two-pore K^+ channels (Goldberg et al. 2011; Okaty et al. 2009), one possible method of selectively increasing the excitability of PV cells focuses on targeting part of the leak K^+ conductance. This prominent background conductance, present in both excitable and non-excitable cells – although most non-PV cells will express other two-pore K^+ channels instead of the TASK subfamily - is a major factor in the maintenance of the negative resting membrane potential (RMP) of all neurons in the brain. The magnitude of the RMP is determined by the equilibrium potentials for all permeant ions and their relative conductances through the membrane. In most neurons, K^+ governs the background conductance which drives the RMP towards the K^+ equilibrium potential (E_K), while the influences of other permeant ions (such as Cl^-, Na^+ and Ca^{2+}) move the RMP away from E_K. Thus, due to the electrochemical gradient of K^+ across the membrane, the blockade of a leak K^+ channels will prevent the efflux of K^+, thereby resulting in membrane depolarisation. The blockade of leak K^+ channels could therefore be a useful method of increasing the excitability of PV cells. Blocking part of the K^+ leak conductance would result in the depolarisation of the RMP, thereby increasing electrical activity and enhancing calcium entry to provoke transmitter release. Although leak K^+ channels belong to large family that are expressed in all cell types within the brain, the specific targeting of a subset of K^+

channels exclusive to PV cells should only result in membrane depolarisation in the PV cell population.

In addition to membrane depolarisation, blocking a subset of leak K^+ channels will also increase the membrane resistance of the cell. This could have a substantial effect on the integration of synaptic inputs because postsynaptic potentials will be amplified. An increase in input resistance not only increases the amplitude, but also the duration of EPSPs that the cell receives, thereby increasing the time window for temporal summation of inputs. Thus, blocking the leak K^+ conductance incorporates two mechanisms that boosts the excitability of the cell: First, the combined effect of passive membrane depolarisation (via the preventability of K^+ efflux) and larger amplitude EPSPs (due to higher input resistance) will bring the cell closer to firing threshold. Second, the increase in input resistance will increase the membrane time constant of the cell, widening the window for temporal summation, consequently increasing the likelihood of action potential generation in response to multiple inputs.

1.3.6 Two-pore-domain K^+ channel family

Mammalian K^+ channels form the largest and most diverse ion channel family in the genome, with almost 80 separate genes encoding the principal pore-forming subunits (Wei et al. 2005; Gutman et al. 2005; Kubo et al. 2005; Goldstein et al. 2005). These subunits can be divided into four major structural classes comprising either two or four transmembrane segments, which relate to inwardly rectifying (K_{ir}) and two-pore domain (K_{2P}) K^+ channels (Kubo et al. 2005; Goldstein et al. 2005), respectively; or six transmembrane segments, constituting voltage-gated (Kv) and Ca^{2+}-activated (K_{Ca}) K^+ channels (Gutman et al. 2005; Wei et al. 2005). All K^+ channels share a common conserved pore loop motif called the P domain, which establishes part of the K^+ conduction pathway, however the number of P domains vary between the distinct classes. K_{ir} channels, which contain a single P domain and are formed of tetramers of pore-forming subunits, operate at negative membrane potentials and

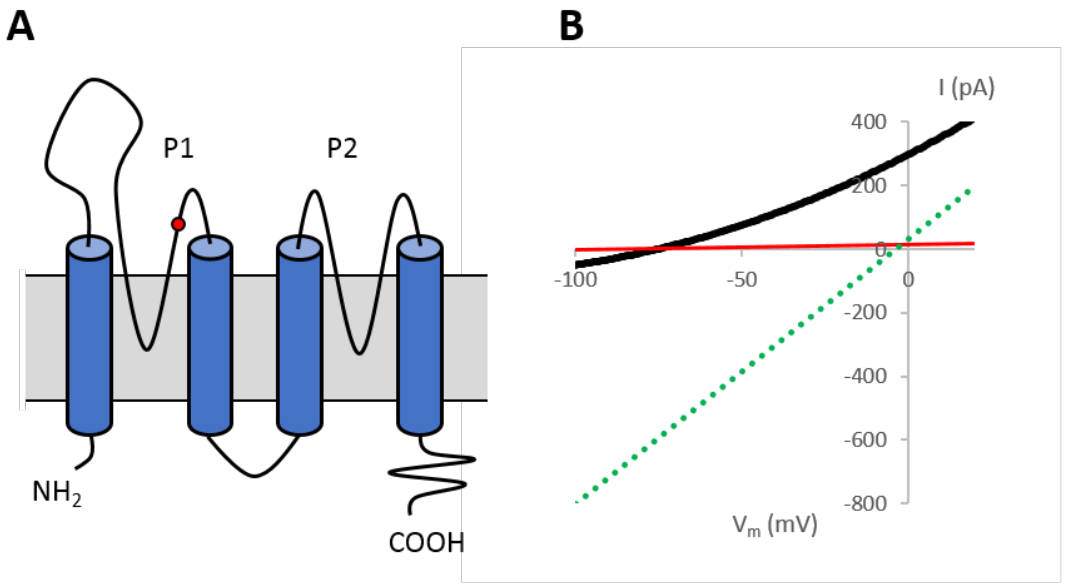

Figure 1.6 K_{2P} channels contribute to the leak K^+ background conductance (A) Schematic diagram of the presumed topology of a TASK-1 channel subunit, which shares a similar structure to all K_{2P} channel subunits. Each subunit has two P domains and four transmembrane segments and assembles into functional channels with other TASK-1 subunits, forming homodimers, or with TASK-3 subunits, forming heterodimers. Sensitivity to external acidification is conferred by a histidine residue at position 98 (red circle) that is situated near the selectivity filter of the channel pore. (B) Current-voltage (I-V) relationship of heterologous expression of TASK-1. In physiological conditions the TASK-1 current closely follows the Goldman-Hodgkin-Katz equation (black line), and is blocked in acidic external conditions (red line). A near linear IV relationship under symmetrical [K+] (green dashed line) suggests that they function as open rectifiers, a typical feature of background leak channels.

influence the RMP (Kubo et al. 2005). K_v and K_{Ca} channels, which similarly contain a single P domain and consist of tetramers, are predominantly activated at depolarised potentials, and mediate the repolarisation phase of the action potential (Gutman et al. 2005; Wei et al. 2005). By contrast, K_{2P} channels contain two P domains per one subunit stoichiometry forming functional channels as dimers (Fig 1.6 A) (Goldstein et al. 2005). Each P domain is therefore flanked by two transmembrane segments which assemble in the membrane as dimers forming a K^+-selective pore. The leak activity of these channels contributes to the setting of the RMP and therefore reduce excitability (Goldstein et al. 2005).

The K_{2P} channel family comprises fifteen distinct genes encoding pore-forming subunits (Goldstein et al. 2005), although their diversity is increased due to alternative splicing and translation initiation, heteromerisation and post-translational modifications that also take place (Feliciangeli et al. 2014). K_{2P} channel subunits are further divided into six main groups that display similar molecular architecture: TWIK (Tandem of pore domains in a weak inward rectifying K^+ channel); TREK (TWIK-related K^+ channel); TASK (TWIK-related acid-sensitive K^+ channel); TALK (TWIK-related alkaline-sensitive K^+ channel); THIK (Tandem pore domain halothane-inhibited K^+ channel); and TRESK (TWIK-related spinal cord K^+ channel) (Feliciangeli et al. 2014).

Theoretically, any K^+ channel active near the RMP contributes to the background K^+ conductance, and persistent activity of both voltage-gated (Kv) channels and inwardly rectifying (Kir) channels can indeed play a small part. Nonetheless, K_{2P} channels, appear to be uniquely positioned to maintain a leak K^+ conductance. In contrast to K_v channels, K_{2P} channels display weak voltage dependence, as they lack a voltage sensor and are not gated by the membrane potential (Duprat et al. 1997; Lesage et al. 1996). They can produce non-inactivating currents over a wide range of membrane potentials, and a subset of the K_{2P} family follows the Goldman-Hodgkin-Katz constant field equation – which maintains ionic flux across the cell membrane as a function of transmembrane potential and ionic concentrations inside and outside of the cell. TASK-1 currents fit this equation well (Fig 1.6 B) (Duprat et al. 1997), whereas others display slightly inward or outward rectifications, such as TWIK-1 (Lesage et al. 1996) and TREK-1 (Fink et al. 1996), respectively.

The pharmacology of K_{2P} channels are unique as they are relatively insensitive to classical K^+ channel blockers such as TEA, 4-AP and caesium (Lesage 2003); however, half of the fifteen known K_{2P} channels have been demonstrated to be Ba^{2+} sensitive (Goldstein et al. 2005). Furthermore, K_{2P} channels are responsive to a range of physical and chemical stimuli, including temperature, membrane stretch, acidosis, lipids and inhalational anaesthetics (Patel & Honoré 2001). Except for THIK and

TRESK, K_{2P} channels are regulated by extracellular pH: TASK and TALK channel subfamilies are strongly inhibited by extracellular acidification (Duprat et al. 1997; Kang & Kim 2004), in addition to two TREK subfamily channels, TREK-1 and TRAAK (Sandoz et al. 2009). TWIK-1 also exhibits a marked sensitivity to extracellular acidification although with a very different effect: instead of terminating ion flow at acidic pH, the channel reversibly switches selectivity to Na^+, demonstrating a unique dynamic ion selectivity mechanism (Chatelain et al. 2012). Sensitivity to pH is mediated by a positively charged histidine residue in the P1 domain of TASK-1 (Fig 1.6 A) (Morton et al. 2003) and TASK-3 (Yangmi Kim, Hyoweon Bang 2000) and by a basic residue in the 4th transmembrane segment projected towards the P2 domain of TALK channels (Niemeyer et al. 2007). The pH sensor in TREK-1 is mediated by a histidine residue in the extracellular loop preceding the first P domain (Sandoz et al. 2009).

1.3.7 The modulation of PV cells via TASK and TREK

With the aim of modulating PV cells to increase their excitability, it is necessary to distinguish specific leak K^+ channels that substantially contribute to the background conductance so that their blockade will produce a convincing effect. In the mouse cortex, PV cells undergo a dramatic developmental transition both molecularly and electrophysiologically during the second and third postnatal weeks (Goldberg et al. 2011). During this time period, the high frequency discharge pattern that defines PV cells emerge, driven by the expression of specialised $K_v3.1$ channels. This is paralleled by a reduction in PV cell input resistance, thought to be induced by the developmentally regulated expression of K_{2P} and K_{ir} channels (Goldberg et al. 2011). As numerous channels exist within these two families, the elucidation of a specific target is therefore required to generate a change that should significantly increase the input resistance and depolarise PV cells closer to firing threshold.

Recent studies looking at electrophysiological, pharmacological and molecular properties indicate that distinct subfamilies of leak K^+ channels are responsible for

K^+ leak conductances in PV cells. For a start, the application of Ba^{2+} (which blocks half of the K_{2P} channel family in addition to K_{ir} channels) has been demonstrated to block at least part of the linear leak current in PV cells putatively mediated by K_{2P} channels, in addition to the blockade of a strong inwardly rectifying current in PV cells, suggesting the presence of both K_{2P} and K_{ir} channel families in the background conductance (Goldberg et al. 2011). In spite of this, various Ba^{2+}-sensitive K_{2P} channels are known not to be responsible for the background conductance in cortical neurons and can therefore be excluded: THIK-1 has been reported to be blocked by Ba^{2+} in heterologous expression systems however appears not to be expressed in the neocortex (Rajan et al. 2001), and is therefore an unsuitable target. Similarly, TALK-1 and TALK-2 are sensitive to Ba^{2+}, but are essentially blocked at physiological pH, and are expressed specifically in the pancreas. While Ba^{2+}-sensitive TWIK-1 appears to be markedly expressed in PV cells during development (Fig 1.7), and is known to be expressed in the brain (Lesage et al. 1996; Goldberg et al. 2011), it is not known whether it is active in the membrane due to post-translational modifications of TWIK- 1 channels (Rajan et al. 2005). This process known as sumoylation is conserved from yeast to humans, and results in the covalent modification and inactivation of TWIK-1 channels by small ubiquitin-related modifier proteins (Rajan et al. 2005).

TASK and TREK channels however may represent a subfamily of K_{2P} channels that make a significant contribution to the K^+ leak conductance in PV cells. These channels, known to be expressed in various tissues including the brain (Goldstein et al. 2005), are sensitive to Ba^{2+}, and are strongly inhibited by extracellular pH as well as to the anaesthetic bupivacaine (Kindler et al. 1999; Leonoudakis et al. 1998). Moreover, TASK-1 expression has been shown to increase developmentally in cortical PV cells using microarrays (Okaty et al. 2009). Furthermore, qPCR data from fluorescence-activated cell sorting (FACS) of PV cells in mice reveal a high abundance of TASK-1 and TASK-3 mRNA expression in the neocortex, which increases between P10 and P18 (Fig 1.7) (Goldberg et al. 2011). Interestingly, this increase in expression correlates with a negative shift in the RMP as well as with a decrease in input resistance during the same time period (Goldberg et al. 2011),

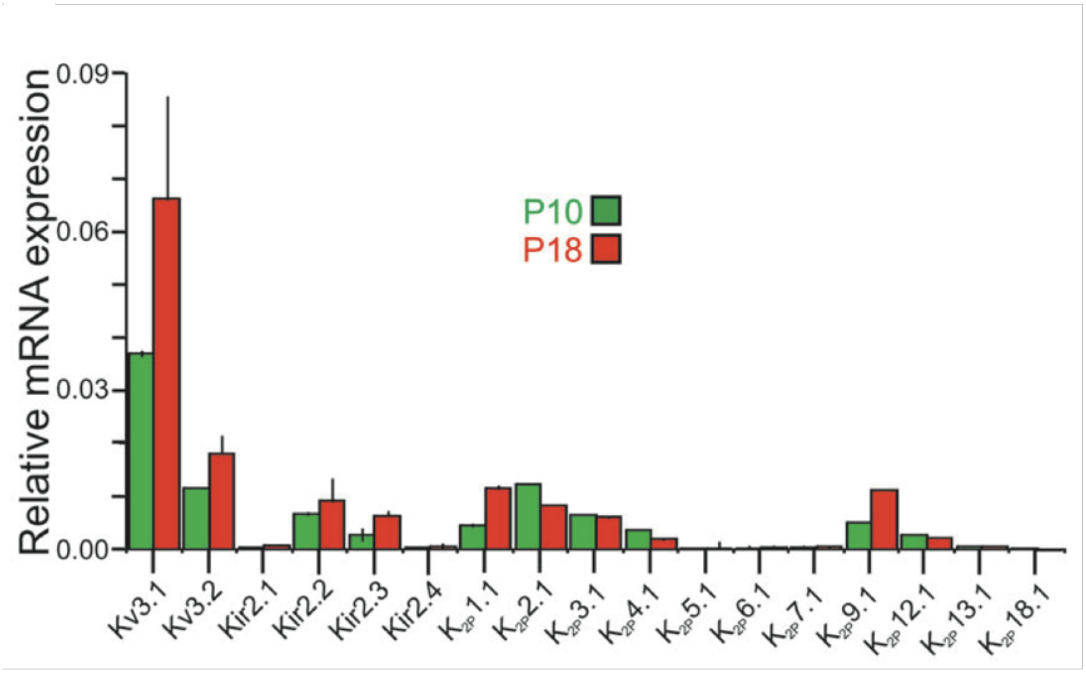

Figure 1.7 Relative expression of K^+ channels in PV cells Bar plot showing qPCR data of PV mRNA purified using FACS at P10 (green) and P18 (red). Note the relatively high expression levels of $K_{2P}1.1$ (TWIK-1), $K_{2P}2.1$ (TREK-1), $K_{2P}3.1$ (TASK-1) and $K_{2P}9.1$ (TASK-3) compared to other K_{2P} channels. Figure from Goldberg et al. 2010.

consistent with the properties of a developing leak K^+ channel. The input resistance and membrane time constant in PV cells are also increased in TASK-1/3 double knockout mice (Goldberg et al. 2011), further demonstrating a role of TASK channels in the background conductance in PV cells. Immunolabeling also indicates an increase in TASK-1 protein expression in PV cells throughout early development (Okaty et al. 2009). Similarly, TREK-1 is also expressed in the neocortex (Talley et al. 2001), although qPCR data indicate that mRNA transcripts are reduced between P10 and P18 (Fig 1.7) (Goldberg et al. 2011).

TASK, and to a lesser degree TREK channels, could therefore represent suitable targets for the modulation of PV cells. Both channels directly regulate the RMP in heterologous expression systems (Kindler et al. 1999; Leonoudakis et al. 1998), indicating that these channels are well established as background leak channels. The molecular profile of TASK channels in PV cells in addition to pharmacological

evidence of a K_{2P} or TASK-like background conductance in PV cells as well as the physiological effect of ablating TASK in mice makes these channels an ideal target. TASK-1 is known to dimerise with TASK-3, forming TASK-1/3 heterodimers (Goldstein et al. 2005), so it would be appropriate to block these channels with a blocker specific for both TASK-1 and TASK-3.

1.3.8 TASK-1/3 and TREK-1 pharmacology

This thesis represents the first study to analyse the functional effects of blocking TASK-1/3 and TREK-1 channels in PV cells using specific K_{2P} blockers. Three distinct structurally unrelated TASK-1/3 blockers were used in experiments throughout the thesis (Fig 1.8). These blockers were provided by Eli Lilly and Company (Surrey, UK) and include: **A293** (2-(Butane-1-sulfonyl-amino)-N-[1-(R)-(6-methoxypyridin-3-yl)-propyl]-benz-amide) (Decher et al. 2011); **A1899** (2'-{[2-(4-methoxy-phenyl)-acetylamino]-methyl}-biphenyl-2-carboxylic acid 2, 4-difluoro-benzylamide), which acts as an open channel blocker that binds to the 2nd and 4th transmembrane segments forming the central cavity of the channel; (Streit et al. 2011); and **compound 23** (1-{1-[6-(biphenyl-4-ylcarbonyl)-5,6,7,8-tetrahydropyrido[4,3-d]-pyrimidin-4-yl}propan-1-one) (Coburn et al. 2012).

Two TREK-1 channel blockers were used in experiments. They include: **amlodipine** – which is also a classic L-type Ca^{2+} channel blocker but blocks TREK-1 with much higher affinity; and **spadin** – which is a peptide based on a secreted propeptide as a result of the maturation of the neurotensin receptor 3/sortillin protein, which is located in the trans-Golgi network (Mazella et al. 2010).

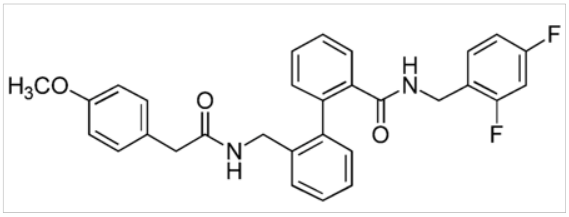

A1899

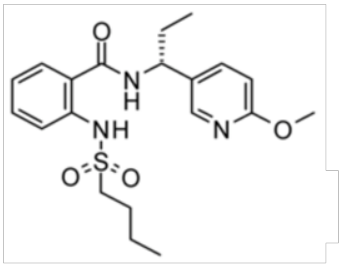

A293

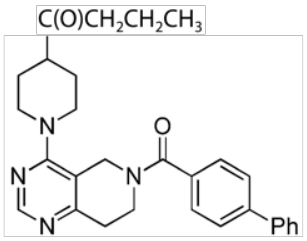

Compound 23

Figure 1.8 Chemical structures of TASK-1/3 channel blockers Structures of A293, A1899 and compound 23 that were used in experiments. All TASK-1/3 channel blockers were synthesised by Eli Lilly and company (Surrey, UK)

1.3.9 Aims of this thesis

The overall aim of the thesis is to increase the excitability of PV cells and thus, increase the probability of action potential firing. If successful, this novel approach of modulating PV cells could be used as a treatment for neuropsychiatric disorders linked to PV cell abnormalities. TASK-1/3 and TREK-1 channels were blocked in PV cells in the attempt to depolarise the RMP and increase the input resistance. Mechanistically, depolarising the cell will bring the cell closer to firing threshold, while increasing the input resistance will increase the amplitude and duration of EPSPs that the cell receives, which could summate and drive the cell to fire.

Direct recordings of PV cells were performed to test whether TASK-1/3 and TREK-1 blockade increased PV cell output and intrinsic excitability. The output of PV cells was assayed using the thalamocortical circuit (see section **3.2.1**). Intrinsic excitability of PV cells was measured based on changes in the RMP and input resistance, and probability of action potential firing. The following chapters test whether TASK-1/3 blockade (chapter 3) and TREK-1 blockade (chapter 4) increases the excitability of PV cells.

Chapter 3: The effect of TASK-1/3 blockade on PV cell excitability

Chapter 4: The effect of TREK-1 blockade on PV cell excitability

Chapter 2

Methods

2.1 Animals and Cell Lines

2.1.1 Housing and Breeding

All animals were housed and maintained in a facility that was subject to 12 hr light/dark cycles with *ad libitum* access to food and water. All procedures were treated in accordance with UK Home Office regulations.

2.1.2 Generation of PV/EYFP mice

PV/EYFP mice were created by crossing a female PV-Cre knockin mouse (Hippenmeyer et al. 2005) with a male Rosa26EYFP mouse (Srinivas et al. 2001). The PV-Cre knockin allele from the female contains the endogenous parvalbumin promoter which directs Cre recombinase expression in parvalbumin-expressing neurons. The R26-stop-EYFP allele from the male contains an Enhanced Yellow Fluorescent Protein gene (EYFP) inserted into the ubiquitously expressed *Gt(ROSA)26Sor* locus (Friedrich & Soriano 1991). Expression of EYFP is halted by an upstream *loxP*-flanked STOP sequence. When crossed together, the STOP sequence is deleted exclusively in parvalbumin-expressing neurons, yielding EYFP expression only in this cell type. Mice homozygous for both PV-Cre and EYFP were maintained for breeding. Both male and female mice were used in experiments.

2.1.3 Genotyping

Animal tissue was collected from ear clips and genotyped in order to select between the littermates to produce PV/EYFP mice:

DNA was extracted using the Hot Shot method: Tissue samples were digested in 600 µl NaOH (50 mM) at 100ºC for 45 min and then neutralised with 50µl Tris-HCl (1 M, pH 8) at 100ºC for a further 2 min. Samples were centrifuged at 13,000 x g for 20 min and subsequently stored at 4ºC. DNA was present in the supernatant.

Each polymerase chain reaction (PCR) contained 12.5 µl of Promega GoTaq master mix, 10.5 µl ddH_2O, 1 µl of total primers (300 nM) and 1 µl of extracted DNA. Thermocycling conditions are summarised in Table 2.1. PCR products were run on a 1.5% agarose gel with SYBR Safe DNA gel stain at 100 V for 45 min with a 1 kb DNA ladder.

For the Cre reaction, two sets of primer pairs were used: Cre537 (5' – CCA CGA CCA AGT GAC AGC AAT G – 3'), Cre538 (5' – AAG TGC CTT CTC TAC ACC TGC G – 3'), which amplifies the 350 bp product of Cre; and Beta-globin forward (5' – CCA ATC TGC TCA CAC AGG ATA GAG AGG GCA GG – 3'), Beta-globin reverse (5' – CCT TGA GGC TGT CCA AGT GAT TCA GGC CAT CG – 3'), which amplifies the control 150 bp band for Beta-globin.

For EYFP, two separate reactions were required, one for the WT allele and one for the mutant allele: Both reactions utilised a common forward primer R26WTF (5' – AAA GTC GCT CTG AGT TGT TAT – 3'); in conjunction with either the WT reverse primer R26WTR (5' – GGA GCG GGA GAA ATG GAT ATG – 3'), or the mutant reverse primer R26KOR (5' – GCG AAG AGT TTG TCC TCA ACC – 3'). A large 550 bp or small 250 bp band indicated that at least one of the alleles was WT or mutant, respectively.

Table 2.1 Thermocycling conditions for Cre and EYFP genotyping

	Cre		**EYFP**	
Step	**Temperature (ºC)**	**Duration**	**Temperature (ºC)**	**Duration**
1	95	5 min	94	15 min
2	95	30 s	94	30 s
3	58	30 s	59	45 s
4	72	30 s	72	2 min
5	Repeat steps 2-4 30X		Repeat steps 2-4 37X	
6	72	5 min	72	10 min
7	4	Indefinitely	4	Indefinitely

2.1.4 Expressing TASK-3 in HEK cells

For TASK-3 channel recordings, human embryonic kidney 293 cells (HEK-293) were cultured in Dulbecco's Modified Eagle Medium (DMEM) with 10% foetal calf serum and 1% ampicillin. The cells were passaged twice weekly and placed onto cover slips precoated in poly-D-lysine (0.05 mg/ml) to assist in binding. The density of cells on the coverslips were approximately 10-30% on the day of recording.

Mouse TASK-3 cDNA constructs were kindly provided by Prof Mathew Nolan. HEK-293 cells were transfected with TASK-3 cDNA using Lipofectamine (Thermofisher). Plasmids containing the TASK-3 construct under the control of a CAMK2 alpha promoter sequence allowed for TASK-3 to be expressed when exposed to the transcription machinery native to HEK-293 cells. 500 ng of DNA was added to each well of a 24 well plate, each containing a coverslip with HEK cells submerged in culture media described above. For each well, plasmids containing the TASK-3 construct and eGFP (enhanced green fluorescent protein) were combined with 25 µl opti-MEM (Thermofisher) before being added to another 25 µl opti-MEM containing 2 µl lipofectamine. This transfection mix was left at room temperature for 20 min. 50 µl of the transfection mix was subsequently added dropwise to each well containing the HEK cells and left to transfect for 2-5 hours. The transfection mix was subsequently replaced with fresh media. Recordings were made 24-72 hours after transfection. HEK-293 cells transfected with TASK-3 were identified by eGFP expression (excitation at 470 nm). Recordings from TASK-3-trasfected cells were interleaved with recordings from untransfected HEK-293 cells, which underwent the same transfection process described above, but without the DNA added to the mix.

2.2 Electrophysiology

2.2.1 Solutions

All chemicals and compounds were obtained from Sigma Aldrich (St Louis, MO, US), Abcam (Cambridge, UK), Tocris (Bristol, UK) or Eli Lilly and Company (Surrey, UK).

Table 2.2 External solution composition

	Sucrose based cutting solution (mM)	**Recording aCSF solution (mM)**
NaCl	80	130
KCl	2.5	2.5
NaH_2PO_4	1.25	1.25
$NaHCO_3$	25	25
Glucose	10	10
Sucrose	90	-
$CaCl_2$	0.5	2.5
$MgSO_4$	4.5	1.5

All solutions were equilibrated with 95% O_2, 5% CO_2 to stabilise the pH to 7.4. CO_2 functions as a pH buffer with HCO_3^-.

Table 2.3 Internal patch pipette solution composition

	$CsMeSO_3$ based internal (mM)	**$KMeSO_3$ based internal (mM)**
$Cs/KMeSO_3$	135	135
NaCl	8	8
Mg-ATP	4	4
Na-GTP	0.3	0.5
HEPES	10	10
EGTA	0.5	0.5
QX 314	5	-

Solutions were adjusted to pH 7.3 with CsOH (for CsMeSO3 based internal) or KOH (for KMeSO3 based internal) and adjusted to have an osmolarity of 295 $mOsm.L^{-1}$ by adding water if required.

2.2.2 Drugs

All drugs were prepared into stock solutions (1000X). All TASK channel blockers were provided by Eli Lilly and Company (Surrey, UK). Final concentrations of most drugs used in experiments are summarised in the table below:

Table 2.4 Drugs dissolved in recording aCSF solution

	Drug (Supplier)	Final Concentration µM (Solvent)
TASK channel blockers	A293 (Eli Lilly)	10 (DMSO)
	A1899 (Eli Lilly)	1 (DMSO)
	Compound 23 (Eli Lilly)	3 (DMSO)
TREK channel blockers	Spadin (Tocris)	1 (H_2O)
	Amlodipine (Abcam)	43 (H_2O)
Isolating TREK currents	CNQX (Abcam)	20 (H_2O)
	D-APV (Abcam)	50 (H_2O)
	Nifedipine (Abcam)	20 (DMSO)
	Picrotoxin (Sigma)	50 (DMSO)
	TEA (Abcam)	1000 (H_2O)
Two-pore potassium channel blocker	Bupivacaine (Sigma)	100 (H_2O)
Cholinergic receptor agonist	Carbachol (Abcam)	30 (DMSO)

Bupivacaine blocks voltage-gated sodium channels as well as two-pore potassium channels. In experiments where bupivacaine was used, the voltage-gated sodium channel blocker QX314 (5 mM) was included in the pipette solution before bupivacaine application, so that its observed effects were mediated exclusively by blocking two-pore channels.

In some control conditions, the pH of the recording aCSF solution was lowered to pH 6.3 by reducing the concentration of $NaHCO_3$. This reduces the concentration of HCO_3^- in the CO_2/HCO_3^- buffer system resulting in an increase in acidity.

2.2.3 Preparation of acute tissue slices

Thalamocortical slices were prepared from male and female P20-26 mice (Fig 2.1) as described previously (Agmon & Connors 1991). Briefly, mice were anaesthetised

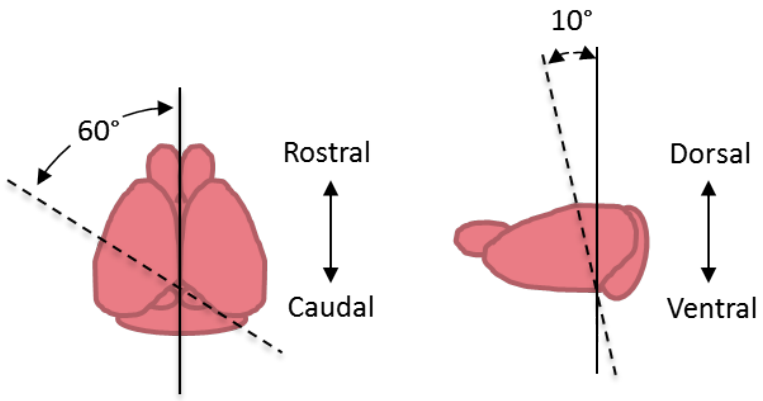

Figure 2.1 Preparation of thalamocortical slices Schematic of mouse brain demonstrating cutting angle required before it is glued to the microtome stage for slicing. Left, 60° cutting angle required from the midline (dorsal view). Right, illustrating that the same cut is required to be angled at 10° from the dorsal-ventral axis.

using isoflurane and decapitated. The brain was quickly removed and placed in ice-cold (<4ºC) sucrose based cutting solution (Table 2.2). It was then cut at ~60º to the midline - angled at 10º from the dorsal-ventral axis - and glued to a vibrating microtome stage on the cut surface. 500 µm slices (unless specified otherwise) were cut in ice-cold sucrose based cutting solution using a Leica VT1200 microtome (Leica, UK) and transferred to a submerged storage chamber where they were maintained in the same solution at 35ºC for 30 min. Slices were allowed to recover for at least 30 min at room temperature before the start of experiments. In a subset of experiments, horizontal hippocampal slices were prepared in identical conditions.

2.2.4 Whole-cell patch clamp recordings

Slices were transferred to a submerged recording chamber and perfused with aCSF solution (Table 2.2) at a rate of 4-5 ml/min and maintained at 31ºC. Cells were visualised with a 40X objective with infrared differential interference contrast optics (Q Imaging, BC, Canada) on a Scientifica Slicescope (Scientifica, UK). Patch pipettes (3-5 MΩ) were made from boroscillate glass capillaries (Harvard Apparatus,

UK) using a P-97 Flaming Brown micropipette puller (Sutter Instrument Company, CA, USA) and filled with internal solution (Table 2.3).

Signal waveforms were amplified and lowpass filtered at 4 kHz with a Multiclamp 700B amplifier (Molecular Devices, CA, USA), digitized at 10 kHz using a Micro1401 (Cambridge Electronic Design Limited, UK) and stored on a computer using Signal 4 (Cambridge Electronic Design Limited, UK). Firing patterns were filtered at 10 kHz and digitized at 40 kHz. Amplifier gain was set at 5 unless stated otherwise.

Whole-cell recording configuration was established once an appropriate neuron was identified. Following the application of positive pressure, a motor micromanipulator (PatchStar, Scientifica, UK) was used to lower the recording electrode to approach the cell. Positive pressure was released when both a dimple was observed on the cell surface and when there was an increase in pipette resistance, measured with a -5 mV square test step function at 10 Hz in Signal 4. Gradual negative pressure was applied until a GΩ seal was obtained, and pipette capacitance was compensated. The cell membrane was then ruptured which was demonstrated by the emergence of large capacitive transients in response to the test pulse. Recordings were only acquired from cells with a series resistance <25 MΩ and that required a holding current less negative than -100 pA when voltage clamped at -70 mV, or with a resting membrane potential (RMP) more negative than -60 mV for current clamp experiments.

2.2.5 Thalamocortical recordings

A 2.5X objective was used to identify layer IV barrels in the somatosensory cortex and ventrobasal thalamus (VB), and to allow quick and easy movement of the electrodes. In order to detect a robust thalamocortical connection, a bipolar stimulating electrode was initially placed in the VB and an extracellular recording electrode placed outside a layer IV barrel. The recording electrode was filled with NaCl (2 M) and broken at the tip to enable better electrical access to the extracellular space. Reliable thalamocortical input was achieved by stimulating different areas within the VB and measuring field EPSPs just outside each barrel with the recording

electrode until a field potential of >0.1 mV was established, indicating a strong connection. Amplifier gain was set at 100 during field recordings to increase signal sensitivity.

Once a good thalamocortical connection was found around a specific barrel, the extracellular recording electrode was removed and replaced with a patch pipette filled with $CsMeSO_3$ based internal (Table 2.3). Stellate cells were located and patched within the same barrel. Whole-cell synaptic currents were measured in voltage clamp, in response to thalamic excitation.

Afferent fibres were electrically stimulated, subsequently activating PV cells in the layer IV barrel, and in turn, transmitting disynaptic feed-forward inhibition onto local stellate cells. Thalamocortical feedforward IPSCs were evoked at a frequency of 0.1 Hz and recorded in the stellate cell clamped at the glutamatergic reversal potential (+5 mV). The amplitude of the IPSC was calculated by subtracting the steady-state holding current from the peak of the IPSC. In multiple stimulation experiments, a 50 Hz triplet of three IPSCs were elicited at 0.1 Hz.

The stimulation intensity was adjusted so that the amplitude of feedforward IPSCs ranged between 200 pA and 2000 pA. This was to ensure that the strength of stimulation was large enough to recruit several PV cells to fire, yet weak enough to prevent saturation of PV-mediated inhibition. Activating several but not all PV cells allowed for the possibility to recruit near-threshold PV cells – in addition to the PV cells activated from baseline period – during the time course of the experiment. As such, an increase in the number of PV cells firing in response to thalamocortical stimulation would translate to an increase in the amplitude of the feedforward IPSC which can therefore be measured (Fig 3.1 A).

2.2.6 PV cell recordings

PV cells were identified by YFP fluorescence. To excite YFP, an X-Cite 120Q illuminator (Excelitas Technologies Corp, Waltham, MA, US) was used with a filter

(Chroma Technology Corp, Bellows Falls, VT, US) with excitation/emission wavelength 500/530 nm.

Thinner 300 μm thalamocortical slices were prepared in order to help distinguish fluorescent PV cells from other non-PV cells. Whole-cell recordings were performed using $KMeSO_3$ based internal (Table 2.3) in current clamp configuration. Recorded cells displayed a fast-spiking phenotype typical of PV cells. These included non-accomodating, non-adapting trains of action potentials during depolarising current steps, occasionally interrupted by intervals with subthreshold oscillations, notably around threshold. In addition to this, they exhibited deep afterhyperpolarising potentials (AHPs) and had a maximum firing frequency of >120 Hz in response to strong current steps.

2.2.7 Measuring RMP, IR and action potential firing in PV cells

10, 250 ms current steps, in 1 s sweeps, were delivered every 30 s to PV cells. The first step was hyperpolarising, with the following steps incrementally depolarising. The current step amplitude was adjusted so that each set of depolarising steps both contained subthreshold and suprathreshold firing. The input resistance was obtained from the average of 4 hyperpolarising steps, 5 s apart, that were interleaved between each set of the 10 current steps described above. This allowed for a more accurate input resistance measurement.

The RMP (V_m) was the average potential during the first 50 ms of the first sweep before any current step was injected. Input resistance (R_{in}) was calculated using Ohm's law ($R_{in} = \Delta V / I$) by subtracting V_m during the last 50 ms of the hyperpolarising current step from V_m during the preceding 50 ms to the step, and dividing it by the injected current. R_{in} was determined from the average of 4 traces.

The number of action potentials per 250 ms was plotted against injected current. Rheobase was classified as the first current step to elicit at least one action potential. Action potential threshold was determined from a membrane potential change greater than 30,000 $mV.s^{-1}$.

2.2.8 Whole-cell TREK currents in PV cells

TREK currents were analysed in relation to their current-voltage function. To isolate TREK currents, synaptic blockers and ion channel blockers were added to the recording aCSF solution (Table 2.4). Whole-cell recordings were performed using $CsMeSO_3$ based internal (Table 2.3) in voltage clamp configuration. 14, 500 ms voltage steps (-90 mV to +40 mV, Δ10 mV) were injected into PV cells from a holding voltage of -70 mV, followed by a 500 ms ramp (-90 mV to +40 mV) in the final. The duration of each sweep was 1 s. Data were normalised to the current response at +40 mV for analysis.

The gradient of the current-voltage relationship in response to voltage ramps was determined from the positive voltage range between +30 mV to +40 mV. The rectification index of the measured current was calculated by dividing the conductance at +40 mV by the conductance at -90 mV. The conductance was calculated by the following equation: $I / V_m – E_{rev}$ where I = normalised current, V_m = membrane voltage and E_{rev} = reversal potential of current response.

2.2.9 Hippocampal gamma oscillations

The cholinergic agonist carbachol was used to trigger synchronous rhythmic oscillations in pyramidal cells in the CA3 region of the hippocampus (McMahon et al. 1998). To induce gamma oscillations in hippocampal slices, carbachol (30μM) was added to the aCSF solution (Table 2.2) and perfused at a rate of 10-12 ml/min. A high flow rate allowed for an increased oxygen supply to the slices to induce the network activity (Hájos et al. 2009).

An extracellular recording electrode was placed into the pyramidal cell layer in CA3 of the hippocampus. Gamma power (35-50 Hz) was computed using Signal 4.

2.2.10 Data analysis

All recordings were normalised to baseline values. These data were averaged across groups and presented as means and the standard error of the mean (SEM; error bars). Comparisons between multiple means were carried out by ANOVA while comparisons between multiple means where there were several drug conditions within experiments were performed by repeated measures ANOVA (RM-ANOVA). Comparisons between two means were performed by two-tailed *t*-tests. The significance level used was $p<0.05$, and corrected for multiple comparisons using the Bonferroni method where stated.

Chapter 3

Effect of TASK-1/3 blockade on fast-spiking interneuron excitability

3.1 Introduction

The balance between excitation and inhibition is essential for cortical function (Yizhar et al. 2011). This balance relies on the maintenance of appropriate ratios of excitatory and inhibitory synaptic inputs which are dynamically regulated throughout development and into adulthood (Maffei et al. 2006; Haider & McCormick 2009). GABAergic interneurons are the major cellular elements that control hyperexcitability in the brain, and consequently, many of the genes that regulate interneuron development and function have been linked to epilepsy (Dichter & Ayala 1987). Furthermore, imbalances in cortical network activity as a result of disrupted interneuron function have been associated with other neurological disorders including schizophrenia and autism (Marín 2012).

Knowledge of functional roles that interneurons play in the healthy brain should yield insight into the possible contribution of aberrant interneuron function to psychiatric diseases. Due to the large diversity of interneurons however, development of such knowledge has been challenging, with more than 20 different classes in the cortex alone (Markram et al. 2004). Nonetheless, growing evidence suggests that functional abnormalities particularly in PV cells are implicated in these diseases (Marin 2012, and see sections **1.2.8** and **1.2.9**) These cells maintain fast, rhythmic inhibition through the generation of gamma oscillations to create narrow time windows for effective excitation, synchronising pyramidal cells to fire at precise oscillatory patterns (Bartos et al. 2007). This is essential for the integration of information between different brain regions, believed to underlie cognition, memory and behaviour. Thus, abnormalities in the function of PV cells may lead to desynchronisation across neuronal ensembles, resulting in deficits in working memory, attention and perceptual organisation found in schizophrenia and autism (Wang & Buzsáki 1996).

The ability to selectively modulate PV cells and increase their activity could be extremely useful as a treatment for patients with neuropsychiatric disorders. As PV cells have a distinctively low input resistance presumed to be mediated in part by TASK subfamily K_{2P} channels (Goldberg et al. 2011), the blockade of these channels could therefore be applied to increase the basal activity of PV cells. Mechanistically, this would prevent the passive efflux of K^+ through TASK channels, resulting in membrane depolarisation which would bring the cell closer to firing threshold. Additionally, their blockade would increase the input resistance which produces two effects: Firstly, an increase in input resistance will increase the depolarisation produced by a given inward current. Secondly, it will increase the membrane time constant which will widen the window for temporal summation of excitatory inputs.

This chapter focuses on the effects of blocking TASK-1 and TASK-3 channels in PV cells predominantly in the mouse primary somatosensory cortex. Initially, the effects of TASK-1/3 blockers on the output of cortical PV cells were analysed using the thalamocortical circuit (Fig 3.1), where PV cell-mediated IPSCs can be reliably measured in voltage-clamped principal cells. Finally, the effects of TASK-1/3 blockers on the intrinsic properties of PV cells were assessed using direct recordings of patch-clamped PV cells.

3.2 Modulation of PV cell output using TASK channel blockers

Two distinct TASK-1/3 channel blockers, A293 and compound 23 were used in an attempt to increase the intrinsic excitability of PV cells and subsequently increase the probability of action potential firing. In doing so, PV cells close to firing threshold that would have remained silent may therefore activate. When incorporated into the global network, an increase in firing will lead to an increase in the frequency of PV cell-mediated IPSCs. Moreover, the amplitude of feedforward inputs onto excitatory cells in response to sensory stimuli will be enhanced as more PV cells are recruited.

The amplitude of stimulus-evoked PV cell-mediated IPSCs can therefore be exploited to provide a suitable measure of network PV cell output as part of a circuit.

3.2.1 Thalamocortical circuit as an assay of PV cell output

In order to assess the effect of a drug on the activity of PV cells, a reliable assay of cell output is required. A conclusive method for analysing PV cell output lies within the thalamocortical network, and incorporates the barrel cortex, where the thalamus provides robust excitatory input to the neocortex (Daw et al. 2007; Cruikshank et al. 2007). In the intact rodent brain, vibrissal sensory input from the thalamus contacts both excitatory and inhibitory neurons, predominantly in layer IV of the somatosensory cortex (Daw et al. 2007). This region of the cortex contains a precise topographic map of the whiskers, where each whisker input stimulates its corresponding layer IV barrel (Fox 2002). Thalamocortical input into layer IV has since been demonstrated to activate inhibitory interneurons more strongly than excitatory neurons, producing powerful feedforward inhibition (Cruikshank et al. 2007). Importantly, PV cells are activated even more robustly than other interneurons, due to strong thalamocortical excitatory conductances, which allows them to fire before feedforward inhibition emerges in the recipient cells in layer IV (Cruikshank et al. 2010). Paired recordings in the barrel cortex demonstrated that unitary IPSCs from fast-spiking cells onto principal cells occurred without failures and produced similar decay kinetics to thalamically stimulated feedforward IPSCs, further supporting the role of PV cells as a primary mediator of thalamocortical feedforward IPSCs (Gabernet et al. 2005). Direct thalamocortical excitation of PV cells *in vitro* provides robust, disynaptic, feedforward inhibition onto excitatory stellate cells in the same barrel (Daw et al. 2007).

PV cell-mediated IPSCs can therefore be accurately measured with very little contamination from other cell types. A bipolar stimulating electrode placed in the ventrobasal thalamus (VB) can be used to electrically stimulate afferent thalamocortical axons, activating PV cells in layer IV, and subsequently producing

GABAergic inhibition onto stellate cells in the same barrel (Fig 3.1 A). IPSCs can then be recorded from stellate cells voltage-clamped at the glutamatergic reversal potential. As the feedforward IPSCs are almost exclusively mediated by PV cells (Cruikshank et al. 2010), this assay is therefore a clean and reliable method for examining the output of PV cells as part of a circuit.

3.2.2 Results

Recordings were carried out using thalamocortical slices (P20-26) with identifiable layer IV barrels and a robust thalamocortical connection. Single disynaptic feedforward IPSCs were evoked, and recorded as outward currents in stellate cells voltage-clamped at the glutamatergic reversal potential in response to extracellular stimulation of the VB at 0.1 Hz (Fig 3.1 B). A stable 5 min baseline IPSC amplitude was obtained in all experiments before a TASK channel blocker was applied for 10 min.

In all experiments, it was imperative to stimulate the VB at a suitable intensity to recruit several but not all PV cells to fire (Fig 3.1 A). This was to ensure that a reliable feedforward IPSC was generated whilst allowing for the opportunity to recruit other PV cells that had initially failed to fire during baseline period, but were close to threshold. Thus, PV cells that may have been close to firing threshold in response to thalamocortical stimulation during the baseline period of experiments could then begin to fire during drug application if they became more excitable. The GABAergic inhibition transmitted from these newly recruited PV cells in addition to the GABAergic inhibition from the PV cells already activated during the baseline period would therefore summate and translate to an increase in IPSC amplitude in the stellate cell (Fig 3.1 A). On the other hand, if the drug had no effect on the excitability of PV cells then the IPSC amplitude recorded in the stellate cell would remain unchanged.

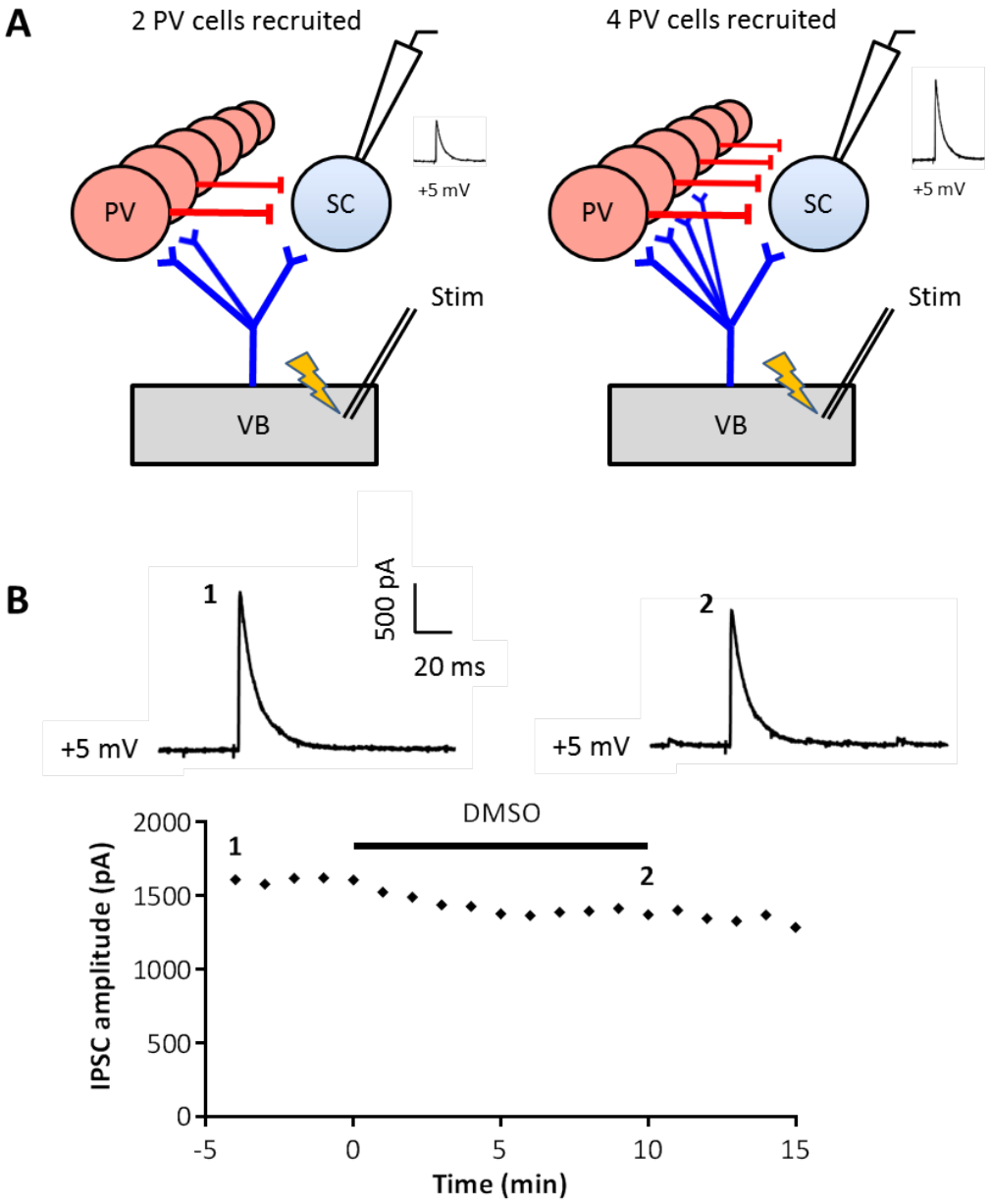

Figure 3.1 Measuring PV cell output using the thalamocortical circuit Extracellular stimulation of the ventrobasal thalamus (VB) elicits disynaptic PV cell-mediated IPSCs in layer IV stellate cells (SC) in the barrel cortex. (A) Schematics of a thalamocortical recording of a voltage-clamped SC in response to VB stimulation at 0.1 Hz. Left, stimulation intensity was initially adjusted before the start of each experiment so that several but not all PV cells fired in response to VB stimulation. Right, an example of a scenario where more PV cells are excited during the course of the experiment, which translates to an increase in IPSC amplitude recorded in the stellate cell. (B) Top, example of an IPSC at baseline (left) and an IPSC in the presence of the solvent DMSO (right), taken at time points 1 and 2, respectively. Bottom, example timecourse showing peak IPSC amplitude. Each point on the graph represents the peak amplitude of an average of 6 traces.

Due to poor solubility of all TASK channel blockers in water, all drugs were dissolved in dimethyl sulfoxide (DMSO) yielding a final DMSO concentration of 0.1% when dissolved in the recording solution. Trials were interleaved between drug application and DMSO (control), and their effect on IPSC amplitude was compared between the two groups.

3.2.3 TASK-1/3 channel blockers have no effect on PV cell output

The TASK-1/3 channel blocker A293 (Decher et al. 2011) was initially used in thalamocortical experiments. A293 has IC_{50}s of 0.2 μM and 0.95 μM for TASK-1 and TASK-3, respectively at heterologously expressed TASK channels in Xenopus oocytes (Putzke et al. 2007). 3 μM of A293 was therefore used in all experiments (approximately tenfold of the IC_{50} value for TASK-1 and threefold of the IC_{50} value for TASK-3) to ensure saturation of TASK-1/3 channels in the slice without inducing a non-specific effect on other channels.

No difference in IPSC amplitude was detected between A293 and DMSO groups (Mean amplitude 5-10 min after application as a percentage of baseline 0-5 min before application, DMSO 85.1% ± 7.2, n=9 cells; A293: 101.1% ± 7.8, n=9 cells; p=0.13, Student's unpaired *t*-test; Fig 3.2).

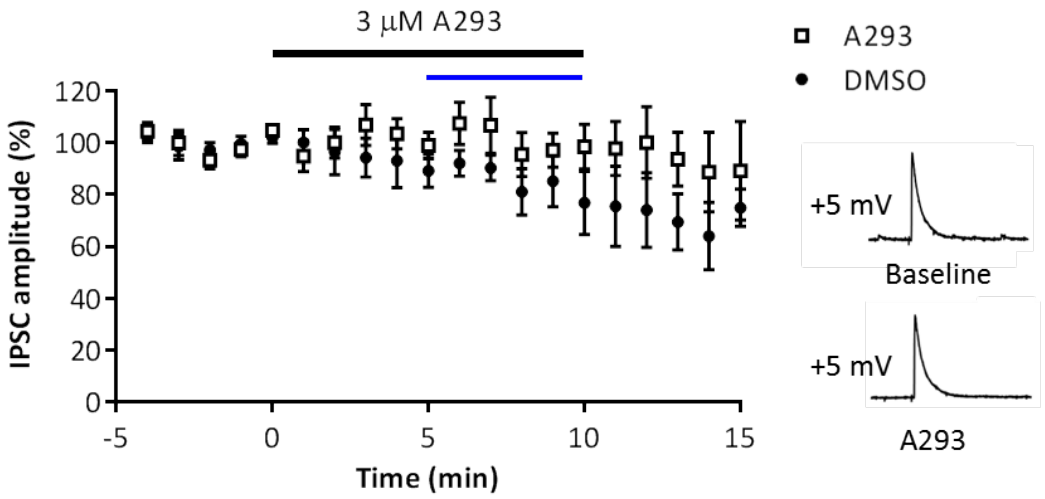

Figure 3.2 TASK-1/3 channel blocker A293 does not affect PV cell output Timecourse of peak PV cell-mediated IPSCs normalised to the baseline average of the first 5 min in the presence of DMSO or 3 µM A293 TASK-1/3 channel blocker. Blue line represents the time period used for statistical test comparison between the two groups. Data as means ± SEM. n=9 cells in both A293 and DMSO groups.

3.2.4 TASK-1/3 channel blockers have no effect on PV cell output during multiple stimulation

The assay so far has only examined PV cell output in response to single thalamocortical stimulation, however neurons *in vivo* typically receive multiple inputs at high frequency. The integration of these inputs depends upon the amplitude and duration of EPSPs that cells receive, which can summate and propagate to the soma, resulting in action potential firing. The duration of EPSPs is set in part by the time constant which sets the time window for temporal summation of inputs. Cells with a low input resistance will have a fast time constant and therefore EPSPs will be brief. By increasing the input resistance and therefore the time constant, the duration of EPSPs will increase, making them more likely to summate with temporally impeding inputs and result in action potential firing. Thus, repetitive stimulation of PV cells at high frequency would also examine changes in the amplitude of PV cell-mediated IPSCs induced by changes in the integration of PV cell inputs.

As A293 failed to alter the amplitude of IPSCs in response to single thalamocortical stimulation, multiple stimulation at high frequency was then tested. This would elicit multiple EPSPs onto PV cells which could summate and result in action potential firing. Such an assay would then be sensitive to changes in the membrane time constant. An increase in the input resistance during TASK-1/3 blockade could increase the time constant of PV cells and therefore increase the time window for temporal summation of inputs. This would increase the amplitude and duration of EPSPs that PV cells receive, which could summate with subsequent EPSPs and drive the cells to fire. By stimulating PV cells repetitively at high frequency, the effects of blocking TASK-1/3 channels on the summation of multiple inputs can be examined.

The VB was stimulated three times at 50 Hz, eliciting three IPSCs in the recorded stellate cell (Fig 3.3). PV cells that would normally have remained inactive could therefore be recruited during high-frequency stimulation, resulting in an increase in amplitude of subsequent IPSCs. Thus, PV cells that may have been close to firing threshold during the baseline period of experiments could then become excitable from the second or third thalamocortical stimuli. This would translate into an increased amplitude of the second or third IPSC recorded in the stellate cell, corresponding to the temporal stimuli responsible for exciting the PV cell. The amplitudes of all three IPSCs were analysed.

All recordings were used for analysis of the 1st peak, however a subset of recordings was excluded from analysis due to failures in the 2nd and 3rd IPSCs during the first 5 min baseline period of experiments. Out of the 20 cells recorded in total, 3 cells from DMSO and 4 cells from A293 groups were excluded from analysis of the 2nd and 3rd IPSCs in the triplet.

No difference in the amplitude of any of the three IPSCs was detected between A293 and DMSO groups (Mean amplitude 5-10 min after application as a percentage of baseline of respective IPSC 0-5 min before application. IPSC 1, DMSO: 82.0% ±

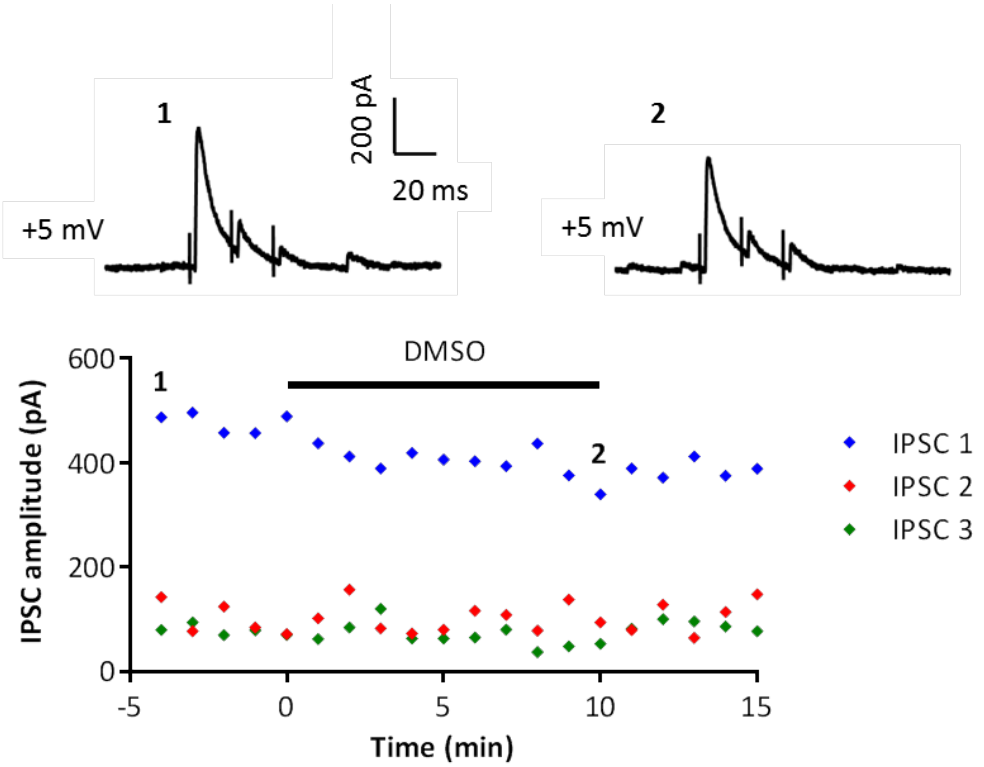

Figure 3.3 Measuring high frequency PV cell output using the thalamocortical circuit A 50 Hz triplet of thalamocortical PV cell-mediated IPSCs was evoked at 0.1 Hz. Top, example of a triplet of IPSCs at baseline (left) and in the presence of DMSO (right), taken at time points 1 and 2, respectively. Bottom, example timecourse showing peak IPSC amplitudes. Each point on the graph represents the peak amplitude of an average of 6 traces.

9.0; A293: 95.5% ± 8.5; p>0.99. IPSC 2, DMSO: 76.4% ± 11.4; A293: 111.9% ± 12.3; p=0.18. IPSC 3, DMSO: 84.0% ± 31.6; A293: 75.6% ± 9.6; p>0.99. n=7 cells for DMSO, n=6 cells for A293, Two-way ANOVA with Bonferroni correction; Fig 3.4). Similarly, no difference in the amplitude of the 1st IPSC in the triplet was detected between A293 and DMSO groups (Mean amplitude 5-10 min after application as a percentage of baseline of respective IPSC 0-5 min before application, DMSO: 80.7% ± 6.6, n=10 cells; A293: 98.4% ± 6.4, n=10 cells; p=0.06, Student's unpaired *t*-test; Fig 3.4 B).

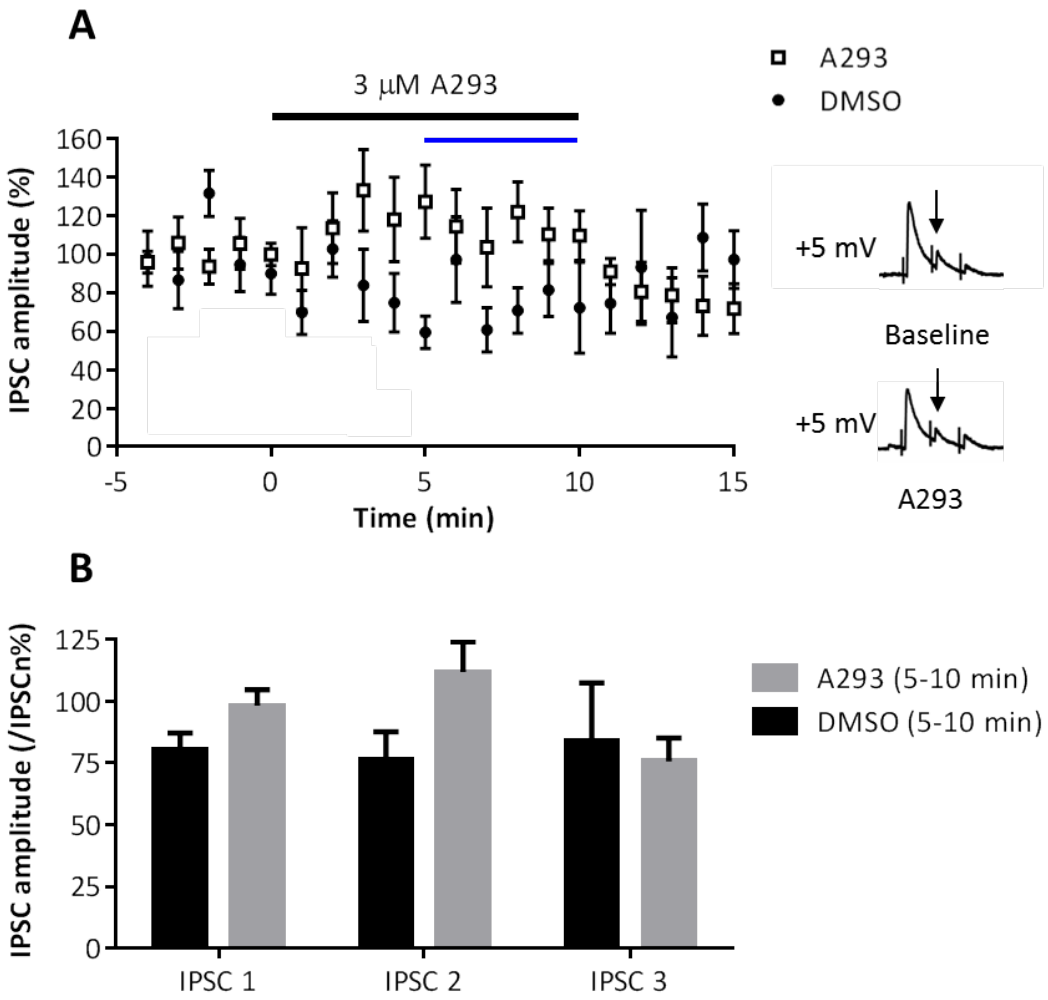

Figure 3.4 TASK-1/3 channel blocker A293 does not affect PV cell output during multiple stimulation A 50 Hz triplet of thalamocortical PV cell-mediated IPSCs was evoked at 0.1 Hz. (A) Timecourse of peak of 2nd IPSC in the triplet (indicated by arrow in inset) normalised to the baseline average of the first 5 min of the 2nd IPSC in the presence of DMSO or 3 µM A293 TASK-1/3 channel blocker. Blue line represents the time period used for statistical test comparison between the two groups. (B) Averages of 1st, 2nd, and 3rd IPSCs during last 5-10 min of DMSO or A293 treatment normalised to the baseline average of the first 5 min of their respective IPSCs. Data as means ± SEM. For IPSC 1: n=10 cells in both A293 and DMSO groups. For IPSC 2 and IPSC 3: n=7 for DMSO, n=6 for A293.

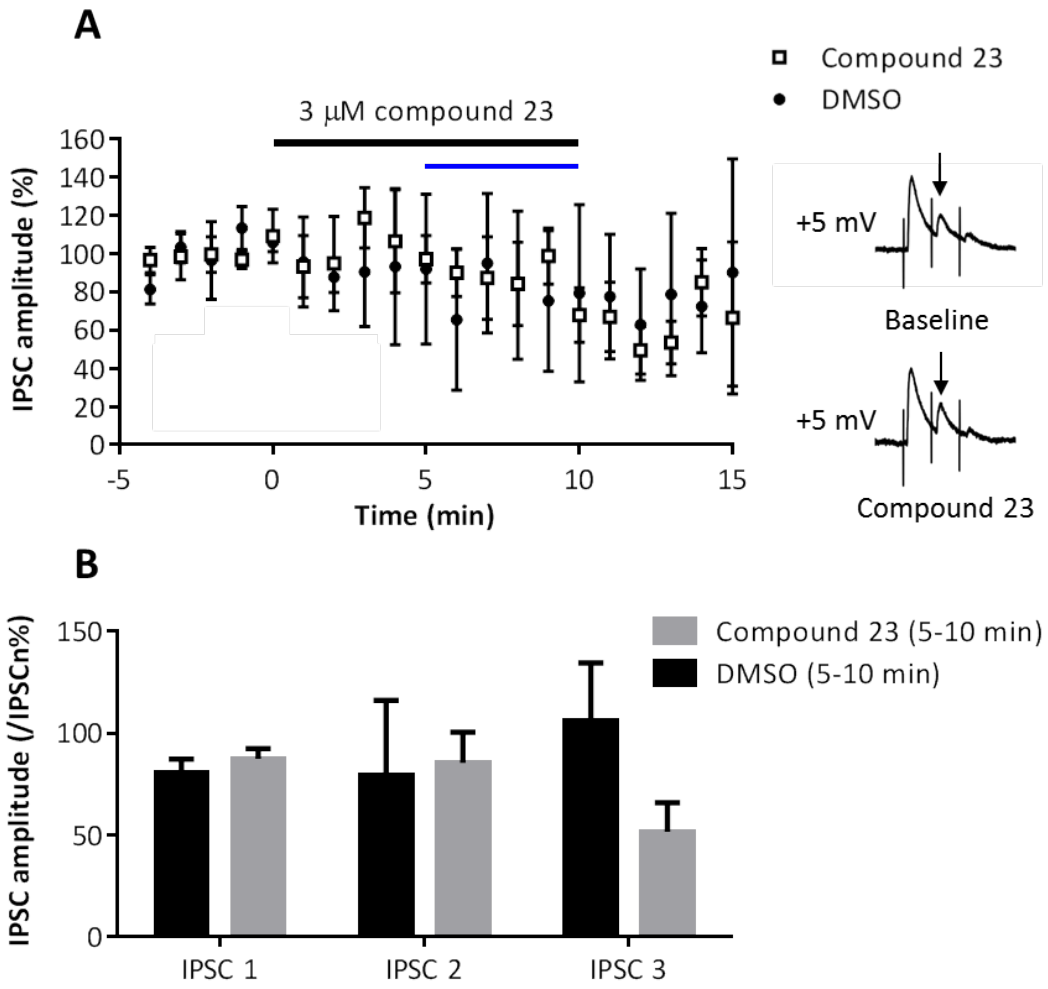

Figure 3.5 More potent TASK-1/3 channel blocker compound 23 does not affect PV cell output during multiple stimulation A 50 Hz triplet of thalamocortical PV cell-mediated IPSCs was evoked at 0.1 Hz. (A) Timecourse of peak of 2nd IPSC in the triplet (indicated by arrow in inset) normalised to the baseline average of the first 5 min of the 2nd IPSC in the presence of DMSO or compound 23 TASK-1/3 channel blocker. Blue line represents the time period used for statistical test comparison between the two groups. (B) Averages of 1st, 2nd, and 3rd IPSCs during last 5-10 min of DMSO or compound 23 treatment normalised to the baseline average of the first 5 min of their respective IPSCs. Data as means ± SEM. n=4 cells for DMSO, n=6 cells for compound 23.

Given the lack of an effect of A293 on the amplitude of IPSCs, other structurally unrelated TASK-1/3 channel blockers were tested. The drug compound 23 has been demonstrated to be a more specific and much more potent TASK-1/3 channel blocker than A293 (Coburn et al. 2012). Although the mechanism for blocking TASK-1/3 channels is not fully understood in both agents, they are structurally dissimilar from each other (see section **1.3.8**), and therefore offer alternative approaches in blocking TASK-1/3 channels. This would help verify the results observed with A293. Compound 23 has IC_{50}s of 0.3 μM and 0.035 μM for TASK-1 and TASK-3, respectively (Coburn et al. 2012). 3 μM of compound 23 was used in all experiments (tenfold of the IC_{50} value for TASK-1 and a hundredfold of the IC_{50} value for TASK-3). This increase in potency was to assure that all TASK-1 and TASK-3 channels were completely blocked.

Compound 23 equally failed to influence PV cell output in response to stimulation at 50 Hz (Fig 3.5). Again, none of the three IPSCs in the triplet were altered by the more potent TASK-1/3 channel blocker between drug and DMSO (Mean amplitude 5-10 min after application as a percentage of baseline of respective IPSC 0-5 min before application. IPSC 1, DMSO: 88.3% ± 7.6; Compound 23: 87.4% ± 5.1; $p>0.99$. IPSC 2, DMSO: 79.6% ± 36.6; Compound 23: 85.5% ± 15.0; $p=0.18$. IPSC 3, DMSO: 105.9% ± 28.7; Compound 23: 51.6% ± 14.3; $p=0.09$. $n=4$ cells for DMSO, $n=6$ cells for A293, Two-way ANOVA with Bonferroni correction; Fig 3.5 B).

3.3 Effects of TASK channel blockers on PV cell excitability

As both TASK-1/3 channel blockers A293 and compound 23 did not appear to increase the output of PV cells, it was imperative to look more closely at PV cells themselves. It would be expected that the blockade of a key K^+ channel thought to be important in the maintenance of the background K^+ conductance would result in membrane depolarisation and an increase in input resistance. PV cells are presumed

to express a high level of TASK-1/3 channels (Goldberg et al. 2011; Okaty et al. 2009) and should therefore depolarise and increase in input resistance during the application of a TASK-1/3 channel blocker. To test if this was the case, direct PV cell recordings were performed to observe the effects of TASK-1/3 channel blockers on their RMP and input resistance.

Recordings were performed on PV cells which displayed electrophysiological properties typical of the fast-spiking cell type. These included rapid firing frequencies (>120 Hz), short width action potentials (<0.6 ms) and deep AHPs with fast rise times in response to strong current injection (Erisir et al. 1999; Rudy et al. 2001). In the majority of experiments, mice with a PV-Cre knocking allele containing the endogenous PV promotor were crossed with lox-P flanked EYFP mice generating PV/EYFP reporter mice. This enabled visualisation of PV cells under blue light, allowing them to be targeted for direct recordings.

3.3.1 TASK-1/3 channel blockers have no effect on RMP and input resistance in PV cells in cortex

Recordings were carried out in thalamocortical slices and in the same region of the cortex. PV cells were targeted in layer IV of the barrel cortex and recorded in current clamp configuration to determine RMP as well as input resistance. Both parameters were monitored to ensure a stable 5 min baseline was acquired before a TASK-1/3 channel blocker was applied. Once again, trials were interleaved between drug treatment and DMSO (control), and their effect on RMP and input resistance was compared between the groups.

When compared between control and drug groups, the potent TASK-1/3 channel blocker compound 23 did not alter the RMP or input resistance (Fig 3.6). No significant difference in RMP was found between DMSO and compound 23 (Difference in mean potential 5-10 min after application from baseline 0-5 min

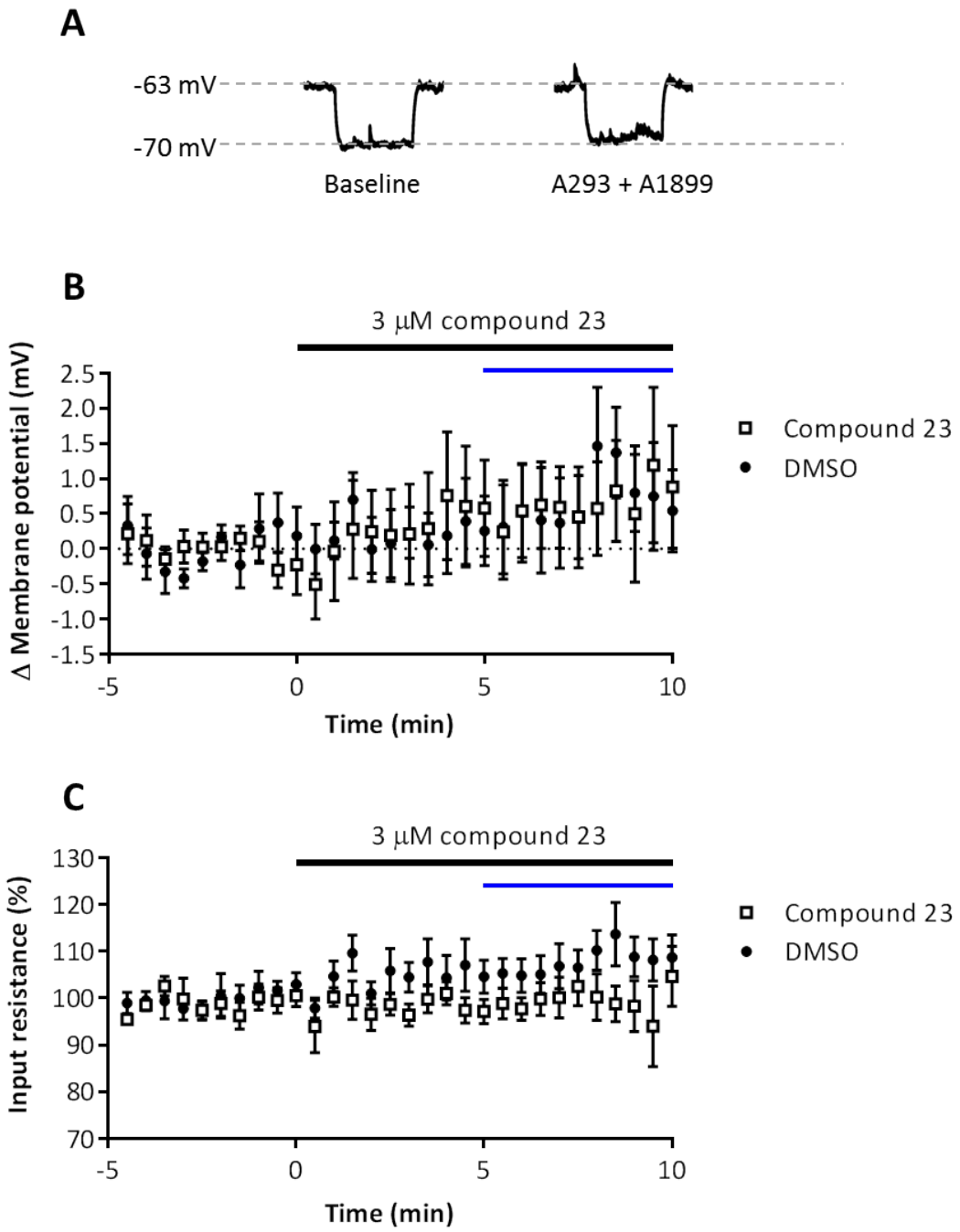

Figure 3.6 TASK-1/3 channel blocker compound 23 does not alter PV cell RMP or input resistance Example voltage traces (A) and timecourse of whole-cell current clamp recordings of PV cells showing RMP (B) and input resistance (C) in the presence of compound 23. Blue line represents the time period used for statistical test comparison between the two groups. Data as means ± SEM. n=7 cells for DMSO, n=8 cells for compound 23.

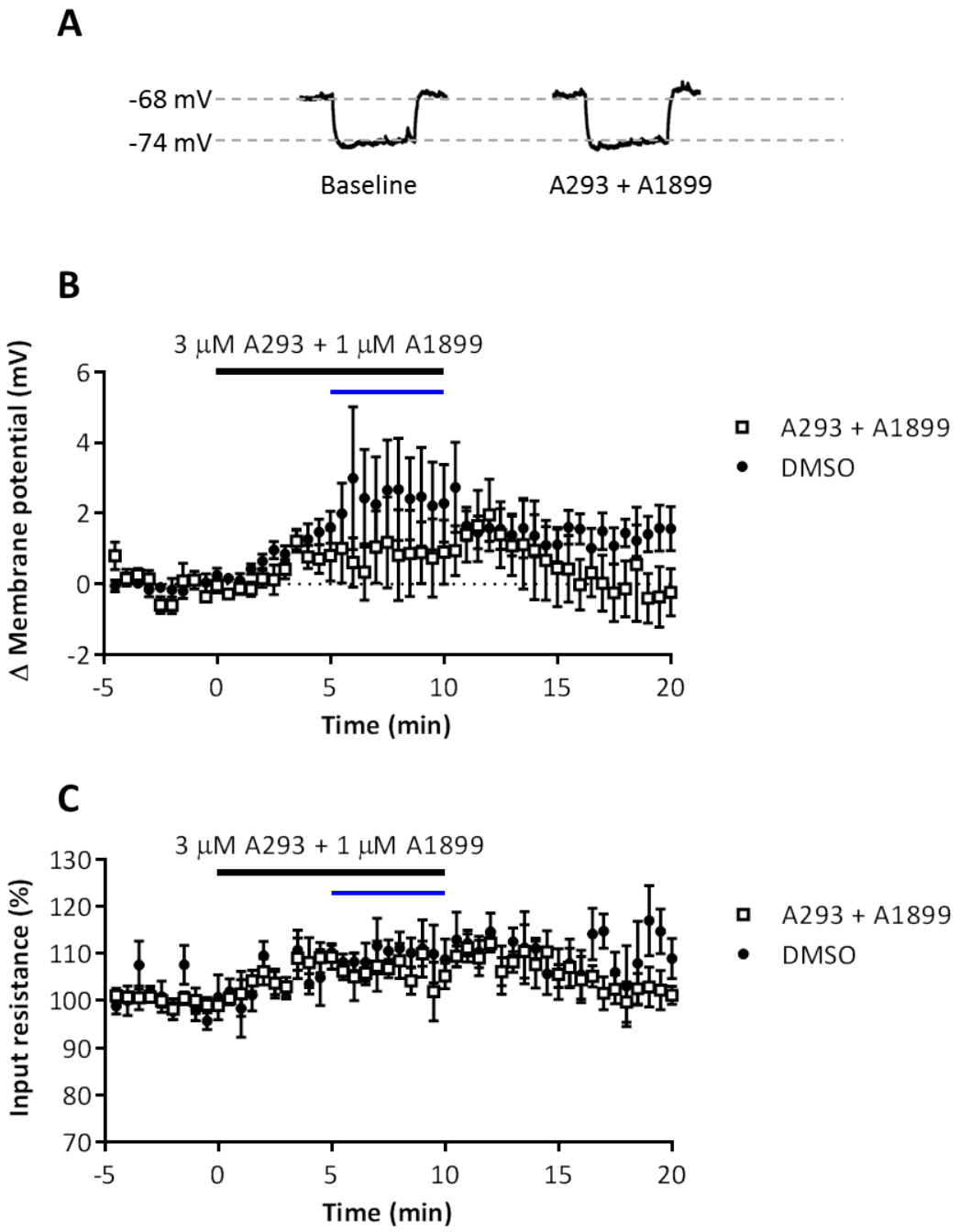

Figure 3.7 TASK-1/3 channel blockers A293 and A1899 does not alter PV cell RMP or input resistance Example voltage traces (A) and timecourse of whole-cell current clamp recordings of PV cells showing RMP (B) and input resistance (C) in the presence of A293 and A1899 (0-10 min). Blue line represents the time period used for statistical test comparison between the two groups. Data as means ± SEM. n=6 cells for DMSO, n=5 cells for A293/A1899.

before application, DMSO: 0.7 ± 0.6 mV, n=7 cells; Compound 23: 0.6 ± 0.7 mV, n=8; p=0.92, Student's unpaired *t*-test; Fig 3.6 B). Importantly, both groups displayed similar absolute RMP values confirming that similar populations of cells were sampled in each group (Mean baseline potential, DMSO: -69.6 ± 2.5 mV, n=7 cells; Compound 23: -64.8 ± 1.4 mV, n=8 cells; p=0.08, Student's unpaired *t*-test). Similarly, no significant difference in input resistance was found between the two groups (Mean resistance 5-10 min after application as a percentage of baseline 0-5 min before application, DMSO: 107.9% ± 4.0, n=7 cells; Compound 23: 99.6% ± 4.1, n=8 cells; p=0.15, Student's unpaired *t*-test (Fig 3.6 C).

To further validate these results, two other TASK-1/3 channel blockers were applied together to establish their effects on RMP and input resistance. 3 μM A293 was combined with the 1 μM of the TASK-1/3 channel blocker A1899. IC_{50} values for A1899 were 0.035 μM and 0.32 μM for TASK-1 and TASK-3 respectively, at heterologously expressed TASK channels in Xenopus oocytes (Streit et al. 2011). Once again, the combined application of A293 and A1899 did not alter the RMP or input resistance between control and drug groups (Fig 3.7). No significant difference in RMP was found between DMSO and A293/A1899 (Difference in mean potential 5-10 min after application from baseline 0-5 min before application, DMSO: 2.4 ± 1.3 mV, n=6 cells; A293/A1899: 0.8 ± 0.9 mV, n=5; p=0.32, Student's unpaired *t*-test; Fig 3.7 B). Both groups displayed similar absolute RMP values (Mean baseline potential, DMSO: -70.3 ± 2.3 mV, n=6 cells; A293/A1899: -66.4 ± 1.5 mV, n=5 cells; p=0.17, Student's unpaired *t*-test). Similarly, no significant difference in input resistance was found between the two groups (Mean resistance 5-10 min after application as a percentage of baseline 0-5 min before application, DMSO: 109.8% ± 2.9, n=6 cells; A293/A1899: 106.2% ± 2.6, n=5 cells; p=0.34, Student's unpaired *t*-test; Fig 3.7 C).

3.3.2 Acidification and bupivacaine depolarises RMP and increases input resistance in PV cells

As three different TASK-1/3 channel blockers had no effect on the RMP and input resistance in PV cells, it was important to determine whether it was possible to detect the effects of TASK blockade with this recording procedure. Since TASK-1/3 channels mediate K^+ efflux at rest, a control experiment was performed to test whether the blockade of background K^+ currents could be detected through changes in the RMP and input resistance. A control leak potassium channel blocker was used to confirm whether it was possible to detect the effects of blocking a large population of the background K^+ conductance in this recording procedure. Problems in the experimental procedure could have impacted a potential effect of the drug which may have masked its overall outcome. A positive control was therefore used to confirm that changes in the RMP and input resistance could reliably be measured in PV cell recordings.

Extracellular acidification (pH 6.4) and the anaesthetic bupivacaine are known to strongly inhibit background TASK-like currents, typical of most K_{2P} channels with open rectification properties (Taverna et al. 2005; Torborg et al. 2006). The blockade of the TASK-like conductance should dramatically depolarise the RMP and increase the input resistance in PV cells.

Extracellular acidification (pH 6.4) and bupivacaine were applied separately for 10 min after the initial 5 min baseline period was established in PV cells. Although the effects of acidification were obtained from the last 5 min of the treatment, the effects of bupivacaine were instead obtained from the last 2 min of drug application as it did not plateau until the last 2 min. As bupivacaine is known to block voltage-gated Na^+ channels (Olschewski et al. 1998; Zhang et al. 2014), QX314 was included in the internal pipette solution to ensure full blockade of Na^+ channels prior to the start of recordings. A robust depolarisation of the RMP and a strong increase in input resistance was confirmed from these recordings (Fig 3.8). The RMP was

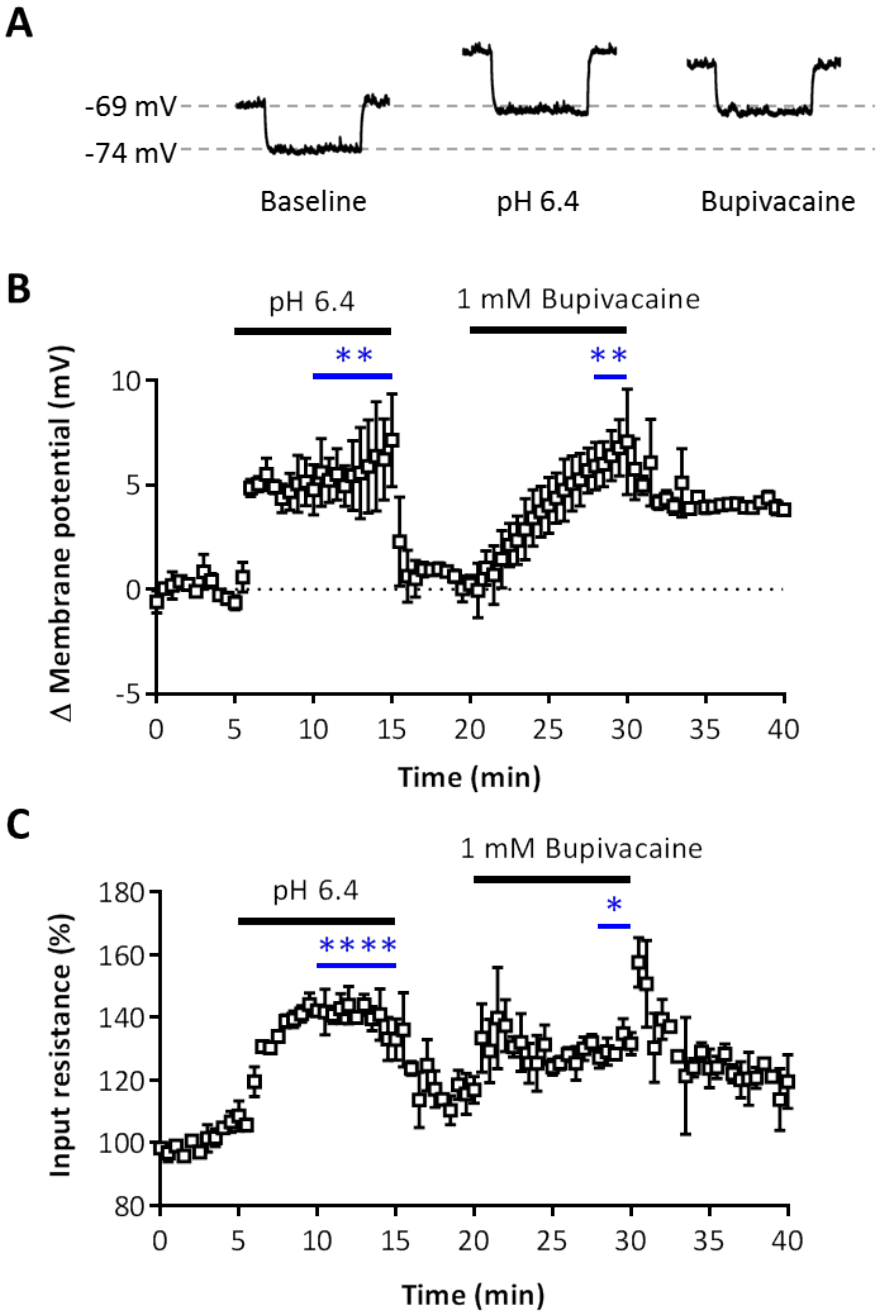

Figure 3.8 Acidification and bupivacaine depolarises RMP and increases input resistance in PV cells External pH 6.4 and the anaesthetic bupivacaine strongly inhibits the TASK-like conductance. Example voltage traces (A) and timecourse of whole-cell current clamp recordings of PV cells showing RMP (B) and input resistance (C) in the presence of pH 6.4 (5-15 min) and bupivacaine (20-30 min). Statistical test performed between treatment effect (blue line) and pretreatment control period. Data as means ± SEM. n=3 cells; *p<0.05, **p<0.01, ****p<0.0001 (One-way RM-ANOVA with Bonferroni correction) compared to the corresponding pretreatment control period.

significantly depolarised between baseline and pH 6.4 conditions (Difference in mean potential at pH 6.4 5-10 min after application from baseline 0-5 min before application: 5.6 ± 1.6 mV; n=3 cells, p=0.008, One-way RM-ANOVA with Bonferroni correction; Fig 3.8 B) and between baseline and bupivacaine (Difference in mean potential 8-10 min after application from baseline 0-2 min before application, Baseline: 0.4 ± 0.4 mV; Bupivacaine: 6.3 ± 1.1 mV; n=3 cells, p=0.006, One-way RM-ANOVA with Bonferroni correction; Fig 3.8 B). Furthermore, the input resistance was significantly increased between baseline and pH 6.4 conditions (Mean resistance at pH 6.4 5-10 min after application as a percentage of baseline 0-5 min before application: 140.0% ± 3.2; n=3 cells, p<0.0001, One-way RM-ANOVA with Bonferroni correction; Fig 3.8 C) and between baseline and bupivacaine (Mean resistance 8-10 min after application as a percentage of baseline 0-2 min before application, Baseline: 115.2% ± 4.3; Bupivacaine: 129.9% ± 0.8; n=3 cells, p=0.01, One-way RM-ANOVA with Bonferroni correction; Fig 3.8 C). This result confirms that a general blockade of background currents can be targeted, and importantly, that this blockade can be detected from changes in the RMP and input resistance.

3.3.3 Compound 23 has no effect on RMP and input resistance in PV cells in CA1 hippocampus

Neurons display distinct molecular profiles depending on their location within the brain (Ko et al. 2013). It is well established that the molecular expression of various proteins including ion channels can be different between brain regions, which may be contingent on a number of circumstances including growth factors during development as well as other molecular cues in the extracellular environment (Sharma et al. 2015; Ko et al. 2013). Different ratios of specific K_{2P} channel subfamilies within different brain areas could explain why some cells would be responsive to their blockade and why some would not. For example, a larger proportion of the leak conductance could be mediated by TREK-1 channels relative to TASK-1/3 channels in the cortex, whereas in the hippocampus this relative proportion might be inversed.

Given that the blockade of TASK-1/3 channels did not alter the intrinsic properties of PV cells in the cortex, the effects of TASK-1/3 blockers on PV cells in other brain areas were explored. In situ hybridisation studies reported TASK-1 and TASK-3 mRNA expression throughout the hippocampus (Talley et al. 2001). Moreover, mRNA expression was also detected in cells – presumably interneurons – in nonpyramidal layers of the hippocampus (Talley et al. 2001). Furthermore, the effect of the TASK-1/3 channel blocker compound 23 was reported to depolarise the RMP in putative fast-spiking cells in CA1 stratum oriens by a collaborator (Keith Phillips, Eli Lilly, data not shown). A set of recordings was therefore performed on PV cells in CA1 to compare results. At the end of each experiment, the acidification control was applied to further validate the presence of a TASK-like conductance in the recordings.

The application of the TASK-1/3 channel blocker compound 23 did not alter the RMP or input resistance in hippocampal PV cells (Fig 3.9). No significant difference in RMP was found between baseline and drug (Difference in mean potential 5-10 min after compound 23 application from baseline 0-5 min before application: 0.5 ± 0.4 mV; n=5 cells, p=0.78, One-way RM-ANOVA with Bonferroni correction; Fig 3.9 B). Similarly, there was no change in input resistance between baseline and drug (Mean resistance 5-10 min after compound 23 application as a percentage of baseline 0-5 min before application: 113.8% ± 5.3; n=5 cells, p=0.27, One-way RM-ANOVA with Bonferroni correction; Fig 3.9 C).

As predicted, the acidification control significantly depolarised the RMP of PV cells (Difference in mean potential 3-5 min after application from baseline 0-2 min before application, Baseline: 0.3 ± 0.6 mV; pH 6.4: 8.0 ± 0.7 mV; n=5 cells, $p<0.0001$, One-way RM-ANOVA with Bonferroni correction; Fig 3.9 B) in addition to increasing the input resistance (Mean resistance 3-5 min after application as a percentage of baseline 0-2 min before application, Baseline: 110.4% ± 3.6; pH: 140.2% ± 13.5; n=5 cells, p=0.008, One-way RM-ANOVA with Bonferroni

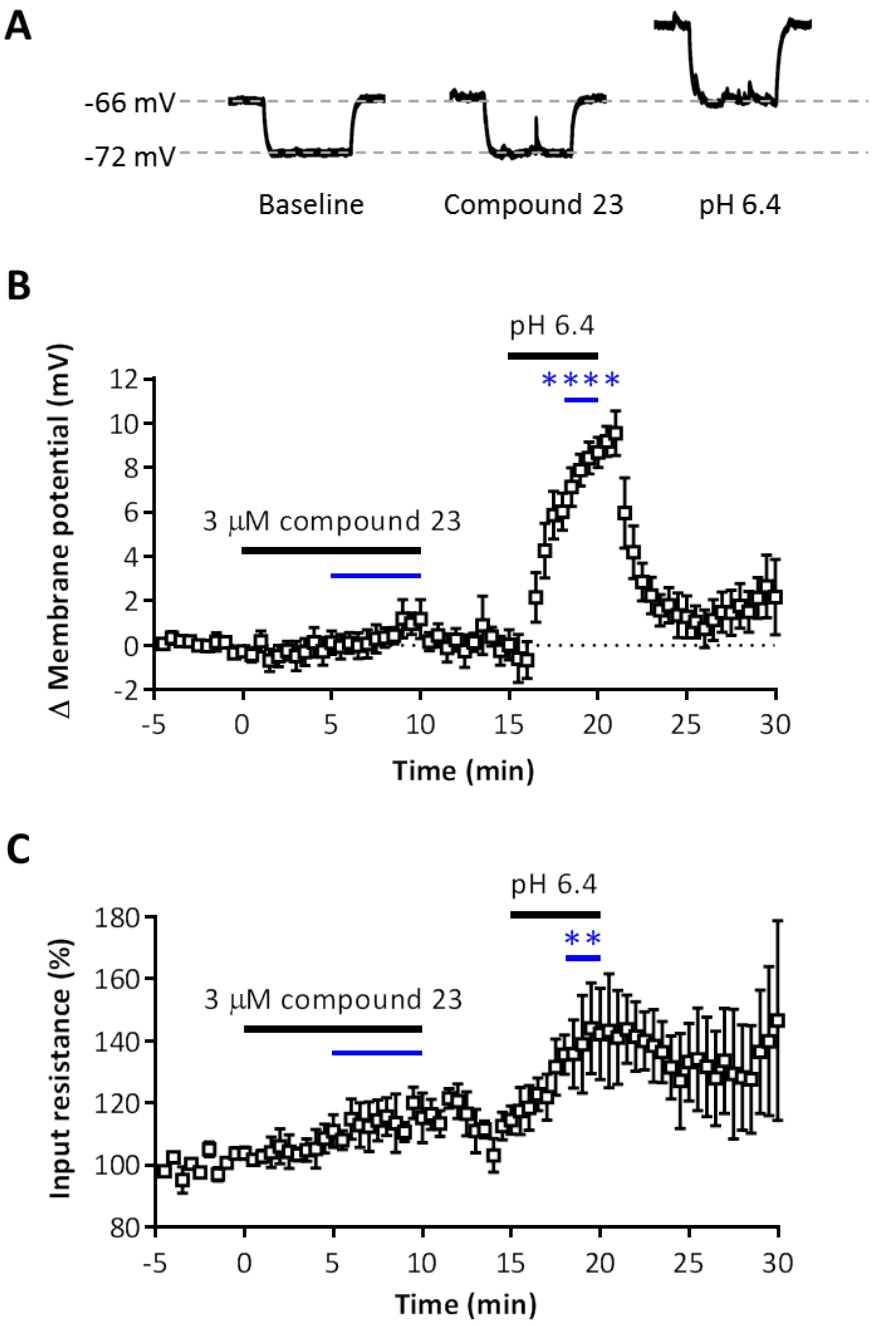

Figure 3.9 TASK-1/3 channel blocker compound 23 does not alter PV cell RMP or input resistance in CA1 hippocampus Example voltage traces (A) and timecourse of whole-cell current clamp recordings of PV cells in CA1 hippocampus showing RMP (B) and input resistance (C) in the presence of compound 23 (0-10 min) and pH 6.4 (15-20 min). Concentration of DMSO was kept constant throughout the experiment. Statistical test performed between treatment effect (blue line) and pretreatment control period. Data as means ± SEM. n=5 cells; **p<0.01, ****p<0.0001 (One-way RM-ANOVA with Bonferroni correction) compared to the corresponding pretreatment control period.

correction; Fig 3.9 C), confirming that a TASK-like conductance remains present in PV cells that was not blocked by compound 23.

3.3.4 TASK-1/3 channel blockers have no effect on gamma oscillation power in CA3 hippocampus

Gamma oscillations (30-80 Hz) are a hallmark of neuronal network function in a number of brain areas including the thalamus, hippocampus and neocortex (Buzsaki & Draguhn 2004). This fast network activity predominantly mediated by PV cell firing (Cardin et al. 2009), contributes to the pacing of pyramidal cell ensembles to fire simultaneously. This activity can be extracellularly recorded *in vitro* in response to the bath application of the cholinergic agonist carbachol. Moreover, although no effect on PV cell activity was established with TASK-1/3 channel blockers, compound 23 was reported to reduce gamma power in carbachol (30 μM)-induced gamma oscillations in CA3 hippocampus by a collaborator (Keith Phillips, Eli Lilly, data not shown). Thus, as a positive control, a set of experiments were performed in CA3 hippocampus, where oscillatory activity can be generated relatively easily.

Horizontal slices were prepared and perfused with 30 μM of carbachol at a high flow rate (10-12 ml/min). Extracellular network oscillations were measured using a field electrode placed in the pyramidal cell layer of CA3. Compound 23 was applied for 10 min three times in 10 min intervals and the power of gamma oscillations was analysed (Fig 3.10). The 35-50 Hz frequency band was used for gamma oscillation analysis as this was the range that consistently displayed the highest power between recordings (Green bars in power vs frequency histogram; Fig 3.10 A). Compound 23 did not alter the power of gamma oscillations in the 35-50 Hz band (Mean power during last 5-10 min of each drug treatment period as a percentage of the mean power during last 5-10 min of each control period: 92.5% ± 9.1; n=8 recordings, p=0.21, Student's paired *t*-test; Fig 3.10 D).

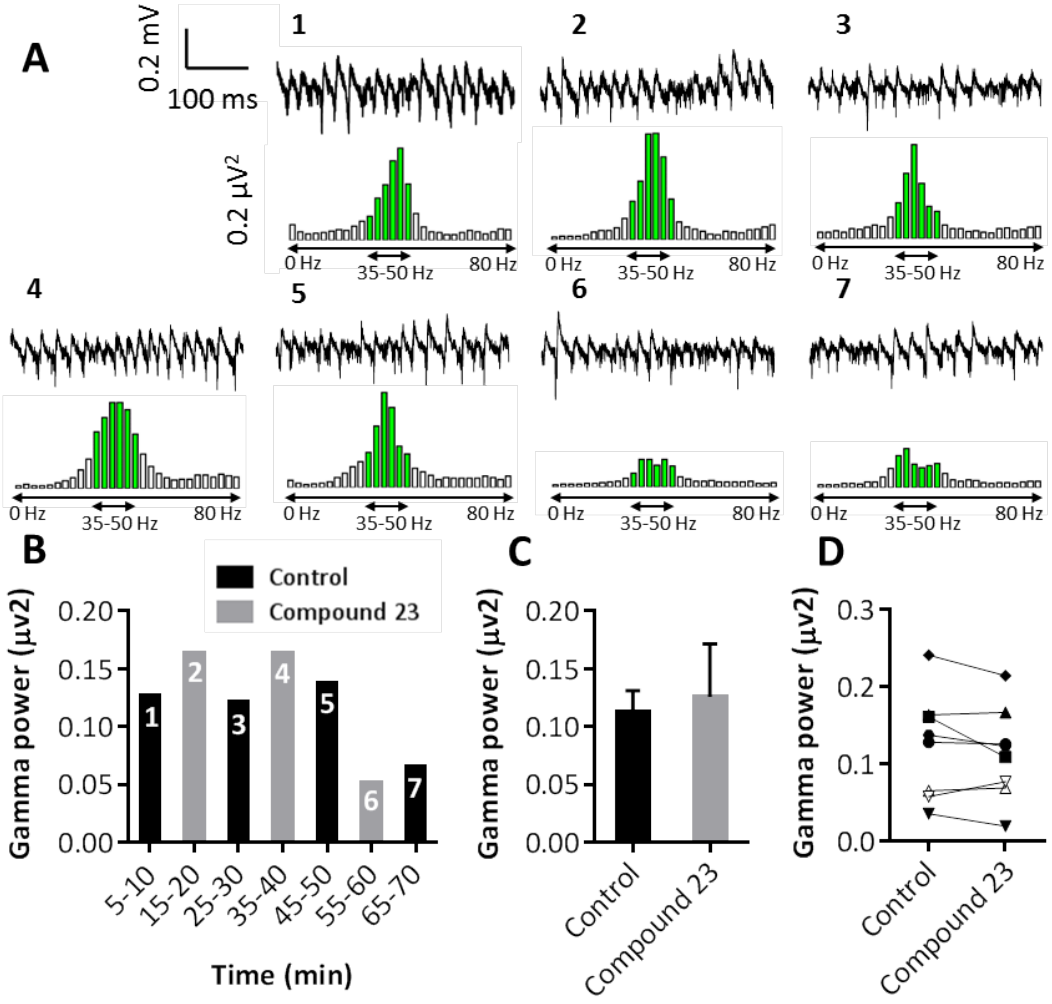

Figure 3.10 TASK-1/3 channel blocker compound 23 does not affect gamma oscillation power in CA3 hippocampus Extracellular field recordings of carbachol-induced gamma oscillations. Compound 23 was applied in 10 min intervals, interleaved with control recording solution. (A) Example traces (top) and power vs binned frequency plots (bottom) at seven consecutive time periods within a recording, as indicated in B. X-axis frequency range 10-80 Hz in 2.4 Hz bins. Green bars indicate gamma bands used for analysis (35-50 Hz). (B) Mean gamma power (35-50 Hz) vs time at the seven time periods in the same recording. (C) Mean gamma power (35-50 Hz) between time periods 1,3 and 5 (control) compared to means of 2,4 and 6 (compound 23) in the same recording. (D) Grouped data of gamma power (35-50 Hz) between baseline and compound 23. Each symbol type represents a different cell. Concentration of DMSO was kept constant thought the experiment. Data as means ± SEM. n=7 recordings.

3.4 Analysis of efficacy of TASK channel blockers

The TASK-1/3 channel blockers A293, A1899 and compound 23 produced no effect on the RMP and input resistance, while the latter two blockers also failed to influence the output of PV cells. Moreover, the corresponding hippocampal data on the effects of compound 23 on the RMP of PV cells in CA1 combined with its effects on gamma oscillations in CA3 did not match between the results in this thesis and results attained from a collaborator (Keith Phillips, Eli Lilly). The effects of compound 23 were therefore assayed in a heterologous system where TASK channels are known to be expressed.

3.4.1 Effects of TASK-1/3 channel blocker compound 23 on heterologously expressed TASK-3 in HEK-293 cells

HEK-293 cells were transfected with TASK-3 constructs to produce cells expressing functional TASK-3 channels. These cells were subsequently patched between 24-72 hours after transfection. The RMP and input resistance was monitored and a 5 min baseline was established before the TASK-1/3 channel blocker compound 23 was applied. Untransfected cells which underwent the same transfection process as transfected cells but with the absence of TASK-3 cDNA in the transfection mix were used as a control.

Current clamp recordings revealed that compound 23 significantly depolarised the RMP between untransfected cells and transfected TASK-3 cells (Difference in mean potential 3-5 min after application from baseline 0-2 min before application, Untransfected: 4.2 ± 1.6 mV, n=7 cells; Transfected: 27.2 ± 2.8 mV, n= 4 cells; $p<0.0001$, Two-way RM-ANOVA with Bonferroni correction; Fig 3.11 B) while the acidification control had a similar effect (Difference in mean potential 3-5 min after application from baseline 0-2 min before application, Untransfected: 0.3 ± 2.2 mV,

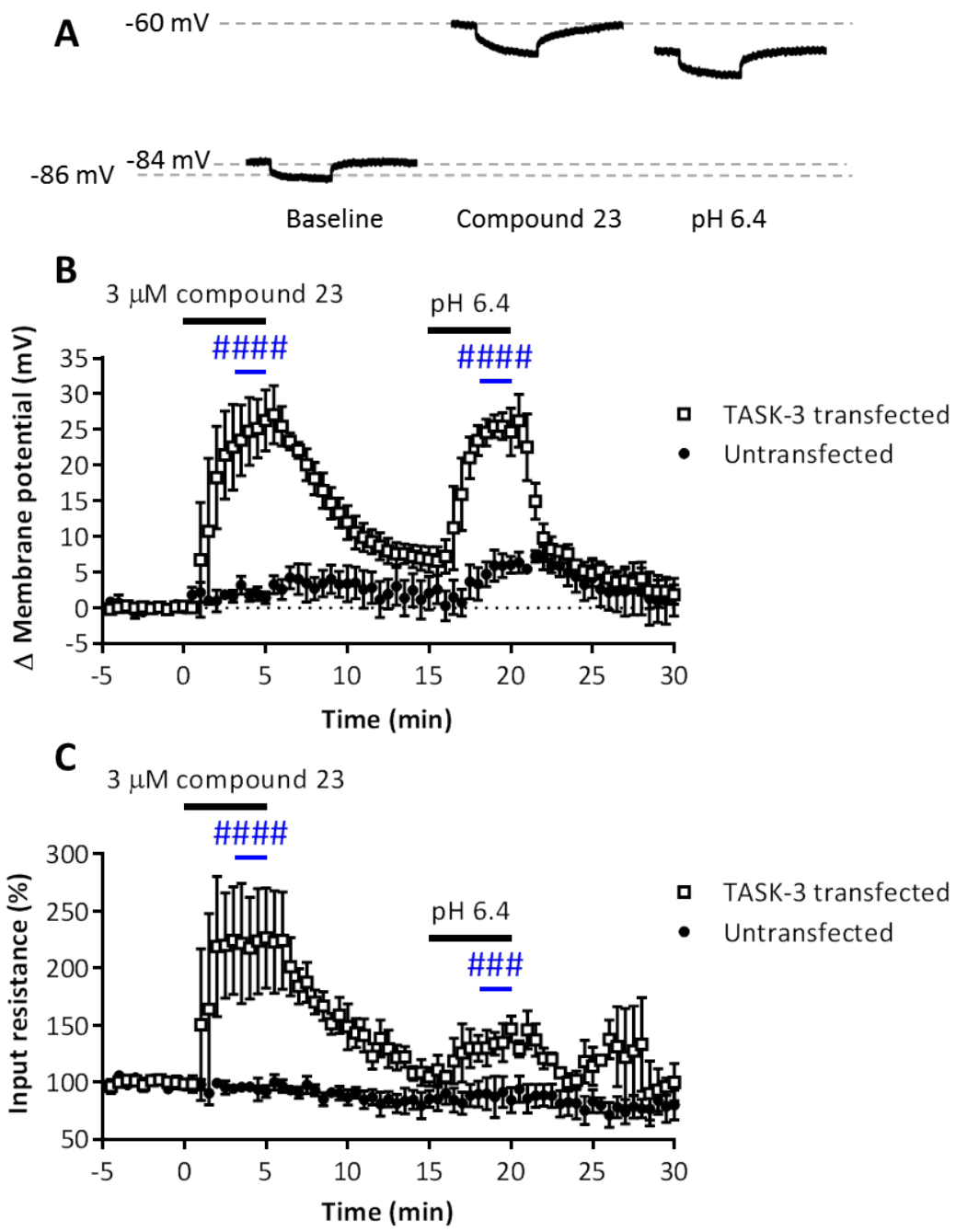

Figure 3.11 TASK-1/3 channel blocker compound 23 depolarises RMP and increases input resistance in HEK 293 cells expressing TASK-3 Example voltage traces (A) and timecourse of whole-cell current clamp recordings of HEK 293 cells expressing TASK-3 showing RMP (B) and input resistance (C) in the presence of compound 23 (0-5 min) and pH 6.4 (15-20 min). Concentration of DMSO was kept constant throughout the experiment. Blue line represents the time period used for statistical test comparison between the two groups. Data as means ± SEM. n=6 for untransfected cells, n=4 for transfected cells; ###p<0.001, ####p<0.0001 (Two-way RM-ANOVA with Bonferroni correction) compared between transfected and untransfected groups.

n=7 cells; Transfected: 29.6 ± 3.8 mV, n=4 cells; p<0.0001, Two-way RM-ANOVA with Bonferroni correction; Fig 3.11 B).

Furthermore, compound 23 also significantly increased the input resistance between untransfected cells and transfected TASK-3 cells (Mean resistance 3-5 min after application as a percentage of baseline 0-2 min before application, Untransfected: 96.4% ± 3.0, n=7 cells; Transfected: 223.5% ± 21.9, n=4 cells; p<0.0001, Two-way RM-ANOVA with Bonferroni correction; Fig 3.11 C) while the acidification control again had a similar effect (Mean resistance 3-5 min after application as a percentage of baseline 0-2 min before application, Untransfected: 107.3% ± 7.5, n=7 cells; Transfected: 170.2% ± 38.8, n=4 cells; p=0.0005, Two-way RM-ANOVA with Bonferroni correction; Fig 3.11 C)

These results validate that compound 23 effectively blocks TASK-3 channels and therefore it can be assumed to be a functional blocker. The similar magnitude of RMP depolarisation between compound 23 and the acidification control in transfected TASK-3 cells further supports its functional efficacy suggesting that it fully blocks all TASK-3 channels that the acidification control is blocking (Difference in mean potential 3-5 min after application from baseline 0-2 min before application, Compound 23: 27.2 ± 2.8 mV; pH 6.4: 29.6 ± 3.8 mV, n=4 cells; p=0.47, Student's paired *t*-test). Despite this conclusion, pharmacological occlusion experiments between compound 23 and external acidification would be required to confirm this.

Finally, to confirm that the effect of compound 23 is mediated by the blockade of an outward cation current, a single TASK-3-transfected HEK-293 cell and a single control HEK-293 cell were voltage-clamped at -70 mV to monitor the effect of the blocker. As expected, the blockade of TASK-3 channels in the TASK-3-transfected cell was paralleled by a strong inward current in the presence of compound 23

(Holding current before application: 295.7 pA; holding current after application: -119.9 pA; Fig 3.12 A) and during acidification (Holding current before application: 165.3 pA; holding current after application: -59.5 pA; Fig 3.12 A). As expected, the holding current required to voltage clamp the untransfected cell at -70 mV was unaffected. The current-voltage relationship of the same TASK-transfected cell in response to a set of voltage steps again indicated that compound 23 and acidification had similar effects in reducing TASK-3-mediated currents (Mean current amplitude during last 5-10 min of each condition, Baseline: 0.46 nA; Spadin: 0.20 nA; pH 6.4: 0.23 nA; Fig 3.12 B).

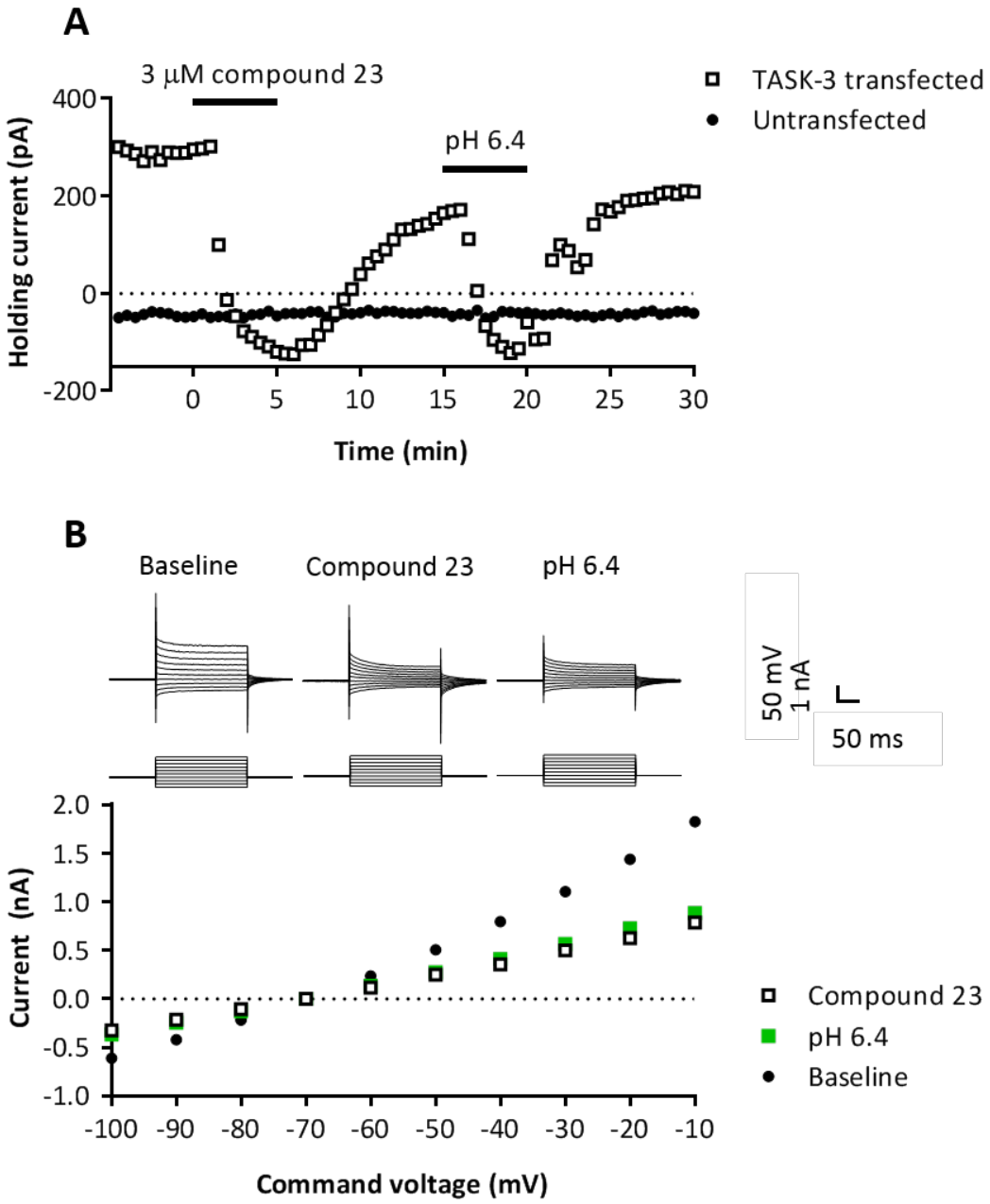

Figure 3.12 Effects of TASK-1/3 channel blocker compound 23 on the current/voltage relationship in a HEK 293 cell expressing TASK-3 Whole-cell voltage clamp recordings of a HEK 293 cell expressing TASK-3 and an untransfected HEK 293 cell. (A) Timecourse of holding currents in a cell expressing TASK-3 and in an untransfected cell voltage-clamped at -70 mV in the presence of compound 23 (0-5 min) and pH 6.4 (15-20 min). (B) Bottom, current/voltage relationship of the same TASK-3-transfected cell in response to a set of voltage steps (200 ms, -100 mV to -10 mV, Δ10 mV) from a holding potential of -70 mV. Top, example traces of TASK-3-mediated currents to the same voltage steps for baseline, compound 23 and pH 6.4 conditions.

3.5 Discussion

In this chapter, I demonstrated that the blockade of TASK-1/3 channels has no effect on the RMP or input resistance in PV cells in the somatosensory cortex and CA1 hippocampus, and therefore does not increase their excitability, contrary to what was predicted. This finding was further validated by the failure of TASK-1/3 channel blockers to increase the amplitude of PV cell-mediated IPSCs. These results were surprising given the high level of TASK-1 and TASK-3 mRNA expression in PV cells (Goldberg et al. 2011; Okaty et al. 2009), as the blockade of TASK-1/3 channels would have been expected to increase cell excitability due to their contribution to the passive background K^+ conductance. A set of positive controls which included extracellular acidification and bupivacaine treatment known to target most K_{2P} channels with open rectification properties demonstrated that blocking this TASK-like conductance had the expected effects on PV cells and that these effects could be measured. Moreover, the TASK-1/3 channel blocker compound 23 failed to alter the power of network gamma oscillations, contrary to results obtained with the same drug from a collaborator (Keith Phillips, Eli Lilly). The efficacy of compound 23 was therefore assayed in TASK-3-expressing HEK-293 cells to confirm that it was indeed an effective TASK channel blocker. It remains possible however that the discrepancy in the effect of compound 23 between PV cells in mice and HEK-293 cells could be explained by differences in the accessibility of the drug between the two systems, or even by differences in the molecular composition of the channels. Native channels in mice are likely to be bound by different subunits which could alter their pharmacological profile. Nonetheless, as all TASK-1/3 channel blockers failed to induce changes in all parameters tested in this chapter, it is likely that the blockers are functional and that the results are consistent with the absence of TASK-1/3 channels in PV cells. In summary, these results confirm that TASK-1/3 channels are either not functionally expressed, or present at extremely low levels relative to other background K^+ channels in PV cells.

3.5.1 TASK-like conductance in PV cells mediated by K_{2P} channels other than TASK-1/3

Whilst the TASK-1/3 channel blockers A293, A1899 and compound 23 did not alter the RMP and input resistance in PV cells, both bupivacaine and acidification controls significantly depolarised the RMP and increased the input resistance in the same population of cells. The bupivacaine- and acid-sensitive background K^+ conductances typically mediated by TASK-like channels function to reduce the input resistance in most cell types (Taverna et al. 2005; Torborg et al. 2006). These results thus confirm two functional properties attributable to PV cells: Firstly, PV cells do not express a large enough population of functional TASK-1/3 channels to significantly modulate the background K^+ conductance that regulates their RMP. Secondly, the RMP in PV cells is evidently maintained by other bupivacaine- and acid-sensitive background conductances.

PV cells have an unusually low input resistance compared to pyramidal cells and other interneurons (Doischer et al. 2008; Taverna et al. 2005). This makes the lack of effect of compound 23 on PV cells even more surprising, especially because of the considerable magnitude of effect observed with both bupivacaine and acidification on the RMP and input resistance. This suggests that there is still a large contribution of background K^+ channels mediating the TASK-like conductance responsible for their low membrane resistivity.

Although bupivacaine and acidification depolarised the RMP by approximately 6 mV and increased the input resistance by approximately 30-40%, it is important to clarify that both these conditions affect many proteins within the membrane other than TASK. Bupivacaine blocks several other channels within the K_{2P} family including TREK-1 and TWIK-1 (Kindler et al. 1999), highlighting other functional background K^+ channels that could be regulating the membrane potential and membrane resistivity in PV cells. In addition to blocking TASK-like channels, bupivacaine also blocks voltage-gated Na^+ channels with high potency (Olschewski

et al. 1998; Zhang et al. 2014) in addition to blocking both high and low voltage-activated Ca^{2+} channels to a lesser effect (Liu et al. 2001). Although the voltage-gated Na^{+} channel blocker QX314 was included in the internal pipette solution to compensate for the blocking action of bupivacaine on Na^{+} channels, other non-specific mechanistic effects may not have been accounted for. Local anaesthetics including bupivacaine have been shown to interact with membrane phospholipids and proteins which can act on a variety of cellular processes. For example, local anaesthetics can modify the signalling of NMDA receptors (Furutani et al. 2010), as well as the signalling of protein kinase C (PKC), adenosine 3', 5'-cyclic monophosphate-dependent kinases (PKAs) and guanosine triphosphate-binding proteins (G proteins) including downstream receptors that they activate (Yanagidate & Strichartz 2006). Electrophysiologically, this could lead to altered levels of intracellular Ca^{2+} which could affect the RMP in addition to the input resistance, as Ca^{2+}-activated K^{+} channels would also be affected (Johnson et al. 2002).

Furthermore, acidification modulates several acid-sensing and proton-sensing channels within the cellular membrane (Wang & Xu 2011). Protons have been shown to decrease neurotransmitter release in presynaptic terminals through feedback inhibition of voltage-gated Ca^{2+} channels and reduce the activity of NMDA receptors in the postsynaptic terminals (Tang et al. 1990; DeVries 2001). Although these effects will not necessarily be detected in whole-cell patch clamp recordings - as glutamatergic terminals are located distally from the soma – their impact may affect other secondary messengers that could influence electrophysiological properties in the soma. Acid-sensing ion channels permeable to Na^{+} and Ca^{2+} are activated by a reduction in extracellular pH to generate rapid depolarising currents (Waldmann et al. 1997). Activation of acid-sensing ion channels has thus been demonstrated to result in substantial intracellular Ca^{2+} elevation, which may contribute to the depolarisation of the RMP observed in this thesis.

Nonetheless, two control conditions (acidification and bupivacaine) both significantly depolarised the RMP and increased the input resistance in PV cells,

consistent with the blockade of a TASK-like conductance. It therefore remains likely that although many non-specific effects of both conditions persist, they are both reasonable indicators showing the presence of a clear majority of the K^+ background conductance that remains to be targeted in PV cells. Furthermore, this suggests that the core aims of the thesis – which is to depolarise the RMP and increase the input resistance in PV cells – can be achieved using blockers that target different leak channels, but might not simply involve canonical TASK-1/3 channels. The effects of blocking other TASK-like currents such as TREK-1 could therefore be explored in PV cells.

3.5.2 Confirmation of efficacy of TASK-1/3 channel blockers

Previous studies assaying the molecular profile of PV cells confirmed the presence of TASK-1 and TASK-3 mRNAs using qPCR and microarrays from FACS-sorted PV cells (Goldberg et al. 2011; Okaty et al. 2009). Moreover, TASK-1 immunolabeling revealed an increase in TASK-1 protein expression throughout early development (Okaty et al. 2009). Although no previous work has used specific blockers to reliably demonstrate the presence of TASK-1/3 currents in PV cells, both acidification and bupivacaine conditions suggested that TASK-1/3 channels may have been functionally expressed in this cell type (Torborg et al. 2006). Furthermore, the membrane resistance of PV cells was reported to be approximately twofold larger in TASK-1/3 double knockout mice (Goldberg et al. 2011).

The lack of an effect that the TASK-1/3 channel blockers had on the RMP and input resistance of PV cells was surprising, given the evidence for TASK-1 and TASK-3 expression and the functional effects in TASK-1/3 double knockout mice. It was for this reason that the efficacy of the blocker compound 23 was tested. Nonetheless, compound 23 significantly depolarised the RMP and increased the input resistance in TASK-3-expressing HEK-293 cells, confirming that it was a successful blocker of TASK. This suggests that the increased input resistance reported in TASK-1/3 double knockout mice could be due to other developmental effects of the TASK-1/3

knockout. Another possibility could involve changes in protein-protein interactions between PV cells and HEK-293 cells, which could alter the pharmacological effects of the drug between the two systems. For example, A1899 was reported to have IC_{50}s of 0.035 μM and 0.32 μM for TASK-1 and TASK-3 respectively, at heterologously expressed TASK channels in Xenopus oocytes, whereas IC_{50}s at heterologously expressed TASK-1 and TASK-3 in Chinese hamster ovary cells were 7 nM and 70 nM respectively (Streit et al. 2011). The discrepancy in the drug affinity between both systems could also be due to differences in the molecular composition of the channels which could alter the binding efficacy of the drug.

3.5.3 The effect of compound 23 failed to replicate findings in hippocampal cells and network gamma oscillations

Prior to testing the efficacy of compound 23 on TASK-3-expressing HEK-293 cells, the effect of the drug was assessed on the power of extracellular gamma oscillations in CA3 hippocampus. This was a simple method to quickly determine the effectiveness of the compound on the rhythmic output of the neuronal network. Compound 23 was previously reported to reduce the power of carbachol-induced gamma oscillations in CA3 (Keith Phillips, Eli Lilly) whereas the results in this thesis did not show a difference. It is difficult to interpret the disparity between these results; however, it is possible that the discrepancy is due to different strains of mice used in the experiments. Mice express distinct levels of mRNA between strains, resulting in various quantities of proteins produced in the brain which can affect the downstream physiology between them (Keane et al. 2011; Korostynski et al. 2006). The fluorescent protein (EYFP) expressed in PV cells in the mice used in this thesis could have influenced the working function of PV cells which may have biased the effects of the drug. In spite of this, a subset of experiments was performed on fast-spiking interneurons from wildtype C57 mice, which displayed similar results to PV/EYFP mice, thus arguing against this possibility.

The effect of compound 23 on the RMP in hippocampal PV cells was also performed and compared with similar data from a collaborator. Compound 23 was previously reported to depolarise the RMP in PV cells in CA1 stratum oriens (Keith Phillips, Eli Lilly), whereas the results in this this thesis did not show an effect. Upon later examination of the cells that were recorded, it was clear that several cells used in the comparable data (Keith Phillips, Eli Lilly) were not exclusively fast-spiking interneurons. These included cells that displayed spike frequency adaptation and exhibited a variety of non-fast-spiking characteristics that included shallow AHPs in addition to AHPs with slow rise times. This diversity in cell population likely explains the discrepancy in the results between the two groups of data.

3.5.4 Dynamics of the output of cortical PV cells upon multiple stimulation

The excitation of thalamic fibres produces robust feedforward inhibition of neurons in layer IV of the somatosensory cortex (Daw et al. 2007). Importantly, the dynamics of thalamocortical feedforward inhibition are governed by mechanisms that extend beyond the properties of each individual synapse. Thalamocortical feedforward IPSCs have been previously shown to reduce in amplitude in response to repetitive stimulation (Gabernet et al. 2005). Whilst the ratio between peak monosynaptic EPSC and peak disynaptic feedforward IPSC conductances remain stable over a range of stimulation intensities in response to single stimulation, the balance is altered during repetitive stimulation where the amplitude of feedforward IPSCs decrease (Gabernet et al. 2005). This effect was observed in this thesis, where high frequency thalamic stimulation triggered IPSCs in voltage-clamped layer IV stellate cells that depressed in amplitude.

Paired recordings from fast-spiking cells to principal cells in layer IV revealed that trains of action potentials triggered at 10 Hz in fast-spiking cells resulted in a reduction in unitary IPSCs by approximately 50% of their original amplitude after the fifth stimulus (Gabernet et al. 2005). This reduction in IPSC amplitude is consistent with a depression in the second GABAergic synapse in thalamocortical

feedforward inhibition. Nonetheless, 10 Hz thalamic stimulation showed an even more striking reduction of approximately 90% in feedforward IPSCs in the same population of principal cells. By comparing the amplitudes of unitary monosynaptic IPSCs and thalamically evoked disynaptic IPSCs between the first and fifth IPSCs, it has been shown that by the fifth stimulus only around 20% of fast-spiking cells were activated (Gabernet et al. 2005). Thus, an effective blockade of the TASK-like conductance could have targeted this element of PV cell depression by increasing the proportion of cells that remained active during multiple stimulation. Furthermore, glutamatergic EPSCs onto fast-spiking cells were found to significantly decrease in amplitude in response to 10 Hz thalamic stimulation. It is therefore clear that although both input and output synapses of PV cells contribute to feedforward IPSCs depression, afferent thalamic stimulation onto PV cells are responsible for most of the effect.

The reduction in IPSC amplitude during multiple stimulation in this thesis can therefore be explained by the depression in one of two synapses: the glutamatergic thalamic inputs onto PV cells, or GABAergic layer IV cortico-cortical inputs from PV cells onto stellate cells. Depression of the first synapse would reduce the proportion of PV cells recruited to fire, and thus participate in the generation of feedforward transmission; whereas depression of the second synapse would directly reduce the amplitude of feedforward inhibition. Paired recordings examining the unitary monosynaptic IPSCs between layer IV PV cells and stellate cells combined with thalamically-evoked disynaptic IPSC recordings would confirm the origin of depression within the thalamocortical circuit used in this thesis.

In summary, PV cells receive thalamic EPSCs which reduce in amplitude with repeated stimulation. GABAergic transmission from PV cells is also reduced following multiple action potential firing. Due to their high probability of release, it is possible that this reduction in transmission is due to the depletion of available vesicles containing neurotransmitter. Moreover, any effect of a drug designed to

increase the excitability of PV cells may have resulted in a reduction in the magnitude of PV cell depression.

3.5.5 DMSO appears to reduce the amplitude of PV cell-mediated feedforward IPSCs

DMSO is a solvent widely employed in cell biology as an effective penetration enhancer for various water-insoluble pharmacological agents. In this thesis, 0.1% DMSO treatment alone appeared to diminish the amplitude of thalamocortical PV cell-mediated IPSCs in single stimulation recordings (Mean amplitude 5-10 min after application as a percentage of baseline 0-5 min before application, DMSO 85.1% ± 7.2, n=9 cells; p=0.04, Student's unpaired *t*-test) as well as the first IPSC in multiple stimulation recordings (Mean amplitude 5-10 min after application as a percentage of baseline 0-5 min before application, DMSO 82.2% ± 5.9, n=12 cells; p=0.005, Student's unpaired *t*-test). During single stimulation, IPSC amplitudes decreased over time in the presence of DMSO by approximately 15%, which appeared to be corrected for, by the application of the TASK-1/3 channel blocker A293 (Fig 3.2). The reduction in IPSC amplitudes may have been caused by a direct effect of DMSO or related to another mechanism which could have exerted its effects over the time course of the experiment. It was therefore important that control vehicle experiments were interleaved with drug trials to ensure that any drug effect was not contaminated by undesirable effects of DMSO.

Although reports on the effects of DMSO exposure are limited, several studies have described changes in cellular activity from whole-cell recordings *in vitro*. DMSO pre-treatment of slices at 0.05% was reported to have no effect on the RMP but significantly reduce the input resistance in hippocampal CA1 pyramidal cells by approximately 30%, compared to untreated tissue slices (Tamagnini et al. 2014). Furthermore, DMSO exposure resulted in a reduction in pyramidal cell firing in response to given current stimuli, thus reducing their excitability. However, unlike experiments in this thesis where DMSO was administered for 10 min, the slices used

for recordings in the Tamagnini et al (2014) study were treated with the solvent for 2-5 hours prior to recordings.

The mechanism of DMSO-treatment on reducing the input resistance in CA1 pyramidal cells is unknown, however it is likely that it increases the number of open ion channels in the plasma membrane. Although its target population of ion channels in not known, one possible candidate is the Cl^- channel. This is supported by DMSO's lack of effect on the RMP which could be expected given that the reversal potential of Cl^- is close to resting potential. The enhanced function of Cl^- channels has been demonstrated in other interactions: One study reported that amyloid beta treatment increased the surface expression of Cl^- channels which resulted in elevated Cl^- conductance (Novarino et al. 2004). In addition to the reduction in input resistance, DMSO was also shown to increase the membrane capacitance of pyramidal cells (Tamagnini et al. 2014). It is therefore possible that DMSO has a direct effect on the capacitive properties of the lipid bilayer which could modulate the integration of multiple synaptic inputs.

Although DMSO did not appear to affect the input resistance of PV cells in this thesis, it did appear to reduce the amplitude of PV cell-mediated feedforward IPSCs to near significance. As the effects of DMSO on input resistance in the Tamagnini et al (2004) study was recorded exclusively from pyramidal cells, it is not known whether PV cells are affected. Although the data in this thesis suggests that PV cell input resistance is not affected by DMSO, these experiments did not pretreat the slices with the solvent for several hours. Nonetheless, it is still plausible that the input resistance of thalamic neurons is reduced in the presence of DMSO, thus depressing their glutamatergic output onto PV cells in layer IV cortex upon thalamocortical stimulation, resulting in a reduction in feedforward inhibition.

Finally, the reduction in IPSC amplitudes may not be related to DMSO at all, as the effects did not appear to wash out. Other factors such as tissue health could be

responsible for this detrimental effect. As the stimulation and recording sites were in different brain areas, the likelihood of adverse effects induced by deteriorating tissue may have increased, given the expanse of tissue that the signal would have to have travelled through. The reduction in IPSC amplitudes may have therefore developed over the duration of the recordings and thus decreased as a function of time. Control recordings would need to be performed with or without the solvent to confirm whether the decline in IPSC amplitude was influenced by DMSO or if another mechanism reduced it over time.

3.5.6 Summary

The aim of this chapter was to increase the intrinsic excitability of PV cells by blocking TASK-1/3 channels. This would have resulted in membrane depolarisation accompanied by an increase in input resistance if the channels were functionally present. Several studies suggested that TASK-1/3 channels may have contributed to the large K^+ leak in PV cells (Goldberg et al. 2011; Okaty et al. 2009), however the application of three distinct TASK-1/3 channel blockers failed to alter the RMP and input resistance, and therefore had no effect on modulating the background K^+ conductance.

External acidification and bupivacaine treatment known to block the TASK-like conductance however significantly depolarised the RMP and increased the input resistance, highlighting a family of background channels that remain to be targeted. As both conditions target TASK-1/3 channels in addition to several other K_{2P} channel subfamilies including TREK-1, it is likely that other acidification- and bupivacaine-sensitive channels regulate the background K^+ conductance in PV cells. Thus, exploring the effects of blocking other leak K^+ channels in PV cells may therefore provide a better target for modulation.

Chapter 4

Effect of TREK-1 blockade on fast-spiking interneuron excitability

4 .1 Introduction

The low input resistance in PV cells presumed to be mediated partly by TASK-like channels could offer novel targets for blockers in the attempt to increase cell excitability. The results from the last chapter suggested that TASK-1/3 channels are not implicated in the resting background K^+ conductance in PV cells, whereas external treatment of acidification and bupivacaine – both of which are known to strongly inhibit TASK-like currents – demonstrated the presence of a large background current that remains to be targeted. Several other K^+ channels known to be acidification- and bupivacaine-sensitive include members of the K_{2P} family, particularly TREK-1 and to a lesser degree, TWIK-1. Thus, the blockade of TREK-1 or TWIK-1 could be applied in PV cells to increase their intrinsic excitability.

In chapter 3, the TASK subfamily of K_{2P} channels believed to contribute to the passive background K+ channel conductance was targeted in PV cells. It was demonstrated, however, that although PV cells express high levels of TASK-1 and TASK-3 mRNA subunits (Goldberg et al. 2011; Okaty et al. 2009), the administration of a variety of TASK channel blockers failed to alter their passive membrane properties, suggesting that TASK channels are not functionally expressed in these cells. Exploring the effects of blocking other K_{2P} channels specific to PV cells may therefore provide a better target.

The substantial effect that external acidification and bupivacaine had on the RMP and input resistance in PV cells suggests that there is a large K^+ background current that remains to be targeted, other than TASK. Other prominent members of the K_{2P} channel family that show acidification and bupivacaine sensitivity are TREK-1 and TWIK-1 channels (Kindler et al. 1999). Mouse qPCR data from FACS-sorted cortical PV cells demonstrated a developmental increase in TWIK-1 mRNA expression (Goldberg et al. 2011) indicating that TWIK-1 channels could provide a useful target for TASK-like inhibition. In spite of this, their currents have been

reported to be small, and display weak inward rectification (Kindler et al. 1999), which makes them less likely to contribute significantly to the large magnitude of inhibition observed during external acidification and bupivacaine treatments.

Within the TREK subfamily however, the acidification- and bupivacaine-sensitive TREK-1 channel is thought to mediate much larger currents (Kindler et al. 1999). A TREK-1 current could therefore be responsible for the depolarisation of the RMP and increase in input resistance observed during acidification and bupivacaine application. In support of this possibility, TREK-1 transcripts have been reported to be highly expressed relative to other background K^+ channels in cortical PV cells (Goldberg et al. 2011). Furthermore, *in situ* hybridisation of K_{2P} channel mRNA reveal a high expression of TREK-1 in several areas including the striatum, hippocampus and predominately layer IV cortex (Talley et al. 2001). Northern blots and real-time reverse transcription PCRs further support high levels of TREK-1 in the neocortex (Meadows et al. 2000). TREK-1 could therefore be a suitable channel to target in PV cells.

In this chapter, the effects of blocking TREK-1 channels in PV cells were assessed in layer IV somatosensory cortex. Direct recordings were made from patch-clamped PV cells and their intrinsic properties were measured in response to TREK-1 channel blockers. Functional expression of TREK-1 should result in RMP depolarisation and an increase in the input resistance during blockade, thus increasing the excitability of cortical PV cells. Finally, the effects of TREK-1 blockade on the firing of action potentials was examined in addition to its effect on the current-voltage relationship.

4.2 Effects of TREK-1 channel blocker amlodipine on PV cell excitability

A suitable TREK-1 channel blocker was required to block TREK-1-mediated currents without modifying the activity of other channels. Several Ca^{2+} channel blockers have been reported to block TREK-1 channels. Interestingly, amlodipine and niguldipine block TREK-1 channels much more potently than Ca^{2+} channels (Liu et al. 2007). The selective serotonin uptake inhibitor fluoxetine and its metabolite norfluoxetine have also been shown to block TREK-1 channels, although with less potency (Kennard et al. 2005). Additionally, the neuroprotective drug sipatrigine blocks TREK-1 but also targets several other voltage-gated Na^{+} and Ca^{2+} channels (Meadows et al. 2001; Xie & Garthwaite 1996; McNaughton et al. 2000).

Amlodipine was chosen for experiments as it was the most potent blocker with an IC_{50} of 0.43 μM for TREK-1 (Liu et al. 2007), compared to 2.4 μM for L-type Ca^{2+} channels (Furukawa et al. 1997). 43 μM was used in all experiments (a hundredfold greater than the IC_{50} value) to ensure full blockade of TREK-1 channels. This concentration of amlodipine would also presumably block L-type Ca^{2+} channels, however, these channels are activated at depolarised potentials and therefore are likely to be in a closed conformation during recordings at resting potential. Nonetheless, any L-type Ca^{2+} channel blockade would hyperpolarise the cell – contrary to the expected effect of blocking TREK-1.

4.2.1 Amlodipine depolarises RMP but has no effect on input resistance

The blockade of a key K^{+} channel known to contribute to the background K+ conductance should result in membrane depolarisation and increase the input resistance of the cell if the channel is functionally present. To test if PV cells functionally express TREK-1 channels at a sufficient level necessary to mediate the

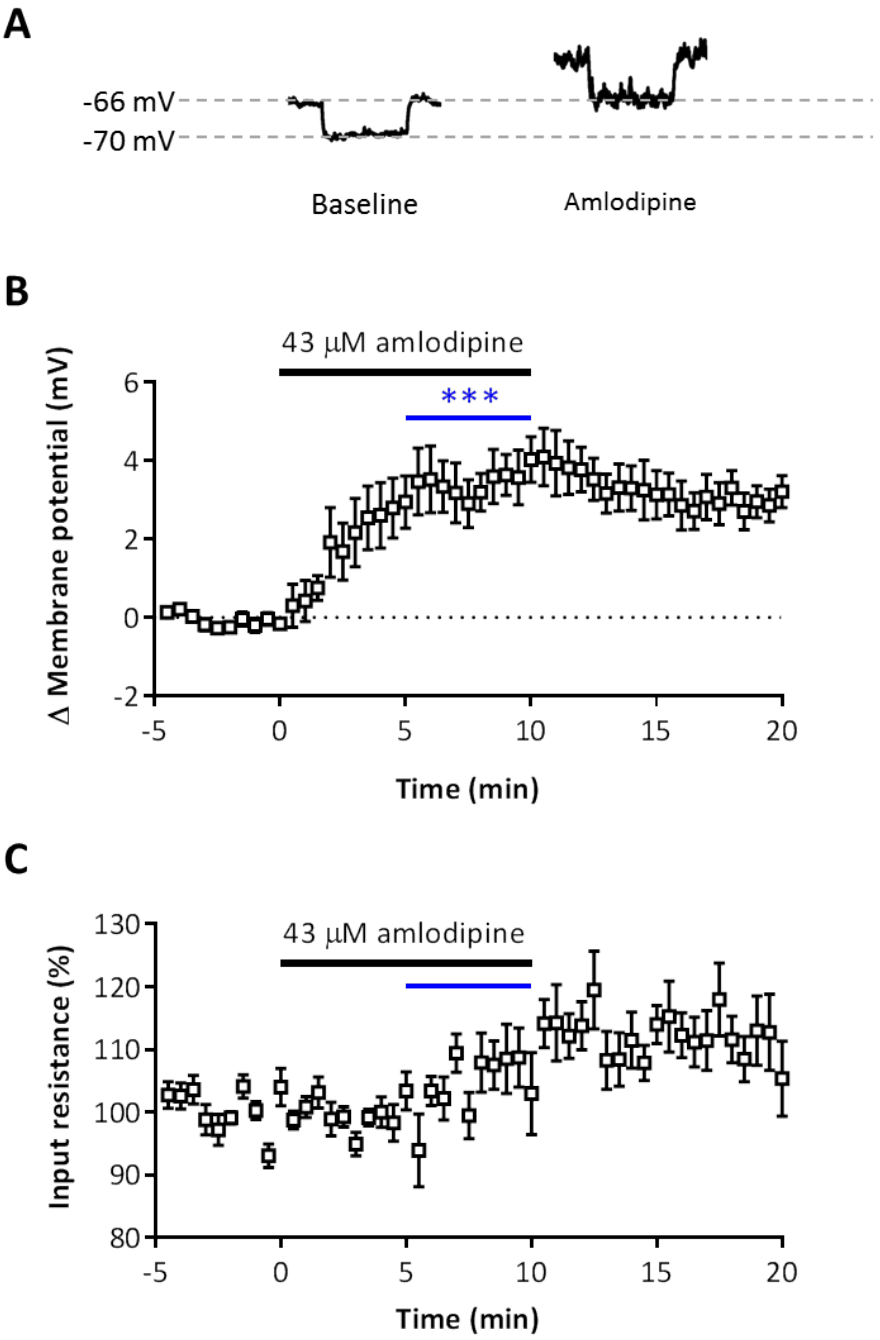

Figure 4.1 TREK-1 channel blocker amlodipine depolarises RMP but does not alter input resistance in PV cells Example voltage traces (A) and timecourse of whole-cell current clamp recordings of PV cells showing RMP (B) and input resistance (C) in the presence of amlodipine (0-10 min). Statistical test performed between treatment effect (blue line) and pretreatment control period. Data as means ± SEM. n=8 cells; ***p<0.001 (Student's paired *t*-test) compared to the corresponding pretreatment period.

passive resting conductance, direct PV cell recordings were performed and amlodipine was applied to assess the blocker's effect on RMP and input resistance. Recordings were carried out on PV cells in layer IV of the barrel cortex which displayed electrophysiological properties characteristic of the fast-spiking cell type (see section **3.3**). As amlodipine was dissolved in external recording solution, a vehicle control was not required.

Amlodipine significantly depolarised the RMP (Difference in mean potential 5-10 min after application from baseline 0-5 min before application: 3.3 ± 0.6 mV; n=8 cells, p=0.0006, Student's paired *t*-test; Fig 4.1 B) suggesting that the intrinsic membrane properties of PV cells are robustly modified. In contrast, amlodipine did not alter the input resistance of PV cells (Mean resistance 5-10 min after application as a percentage of baseline 0-5 min before application: 104.4% ± 2.2; n=8 cells, p=0.06, Student's paired *t*-test; Fig 4.1 C). This was surprising because the blockade of a TASK-like channel would have been expected to alter both parameters simultaneously. Furthermore, it appeared that the input resistance may have increased, but over a longer timescale in relation to the change in RMP, which again was unexpected.

4.2.2 Amlodipine does not alter the firing of PV cells in response to current steps

Cells typically receive multiple inputs *in vivo* which are converted into action potentials once voltage-gated Na^+ channels reach activation threshold. Depolarisation of the RMP will bring the cell closer to activation threshold. As a result, cells become more excitable and fire more action potentials to a given input. As amlodipine depolarised the RMP of PV cells, their active firing excitability was examined in response to a set of current steps, to assess whether the effect of depolarisation resulted a higher probability of action potential firing.

All recordings were performed at resting potential in current clamp configuration where PV cells were subjected to a series of current steps to make them fire. This

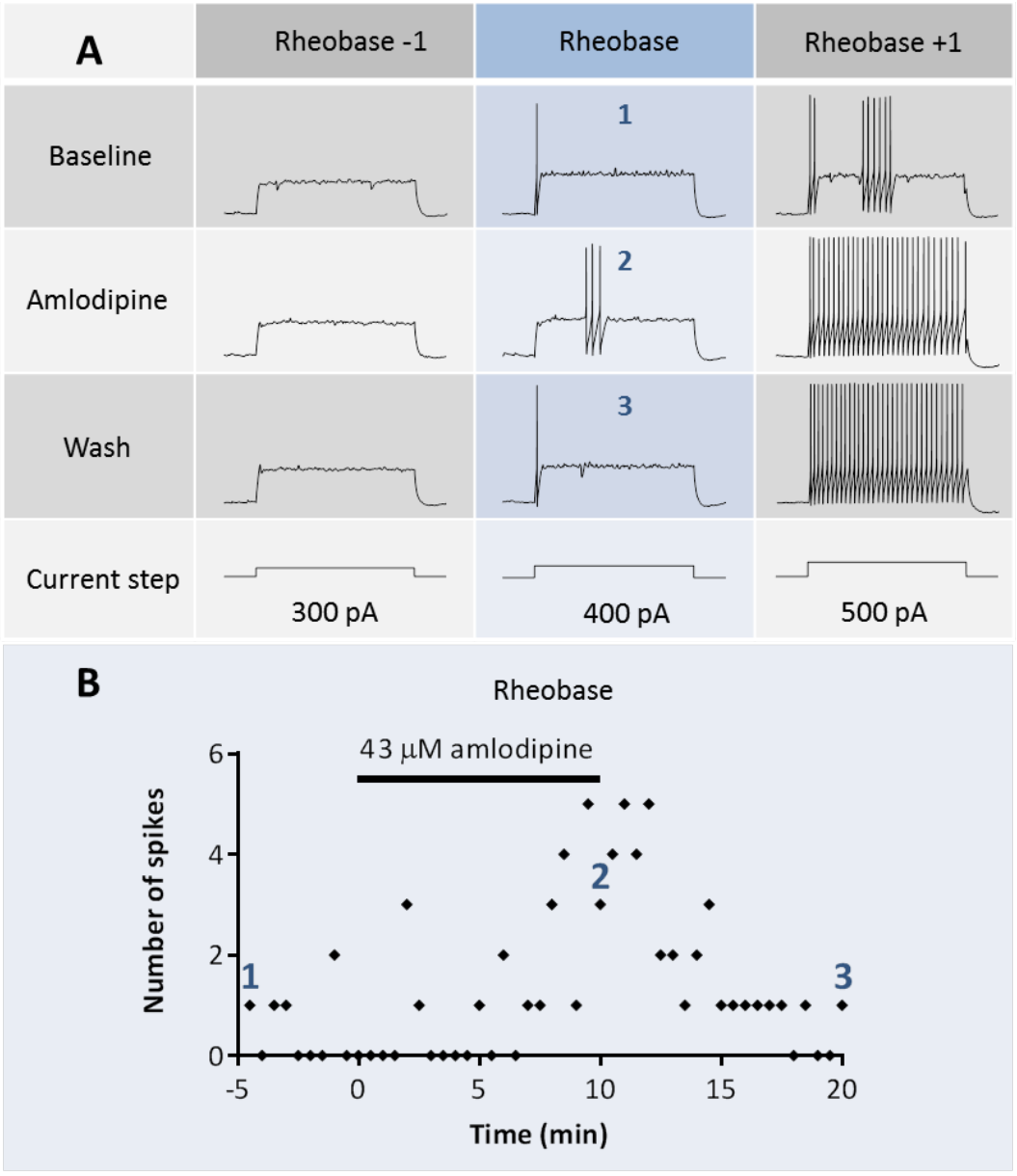

Figure 4.2 Measuring PV cell excitability in the presence of TREK-1 channel blocker amlodipine Current clamp recordings of PV cells in response to a set of depolarising current steps. PV cell firing was recorded in response to a set of 8, 250 ms depolarising current steps stimulated every 30 s in the presence of amlodipine (0-10 min). The current amplitude required to elicit 1 action potential in the baseline period was selected to represent the rheobase current. The previous (smaller) and subsequent (larger) current steps represent the rheobase-1 and rheobase+1, respectively. (A) Example traces of a cell grouped into stimulation intensities (columns) at baseline, spadin and wash conditions (rows). (B) Example timecourse of the same recording showing spike number at the rheobase current step which was determined from the baseline control period. Timepoints 1, 2 and 3 are represented by the middle traces in A (blue column).

allowed for the input resistance to be determined from a negative current step (as performed in previous recordings) in addition to measuring cell excitability calculated from a set of 8 positive current steps. The current amplitude was adjusted to ensure that each set of 8 steps resulted in a number of sweeps that preferably contained the following parameters: the threshold current (rheobase) required to elicit one action potential; the subthreshold current (rheobase -1) that failed to elicit an action potential, as well as the suprathreshold current (rheobase +1) that discharged more than one action potential (Fig 4.2 A). A set of 8, 250 ms current steps were injected into PV cells every 30 s and performed in the presence of amlodipine (Fig 4.2 B).

Amlodipine significantly reduced the rheobase amplitude required to generate one action potential (Mean rheobase 5-10 min after application compared to baseline 0-5 min before application, Baseline: 477.1 ± 59.2 pA; Amlodipine: 404.0 ± 60.3 pA; n=8 cells, p=0.03, Student's paired *t*-test; Fig 4.3 B), although did not return to pretreatment values in the wash (Mean rheobase 5-10 min after application compared to last 5-10 min of wash, Amlodipine: 404.0 ± 60.3 pA; Wash: 390.4 ± 55.2 pA; n=8 cells, p=0.59, Student's paired *t*-test; Fig 4.3 B)

However, amlodipine did not affect the number of action potentials in response to the rheobase -1 current step (Mean number of spikes 5-10 min after amlodipine application compared to baseline 0-5 min before application, Baseline: 0.0 ± 0.0; Amlodipine: 0.7 ± 0.5; n=8 cells, p=0.38, One-way RM-ANOVA with Bonferroni correction; Fig 4.3 C). Similarly, amlodipine did not alter the number of action potentials in response to the rheobase current step (Normalised number of spikes 5-10 min after application compared to baseline 0-5 min before application, Baseline: 1.0 ± 0.0; Amlodipine: 7.5 ± 4.0; n=8 cells, p=0.26, One-way RM-ANOVA with Bonferroni correction; Fig 4.3 C; Absolute number of spikes, Baseline: 0.7 ± 0.4; Amlodipine: 3.7 ± 2.3) and also failed to affect the number of action potentials in response to the rheobase +1 current step (Normalised number of spikes 5-10 min after application compared to baseline 0-5 min before application, Baseline: 1.0 ±

0.0; Amlodipine: 6.2 ± 3.7; n=8 cells, p=0.81, One-way RM-ANOVA with Bonferroni correction; Fig 4.3 C; Absolute number of spikes, Baseline: 8.7 ± 3.5; Amlodipine: 12.5 ± 4.7). These data suggest that although the effects of amlodipine reduce the rheobase current required to elicit one action potential, it does not significantly increase the number of spikes generated in response to given current steps.

Attention must be drawn to the possibility that the dataset used for these experiments might have been underpowered. As the dataset only contained 8 cells, the significant effects that amlodipine had on the RMP (Fig 4.1 B) and rheobase current (Fig 4.3 B) indicate that significant effects on the input resistance (Fig 4.1 C) and number of spikes to given current injections (Fig 4.3 C) might have been discovered if more cells had been recorded. Nonetheless, power analysis of this data revealed that 37 cells would have been required to observe a significant effect on the input resistance of PV cells. Likewise, power analysis revealed that 36-99 cells would have been required to observe a significant effect on the number of spikes generated from given current injections (rheobase-1, rheobase and rheobase+1).

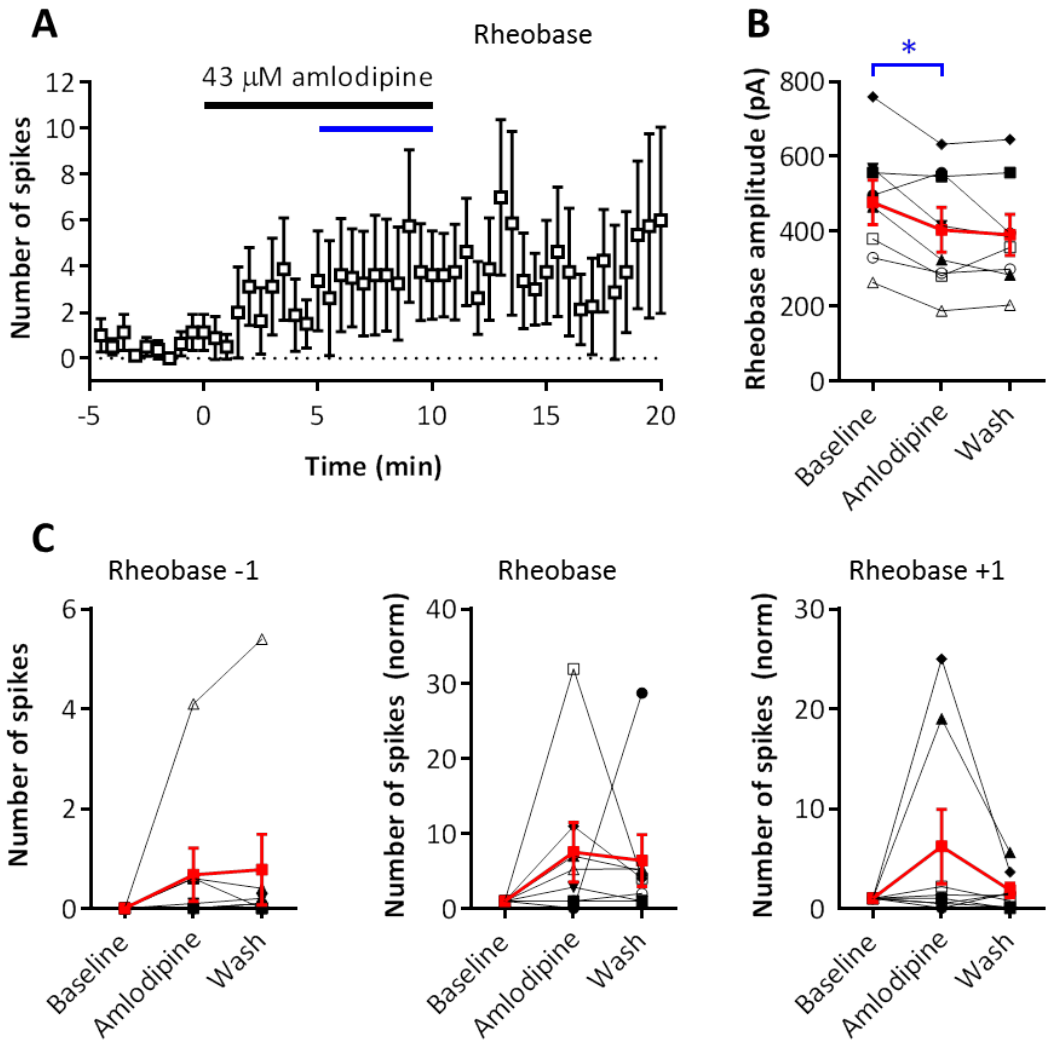

Figure 4.3 TREK-1 channel blocker amlodipine does not alter PV cell excitability
Current clamp recordings of PV cells in response to a set of depolarising current steps. (A) Timecourse of PV cell recordings showing number of spikes during 250 ms rheobase current step in the presence of amlodipine (0-10 min). (B) Amlodipine reduced the mean current amplitude required to elicit 1 action potential (n=8 cells; *p<0.05 (Student's paired *t*-test) compared to the corresponding pretreatment period). (C) Mean number of spikes grouped into stimulation intensities (determined from the baseline control period) compared between baseline, amlodipine and wash. Rheobase-1 graph (left) displays absolute spike number. Rheobase and rheobase+1 graphs (middle and right) are normalised to the baseline average of the first 5 min. Each symbol type in B and C represents a different cell. Data as means ± SEM. n=8 cells.

4.3 Effects of TREK-1 channel blocker spadin on PV cell excitability

Although amlodipine significantly depolarised the RMP in PV cells, a more potent and specific TREK-1 channel blocker was employed, as it was possible that the non-specific effects of amlodipine could have impacted on the full effect of blocking TREK-1. Interestingly, the peptide spadin has been reported to block TREK-1 channels with high affinity (Mazella et al. 2010). Spadin is a peptide based on the sequence of amino acids derived from a propeptide that is secreted during the maturation of the neurotensin receptor 3/sortillin protein, which is located in the trans-Golgi network (Mazella et al. 2010). Moreover, spadin is structurally distinct from amlodipine, and therefore their specific effects can be accurately compared between the two blockers to provide a meaningful conclusion. The effects of blocking TREK-1 with spadin have already been explored as an antidepressant in mice. The excitability of serotonergic neurons in the Dorsal Raphe Nucleus - which express TREK-1 – was reported to increase in response to spadin administration (Mazella et al. 2010). Furthermore, mice treated with spadin were shown to behave exactly as TREK-1 knockout mice which display a clear antidepressant phenotype (Heurteaux et al. 2006; Mazella et al. 2010). This suggests that spadin is a potent blocker of TREK-1 channels. Although the IC_{50} of spadin is 70 nM for TREK-1 - reported from COS-7 TREK-1-transfected cells (Mazella et al. 2010) - 1 μM was used in all experiments (approximately 2.5-fold of the IC_{50}), likely to result in over 75% inhibition of TREK-1 channels.

4.3.1 Spadin depolarises RMP but has no effect on input resistance

Spadin was administered to PV cells for 10 min after a 5 min baseline was established. Similar to the effects of amlodipine, spadin significantly depolarised the RMP (Difference in mean potential 5-10 min after application from baseline 0-5 min before application: 0.9 ± 0.4 mV; n=15 cells, p=0.02, Student's paired *t*-test; Fig 4.4 B) but did not alter the input resistance (Mean resistance 5-10 min after application as a percentage of baseline 0-5 min before application: 102.4% ± 2.0; n=15 cells,

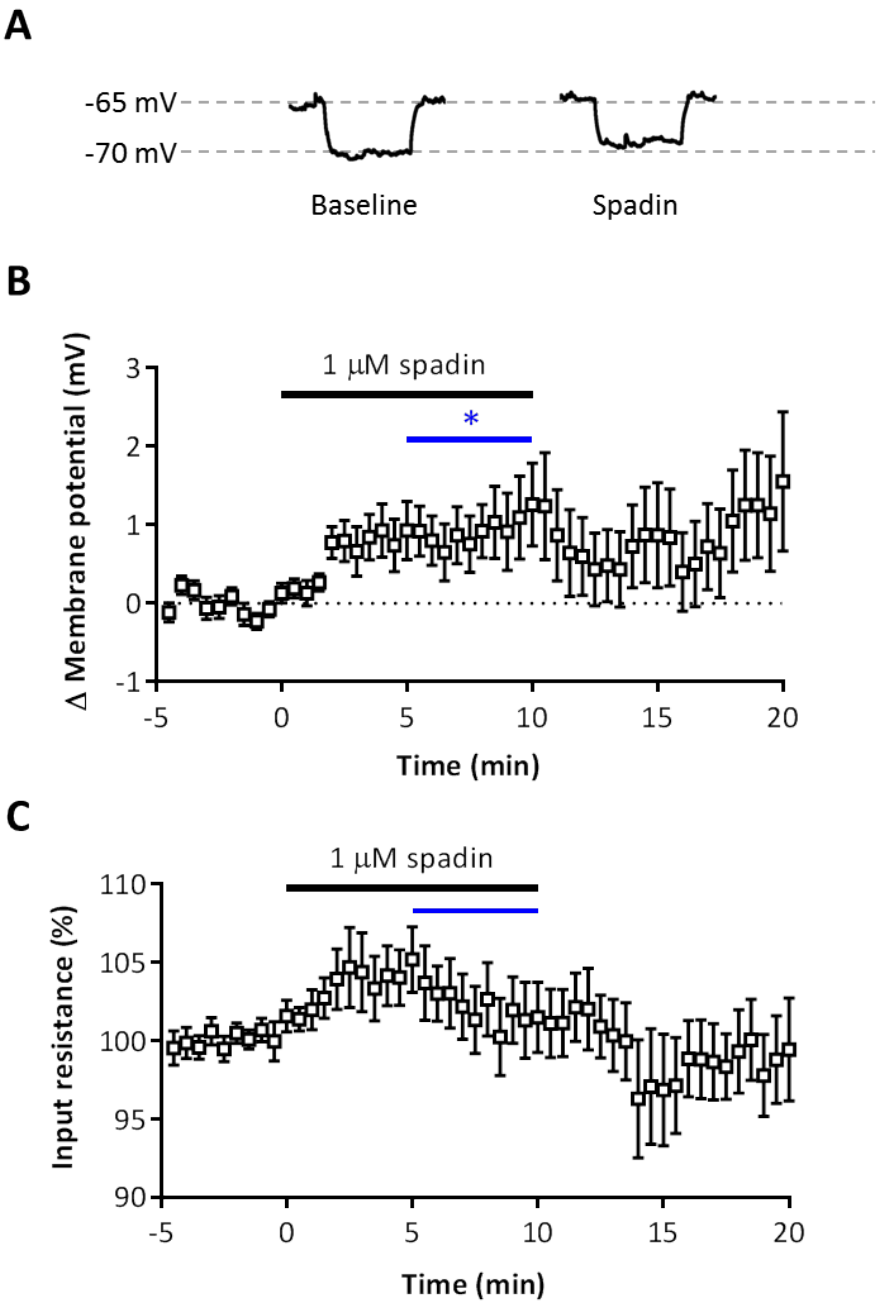

Figure 4.4 TREK-1 channel blocker spadin depolarises RMP but does not alter input resistance in PV cells Example voltage traces (A) and timecourse of whole-cell current clamp recordings of PV cells showing RMP (B) and input resistance (C) in the presence of spadin (0-10 min). Statistical test performed between treatment effect (blue line) and pretreatment control period. Data as means ± SEM. n=15 cells; *p<0.05 (Student's paired *t*-test) compared to the corresponding pretreatment period.

p=0.22, Student's paired *t*-test; Fig 4.4 C). Thus, the results from amlodipine are paralleled by the much cleaner TREK-1 channel blocker spadin although to a lesser magnitude.

4.3.2 Spadin increases the firing of PV cells in response to current steps

The effect of the depolarising action of the TREK-1 channel blocker was investigated on the spiking activity of PV cells in response to 8 positive current steps (Fig 4.5 A) carried out in the same manner as before. 8, 250 ms depolarising current steps were injected every 30 s (Fig 4.5 B).

Spadin significantly reduced rheobase (Mean rheobase 5-10 min after application compared to baseline 0-5 min before application, Baseline: 434.5 ± 64.9 pA; Spadin: 691.0 ± 68.1 pA; n=15 cells, p=0.02, Student's paired *t*-test; Fig 4.6 B), although did not return to pretreatment values in the wash (Mean rheobase 5-10 min after application compared to last 5-10 min of wash, Spadin: 691.0 ± 68.1 pA; Wash: 713.3 ± 70.9 pA; n=15 cells, p=0.09, Students paired *t*-test; Fig 4.6 B).

Furthermore, spadin increased the number of action potentials in response to the rheobase -1 current step (Mean number of spikes 5-10 min after application compared to baseline 0-5 min before application, Baseline: 0.1 ± 0.0; Spadin: 0.4 ± 0.1; n=15 cells, p=0.01, One-way RM-ANOVA with Bonferroni correction; Fig 4.6 C), although did not return to pretreatment values in the wash (Mean number of spikes 5-10 min after application compared to last 5-10 min of wash, Spadin: 0.4 ± 0.1; Wash: 0.3 ± 0.1; n=15 cells, p=0.33, One-way RM-ANOVA with Bonferroni correction; Fig 4.6 C).

Similarly, spadin significantly increased the number of action potentials in response to the rheobase current step (Normalised number of spikes 5-10 min after application compared to baseline 0-5 min before application, Baseline: 1.0 ± 0.1; Spadin: 1.8 ±

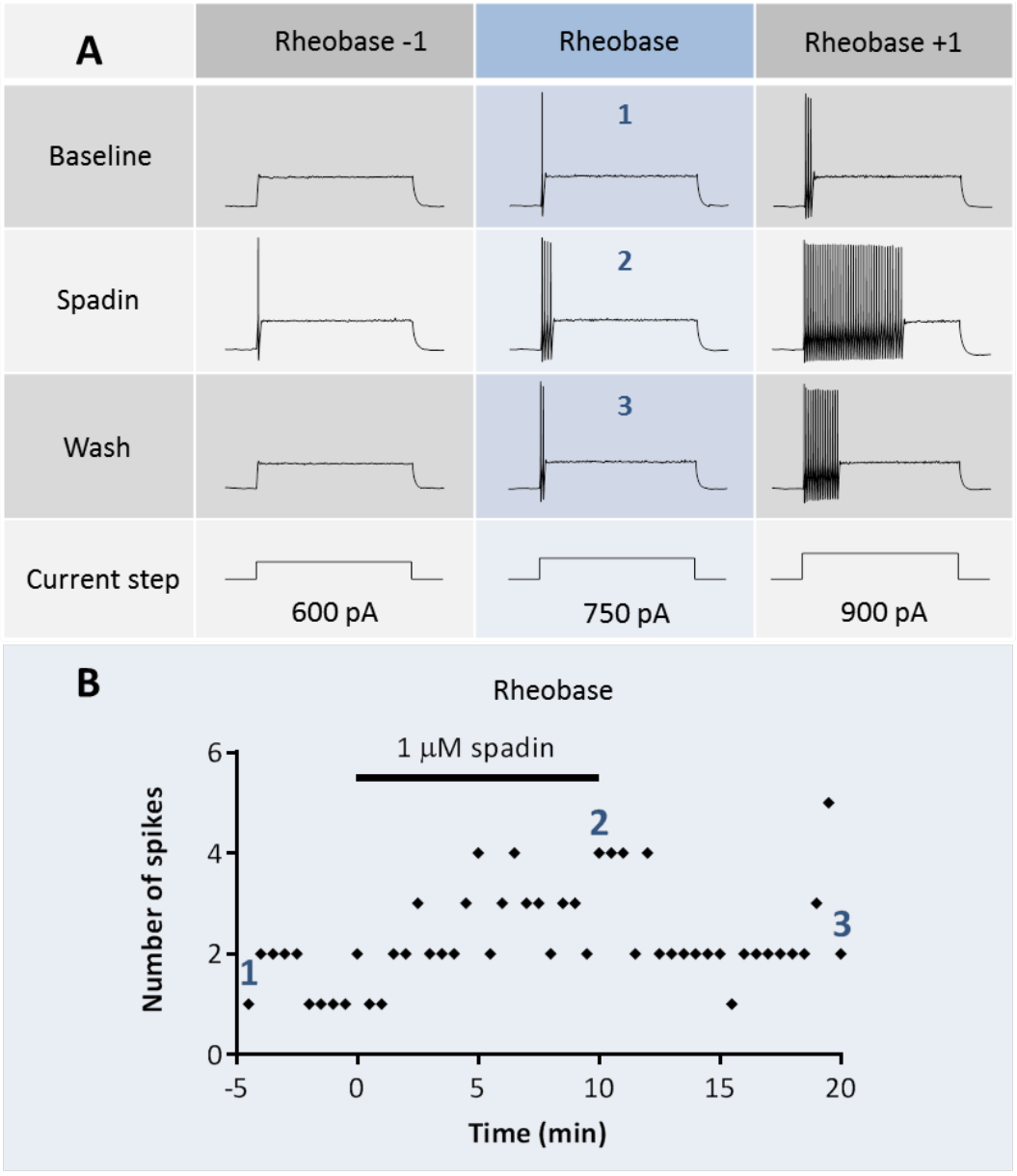

Figure 4.5 Measuring PV cell excitability in the presence of TREK-1 channel blocker spadin Current clamp recordings of PV cells in response to a set of depolarising current steps. PV cell firing was recorded in response to a set of 8, 250 ms depolarising current steps stimulated every 30 s in the presence of spadin (0-10 min). The current amplitude required to elicit 1 action potential in the baseline period was selected to represent the rheobase current. The previous (smaller) and subsequent (larger) current steps represent the rheobase-1 and rheobase+1, respectively. (A) Example traces of a cell grouped into stimulation intensities (columns) at baseline, spadin and wash conditions (rows). (B) Example timecourse of the same recording showing spike number at the rheobase current step which was determined from the baseline control period. Timepoints 1,2 and 3 are represented by the middle traces in A (blue column).

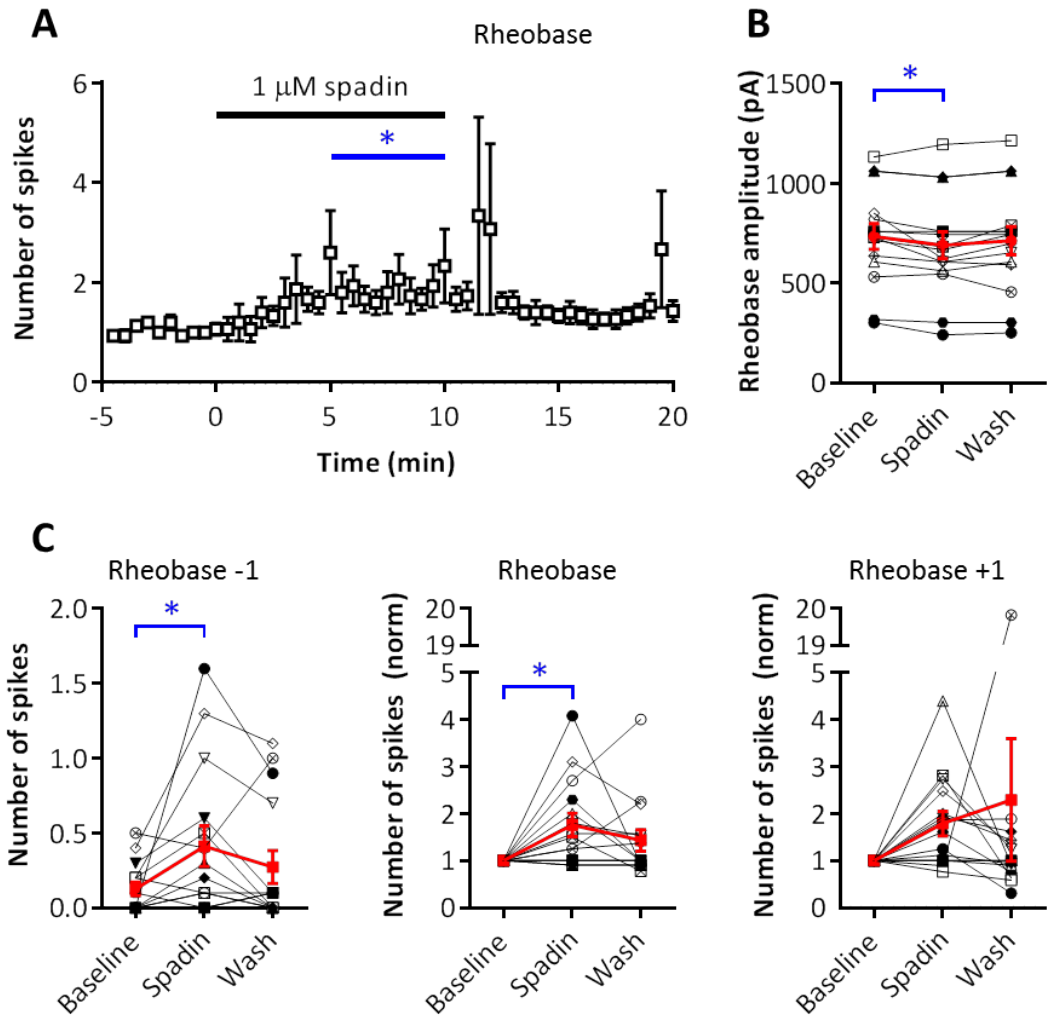

Figure 4.6 TREK-1 channel blocker spadin increases PV cell excitability
Current clamp recordings of PV cells in response to a set of depolarising current steps. (A) Timecourse of PV cell recordings showing number of spikes during 250 ms rheobase current step in the presence of amlodipine (0-10 min) (n=15 cells; *p<0.05 (Student's paired *t*-test) compared to the corresponding pretreatment period). (B) Spadin reduced the mean current amplitude required to elicit 1 action potential (n=15 cells; *p<0.05 (Student's paired *t*-test) compared to the corresponding pretreatment period). (C) Mean number of spikes grouped into stimulation intensities (determined from the baseline control period) compared between baseline, spadin and wash. Rheobase-1 graph (left) displays averaged spike number (last 5 min of each condition). Rheobase and rheobase+1 graphs (middle and right) displays averaged spike number normalised to the baseline average of the first 5 min. *p<0.05 (One-way RM-ANOVA with Benferroni correction). Each symbol type in B and C represents a different cell. Data as means ± SEM. n=15 cells.

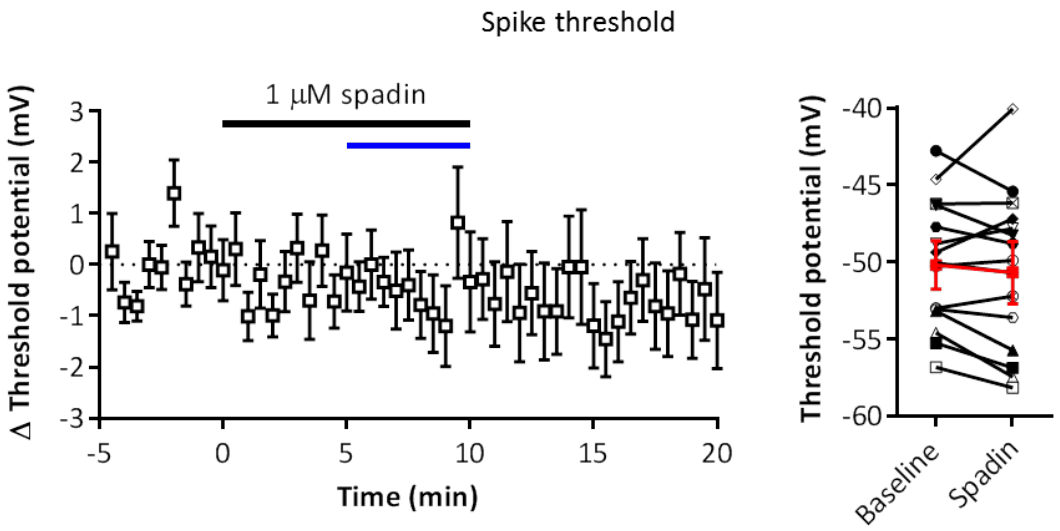

Figure 4.7 TREK-1 channel blocker spadin does not alter firing threshold in PV cells (Left) Timecourse of whole-cell current clamp recordings of PV cells showing action potential threshold potential. (Right) Absolute membrane potential for spike threshold between baseline average of first 5 min and last 5-10 min of spadin treatment. Each symbol type represents a different cell. Data as means ± SEM. n=15 cells.

0.3; n=15 cells, p=0.01, One-way RM-ANOVA with Bonferroni correction; Fig 4.6 C; Absolute number of spikes, Baseline: 1.0 ± 0.1; Spadin: 1.9 ± 0.3), but again did not return to pretreament values (Normalised number of spikes 5-10 min after application compared to last 5-10 min of wash, Spadin: 1.8 ± 0.3; Wash: 1.4 ± 0.2; n=15 cells, p=0.37, One-way RM-ANOVA with Bonferroni correction; Fig 4.6 C; Absolute number of spikes, Spadin: 1.9 ± 0.3; Wash: 1.5 ± 0.2). Nevertheless, spadin did not affect the number of action potentials in response to the rheobase +1 current step (Normalised number of spikes 5-10 min after application compated to baseline 0-5 min before application, Baseline: 1.0 ± 0.0; Spadin: 1.8 ± 0.3; n=15 cells, p=0.51, One-way RM-ANOVA with Bonferroni correction; Fig 4.6 C; Absolute number of spikes, Baseline: 4.4 ± 1.5; Spadin: 8.3 ± 2.9). These data demonstrate that spadin increases the excitability of PV cells.

The effect of spadin on increasing the number of action potentials in response to the rheobase -1 and rheobase steps could have been due to a change in the threshold

potential for action potential initiation rather than a change in RMP. The membrane threshold potential for action potential generation was therefore analysed. Spadin had no effect on the action potential threshold (Mean threshold potential 5-10 min after application compared to baseline 0-5 min before application, Baseline: -50.2 ± 1.1 mV; Spadin: -50.6 ± 1.4 mV; n=15 cells, p=0.43, Student's paired *t*-test; Fig 4.7)

4.3.3 Spadin has no effect on PV cell output

Cells that increase in excitability may generate a higher frequency of action potentials either spontaneously or in response to stimulation from afferent inputs. In the thalamocortical feedforward microcircuit, several PV interneurons in layer IV cortex receive excitatory inputs from the thalamus in response to whisker stimulation (Gabernet et al. 2005). Some of these PV cells will reach firing threshold and participate in feedforward inhibition onto local principal cells whilst other PV cells will not reach firing threshold and remain silent. As spadin depolarises the RMP and increases the excitability of PV cells, a greater proportion of them might rest closer to firing threshold and thus fire action potentials more effectively upon stimulation. PV cell output was therefore examined within the thalamocortical circuit (Fig 3.1 A). The evoked feedforward output of PV cells in response to thalamocortical stimulation was recorded before and after application of the drug. PV cells that become more excitable in response to the application of spadin should contribute to feedforward inhibition upon stimulation, and result in an increase in IPSC amplitude in the recorded voltage-clamped layer IV stellate cell.

The VB was stimulated three times at 50 Hz, eliciting three IPSCs in the recorded stellate cell. No difference in the amplitude of any of the three IPSCs was detected in the presence of spadin (Mean amplitude 5-10 min after application as a percentage of baseline of respective IPSC 0-5 min before application. IPSC 1: 102.8% ± 14.3; p>0.99. IPSC 2: 172.4% ± 68.9; p=0.46. IPSC 3: 173.5% ± 60.7; p=0.45. n=7 cells, Two-way ANOVA with Bonferroni correction; Fig 4.8). This result was surprising

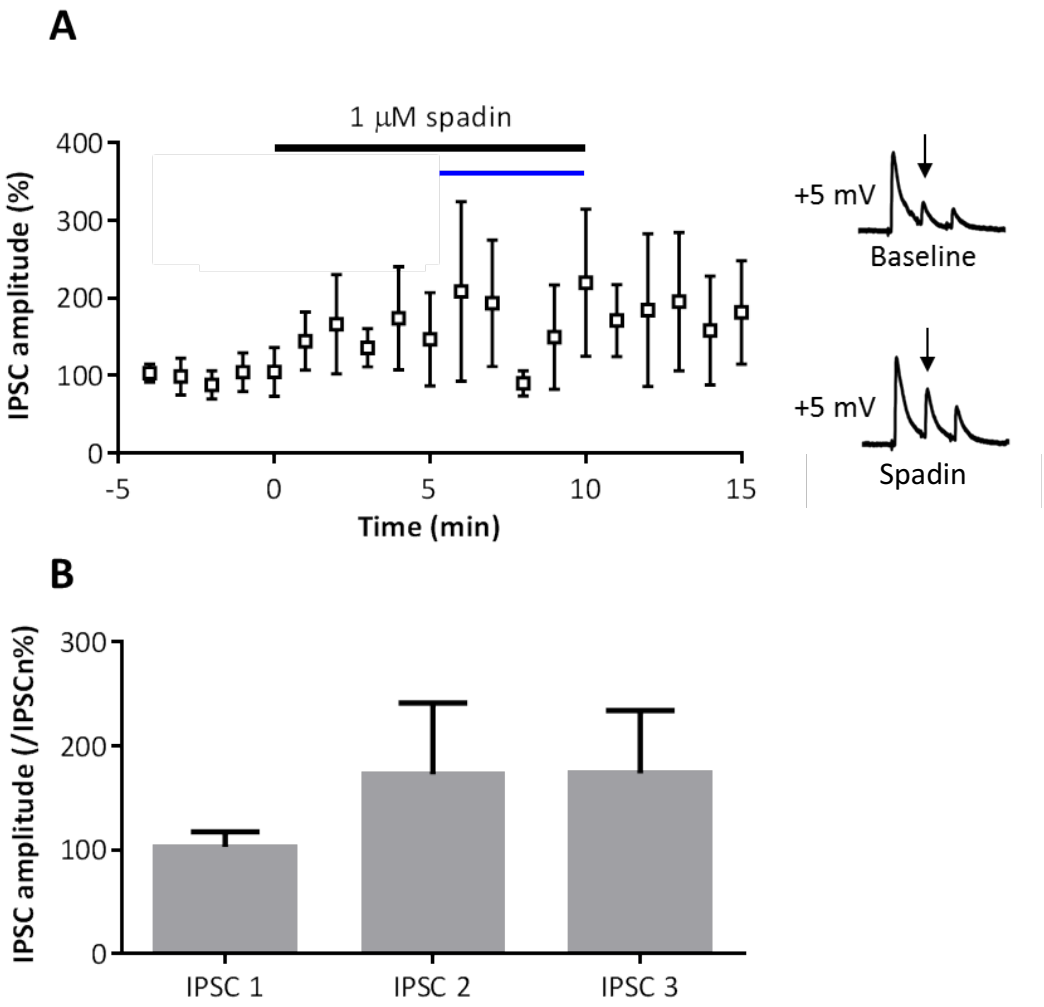

Figure 4.8 TREK-1 channel blocker spadin does not effect PV cell output during multiple stimulation A 50 Hz triplet of thalamocortical PV cell-mediated IPSCs were evoked at 0.1 Hz. (A) Timecourse of peak of 2nd IPSC in the triplet (indicated by arrow in inset) normalised to the baseline average of the first 5 min of the 2nd IPSC in the presence of 1 µM spadin TREK-1 channel blocker (0-10 min). Statistical test performed between treatment effect (blue line) and pretreatment control period. (B) Averages of 1st, 2nd, and 3rd IPSCs during last 5-10 min of spadin treatment normalised to the baseline average of the first 5 min of their respective IPSCs. Data as means ± SEM. n=7 cells.

given spadin's effect on the RMP which presumably would have shifted more cells closer to firing threshold.

4.3.4 Spadin does not affect current-voltage relationship in PV cells

The blockade of a TREK-1 isolated current should reduce its amplitude in response to a series of voltage steps. It was important to try and tease out the TREK-1 current in PV cells in order to validate that spadin's effects on PV cell RMP and excitability is indeed caused by the blockade of TREK-1 channels and not as a result of another non-specific mechanism.

To isolate TREK-1 currents, PV cells were exposed to a cocktail of external glutamatergic blockers, GABAergic blockers, K^+ channel blockers and an L-type Ca^{2+} channel blocker (CNQX, D-APV, picrotoxin, TEA, nifedipine). The current-voltage relationship was measured in response to a series of 500 ms voltage steps (-90 mV to +40 mV, Δ10 mV) from a holding potential of -70 mV (Fig 4.9 A) before and after spadin application. A voltage ramp was also performed in PV cells to measure the effect of spadin on the current-voltage relationship (Fig 4.9 B).

Spadin did not significantly alter the current-voltage relationship of the isolated current in PV cells during square voltage steps (Mean current amplitude 5-10 min after application compared to baseline amplitude 0-5 min before application, Baseline: 37.0 ± 0.6; Spadin: 36.6 ± 1.2; n=5 cells, $p>0.99$, Two-way RM-ANOVA with Bonferroni correction; Fig 4.9 A). There was therefore no effect between spadin and wash (Mean current amplitude 5-10 min after application compared to last 5-10 min of wash, Spadin: 36.6 ± 1.2; Wash: 34.8 ± 1.3; n =5 cells, $p=0.56$, Two-way RM-ANOVA with Bonferroni correction; Fig 4.9 A).

Similarly, spadin did not significantly alter the gradient of the current-voltage slope in response to a voltage ramp (Mean gradient between +30 mV and +40 mV voltage

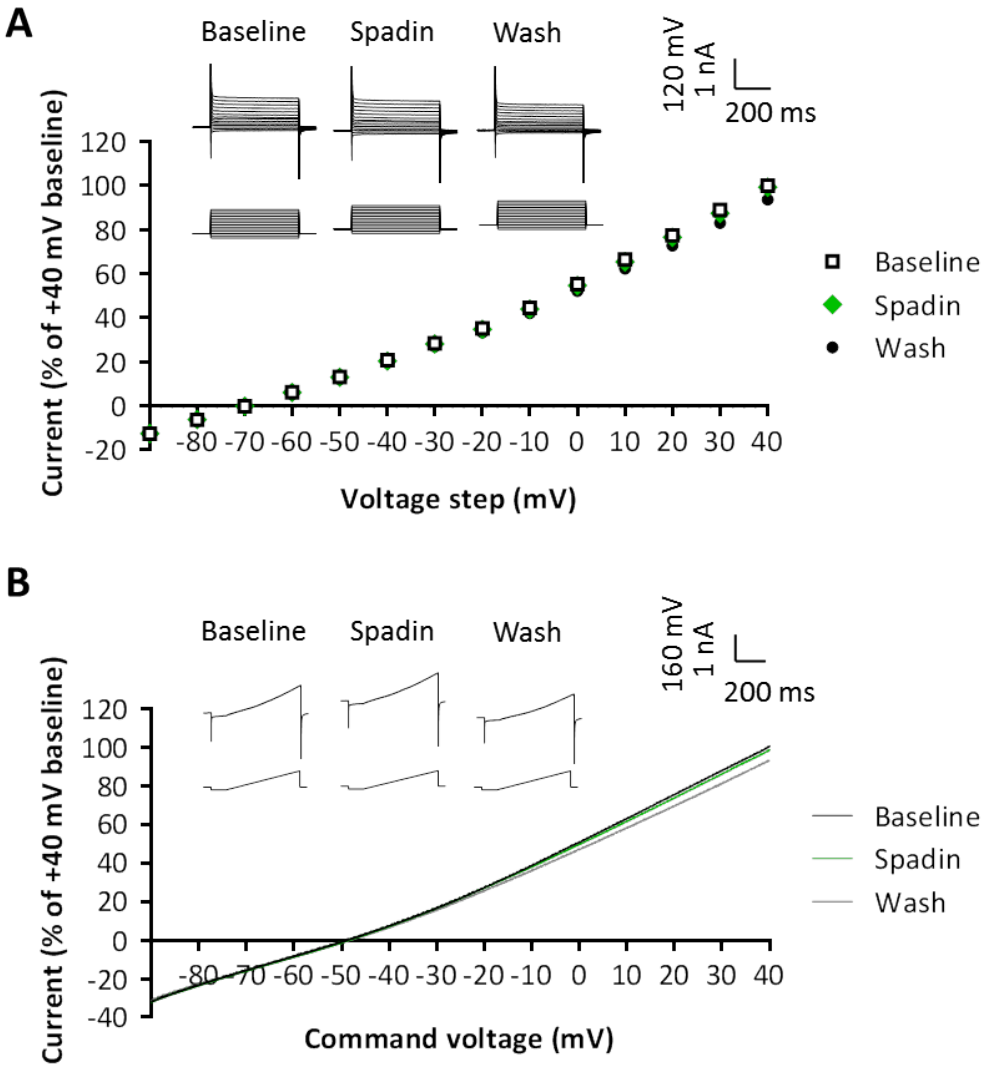

Figure 4.9 TREK-1 channel blocker spadin does not alter the current/voltage relationship in PV cells Whole-cell voltage clamp recordings of PV cells in the presence of spadin. External bath contained CNQX, D-APV, nifedipine, picrotoxin and TEA to isolate TREK-1 currents. (A) Current/voltage relationship in response to a set of voltage steps (500 ms, -90 mV to +40 mV, Δ10 mV) from a holding potential of -70 mV. Example traces showing current responses to the same voltage steps for baseline, spadin and pH 6.4 conditions (inset). (B) Current/voltage relationship in response to a voltage ramp (cells were hyperpolarised to -90 mV from a holding potential of -70 mV and subjected to a 500 ms ramp to +40 mV). Example traces showing current responses to the same voltage ramp for baseline, spadin and pH 6.4 conditions (inset). Data as means ± SEM (in A). n=5 cells

range 5-10 min after application compared to baseline gradient 0-5 min before application, Baseline: 0.9 ± 0.1; Spadin: 0.9 ± 0.1; n=5 cells, p>0.99, One-way RM-ANOVA with Bonferroni correction; Fig 4.9 B) and did not significantly affect the rectification properties of the slope (Rectification index 5-10 min after application compared to baseline 0-5 min before application, Baseline 1.4 ± 0.1; Spadin: 1.4 ± 0.1; n=5 cells, p>0.99, One-way RM-ANOVA with Bonferroni correction; Fig 4.9 B). There was therefore no effect on the gradient of the slope between spadin and wash (Mean gradient between +30 mV and +40 mV voltage range 5-10 min after application compared to last 5-10 min of wash, Spadin: 0.9 ± 0.1; Wash: 0.9 ± 0.1; n=5 cells, p>0.99, One-way RM-ANOVA with Bonferroni correction; Fig 4.9 B) and no effect on the rectification properties of the slope (Rectification index 5-10 min after application compared to last 5-10 min of wash, Spadin: 1.4 ± 0.1; Wash: 1.4 ± 0.1; n=5 cells, p>0.99, One-way RM-ANOVA with Bonferroni correction; Fig 4.9 B).

4.4 Subcellular localisation of TREK-1 channels

PV cells express an extremely high density of voltage-gated Na^+ and K^+ channels in the AIS (Hu et al. 2014). An action potential is initiated once the local region of the AIS is significantly depolarised to induce activation of voltage-gated Na^+ channels. Any excitatory inputs reaching the AIS are either converted into action potentials or filtered out through ion channels. Both spadin and amlodipine depolarise the RMP but have no effect on the input resistance in PV cells, while the more potent and specific TREK-1 channel blocker spadin increases the excitability of PV cells. The discrepancy between RMP and input resistance could be explained by an increased density of TREK-1 channels in the axon initial segment (AIS) instead of a uniform distribution along the somatodendritic axis of the cell. Previous experiments would thus be unable to detect currents carried by TREK-1 channels, and therefore the functional effect of spadin on the RMP and input resistance would not be observed if

they are located mostly outside of the somatic compartment - where the recording patch-pipette would be most sensitive to measuring the input resistance.

If TREK-1 channels are expressed in the AIS, then their blockade should increase the input resistance locally and reduce the filtering of incoming inputs. Furthermore, the 1 mV depolarisation of the RMP observed during spadin application could suggest a much greater depolarising effect occurring locally in the AIS, which would have subsequently propagated towards the soma. The local increase in input resistance however may have been too distally located for the recording pipette to monitor. This could therefore explain the contradicting effects observed with TREK-1 channel blockers between the RMP and input resistance.

To test this hypothesis, a puff pipette could be used to locally apply spadin onto the AIS while the cell is injected with a set of depolarising current steps (as conducted previously). To verify that its effect is AIS-specific, spadin would also be locally applied to the soma and proximal dendrites as a control. An increased expression of TREK-1 channels in the AIS may therefore increase the excitability of PV cells to a given set of current steps only during local puffs of spadin onto the AIS compared with local puffs onto other compartments.

4.4.1 Effects of locally applied tetrodotoxin (TTX) on cell excitability

A pilot study was performed to assess the efficacy of locally puffing a drug onto distinct subcellular compartments. The voltage-gated Na^+ channel blocker tetrodotoxin (TTX) was used as a control to block voltage-gated Na^+ channels when puffed onto the AIS. Cells were filled with standard internal solution containing Alexa Fluor 488 dye enabling the axonal and dendritic processes of the cell to be visualised under blue light. Layer IV cortical pyramidal cells were selected for recordings instead of PV cells as their axons were easily detectable. A pipette filled with recording solution containing 300 nM TTX was positioned either behind the

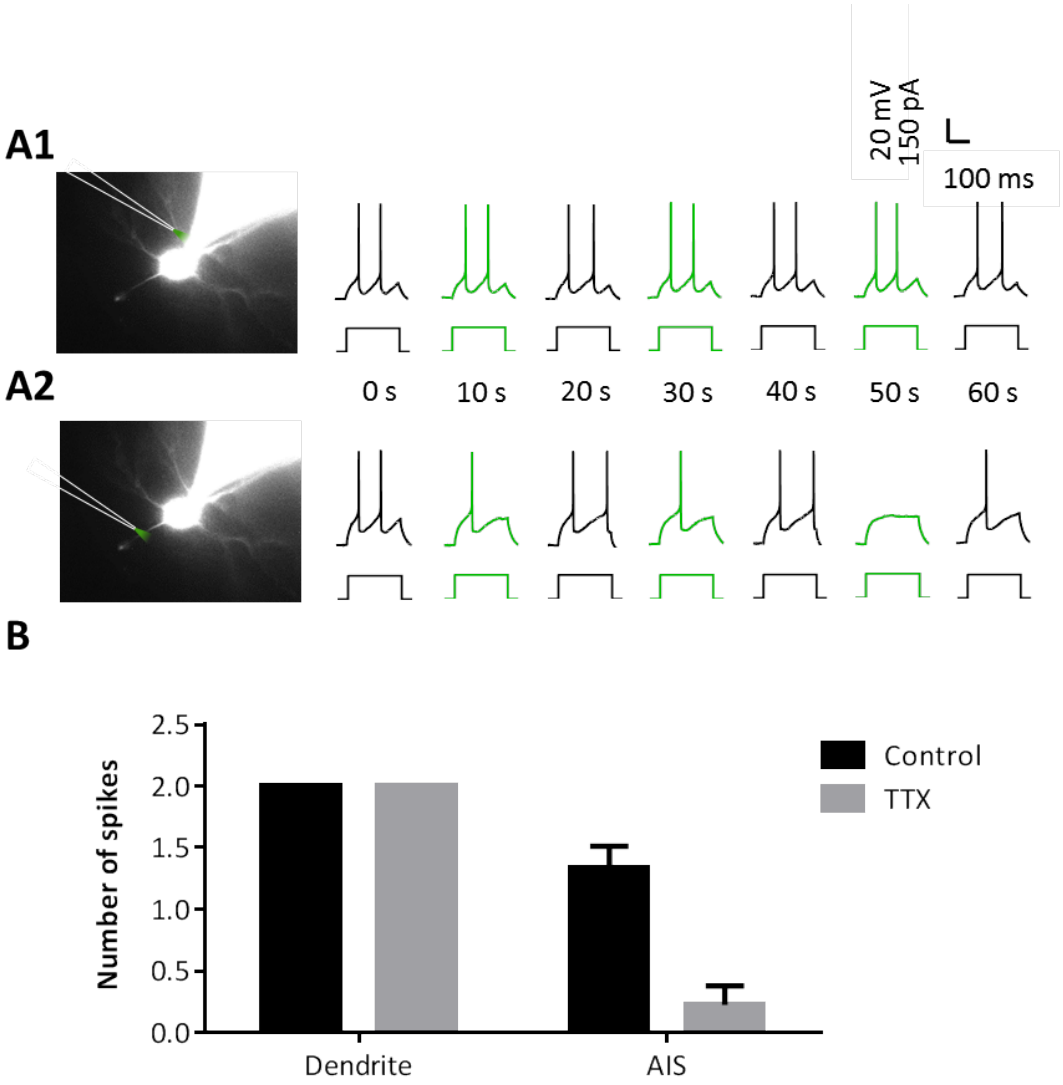

Figure 4.10 Pilot puffing experiments on pyramidal cell processes
Whole-cell current clamp recordings of pyramidal cells in response to TTX puffs on a dendrite vs AIS. Cells were filled with Alexa Fluor 488 to visualise processes under blue light (excitation/emission wavelength 490/525 nm). (A1) Left, live image of cell during recording showing puff pipette (white overlay in top left of image) containing external recording solution with 300 nM TTX, positioned behind a dendrite. Right, the first seven voltage traces (top) in response to square current steps (250 ms, 150 pA; bottom) injected at 0.1 Hz. Recordings were interleaved between control (black traces) and TTX puffing (green traces). Each puff lasted 2 s and preceded the current injection by 1.5 s. (A2) Same as A1 except for that the puff pipette was positioned behind the AIS. (B) Mean number of elicited spikes from between dendrite vs AIS puffing (18 sweeps from each).

AIS – located approximately 40 μm away from the soma (Kole et al. 2008) –, proximal dendrite, or soma.

A single 250 ms depolarising current step was injected into a pyramidal cell at 0.1 Hz to elicit two action potentials (Fig 4.10 A). A 2 s puff of TTX was administered 1.5 s before the start of the current step at 0.05 Hz, to ensure interleaved trials consisting of control spiking followed by spiking in the presence of locally applied TTX. Initially, puffing was applied onto a proximal dendrite (Fig 4.10 A1) for 18 sweeps (9 trials each) before puffing was applied onto the AIS (Fig 4.10 A2). Puffing TTX onto the dendrite had no effect on action potential firing but appeared to decrease firing when administered to the AIS (Fig 4.10 B). In the AIS puffing trial, the effect of TTX on reducing the number of action potentials failed to revert to baseline (two spikes). This is likely due to the poor reversibility of the effects of TTX. Nonetheless, this suggests that localised puffing of a drug can be reliably conducted in this experimental configuration.

Subcellular TTX puffing experiments were subsequently repeated in PV cells. Unfortunately, due to the complexity of the morphology of PV cells, it was difficult to identify the AIS. Another possible approach for this experiment could employ mice in which the AIS is labelled with a fluorescent protein. The protein ankyrin-G is expressed at the AIS and nodes of Ranvier of most neurons, where it binds to voltage-gated Na^+ channels and promotes their clustering (Zhou et al. 1998). Ankyrin-G mice tagged with green fluorescent protein (GFP) could provide a practical method for visualising the AIS of PV cells. Control TTX puffing on distinct subcellular locations during given depolarising steps would initially be performed to confirm that puffing specifically onto the AIS region of PV cells produces a robust decline in action potential firing. This would validate the spatial specificity of drug exposure onto distinct PV cell compartments. Spadin could then be puffed onto distinct subcellular compartments of a PV cell during a set of depolarising current steps to assess whether its firing excitability increased when the drug was applied onto the AIS. An increase in action potential firing during spadin puffing specifically

onto the AIS would suggest that TREK-1 channels are functionally expressed particularly in the AIS.

4.5 Discussion

In this chapter, I demonstrated that the blockade of TREK-1 channels significantly depolarises the RMP but does not alter the input resistance in PV cells. Furthermore, I showed that the potent TREK-1 channel blocker spadin significantly increases the excitability of PV cells in response to a given current stimulus. The significant effect of TREK-1 blockade on the RMP but not on the input resistance was surprising because any modulation of the TASK-like conductance - which includes TREK-1 - should have acted on both properties. Two separate TREK-1 blockers produced consistent results in both parameters, suggesting that this effect is robust. Nonetheless, PV cell output in response to thalamocortical stimulation is unaffected during spadin treatment, and isolated TREK-1 currents in PV cells are unaltered in the presence of the drug. One explanation for the discrepancy in these effects is that TREK-1 is expressed in the AIS, instead of the soma. The blockade of TREK-1 channels may boost cell excitability by depolarising the RMP and increasing the input resistance locally in the AIS, thereby making it easier for action potentials to be generated. A pilot experiment was performed to demonstrate that puffing a drug locally onto specific subcellular compartments of PV cells can affect the firing of a cell depending on the subcellular location. Future experiments could determine whether spadin increases PV cell excitability when applied locally onto the AIS. An increase in excitability upon local AIS puffing could support the conception that TREK-1 channels are not uniformly expressed throughout PV cells, but expressed at higher densities in the AIS.

4.5.1 Effect of TREK-1 channel blockade on RMP and input resistance

Both TREK-1 channel blockers spadin and amlodipine significantly depolarise the RMP but do not alter the input resistance in PV cells. This demonstrates that this effect is conserved between different TREK-1-blocking agents which highlights the true function of TREK-1 channels in PV cells, assuming minimal non-specific effects on other receptors from both drugs. Amlodipine is known to block L-type

Ca^{2+} channels as well as N- and T-type Ca^{2+} channels, although to a lesser degree (Liu et al. 2007; Furukawa et al. 1997). Nonetheless, as two structurally unrelated blockers were employed - and are unlikely to share the same off-target effects - the blockade of Ca^{2+} channels are unlikely to be involved in the effects observed in this thesis.

Both spadin and amlodipine showed a small indication of modulating the input resistance in PV cells - although the effect was not significant. Given the low *n* number and huge variability in input resistance in the amlodipine experimental data, examination of whether the data was underpowered was considered. However, it was discovered that the number of experiments required to reach significance would need to have been increased fivefold. This would have been impractical to achieve in the timeframe of this thesis, given that there were more important experiments to perform with the much more specific and potent drug spadin.

Upon initial spadin administration, the input resistance appeared to increase very slightly but then returned to baseline levels throughout application. Similarly, although amlodipine had no effect on the input resistance after 5-10 min of treatment, it did appear to increase it over a longer timescale. Previous studies in ventricular myocytes described amlodipine as a slow acting blocker on L-type Ca^{2+} channels, suggesting a similar slow mechanism could be implemented with TREK-1 channels (Kass et al. 1989). However, it was surprising to observe an effect where the RMP and input resistance did not change simultaneously, which would have been the case if a background K^+ channel was modified. One explanation for this could be due to non-specific effects of the drug to other channels. This could diminish the effect of the drug by influencing a change in the membrane properties through another mechanism, and thus depress the change in input resistance. Another explanation is that the effects were masked by noise within the recordings. To counteract unwanted noise, the input resistance was calculated from an average of 4 sweeps in response to hyperpolarising current steps, every 30 s. However, it is still possible that this measure of input resistance could have been unreliable.

4.5.2 Concentration and usage of blockers

The concentration of amlodipine used in experiments was 43 μM, which is a hundredfold greater than the IC_{50} - determined from cultured bovine adrenal zona fasciculata cells (Liu et al. 2007). A high concentration of amlodipine ensured a greater efficacy of TREK-1 channel blockade in murine slices. Notably, amlodipine's IC_{50} for L-type Ca^{2+} channels - determined from Xenopus oocytes (Furukawa et al. 1997) - is one-twentieth of the final concentration that was used in experiments. The effects of amlodipine on L-type Ca^{2+} channels cannot therefore be excluded. Nonetheless, it would have been expected that any block of Ca^{2+} channels would hyperpolarise the cell due to the inhibition of an inward cation current. The effects observed with amlodipine in this thesis depolarised the RMP instead, suggesting that any effect caused by L-type Ca^{2+} channels present in PV cells are not correlated with the result. On the other hand, a decline in the intracellular Ca^{2+} concentration resulting from the blockade of L-type Ca^{2+} channels could lead to a reduction in the activity of Ca^{2+}-activated K^+ channels. This would reduce the efflux of K^+ from inside the cell and result in depolarisation of the RMP - comparable to blocking TREK-1 channels. Similarly, the closure of these ion channels could also result in an increase in input resistance.

The magnitude of depolarisation was different between the two TREK-1 channel blockers. The effect of amlodipine on the RMP was over threefold greater than that of spadin. This could have been due to non-specific effects of amlodipine such as the modulation of Ca^{2+}-activated K^+ channels (as described above), which could have augmented the overall depolarising effect of blocking TREK-1. Another possibility is that the discrepancy is due to the use of different concentrations of each blocker. Spadin was only applied at a concentration 2.5-fold greater than the IC_{50} for TREK-1 whereas amlodipine was applied at a hundredfold. It would be interesting to increase the concentration of spadin fortyfold to match the IC_{50} used for amlodipine, to examine whether the effects on the RMP are similar to those observed with amlodipine. However, as the potency of TREK-1 blockade by amlodipine has not yet been investigated on cloned channels - while spadin has been tested at TREK-1

transfected in COS-7 cells (Mazella et al. 2010) – some of the differences in IC_{50}s between the two drugs could have been due to the differences between native TREK-1 channels and cloned channels. Finally, tissue accessibility between the two drugs could be different in slice compared to cultured systems, highlighting the difficulty in determining a reasonable concentration of blockers to apply to the slice.

4.5.3 The effect of spadin on the current-voltage relationship of TREK-1

Spadin failed to influence voltage-clamped TREK-1-isolated currents in PV cells in response to both voltage step and voltage ramp protocols. This was surprising given its effect on the RMP. Although a cocktail of ion channel blockers was added to the bath before spadin was tested, it was possible that other non-TREK-1 currents were masking its effects. Internal caesium and external TEA should have blocked most of the non-K_{2P} K^+ channels, whilst QX314 should have blocked voltage-gated Na^+ channels. Synaptic blockers were also used to remove contamination by synaptic currents. The L-type Ca^{2+} channel blocker nifedipine should have additionally removed a large proportion of Ca^{2+} currents.

Subsequent to the completion of experiments, nifedipine was later discovered to block TREK-1 channels with a low affinity (IC_{50} of 8.2 μM) in cultured cells (Liu et al. 2007). As 20 μM of nifedipine was used in these experiments it is possible that a significant proportion of TREK-1 channels was blocked before spadin was even administered. However, as experiments in this thesis were performed in brain slices, the concentration of pharmacological agents at their receptors is likely to be much lower than in cultured cells. This is partly because cultured cells are readily exposed to the external drug solution, however recordings made in slices are usually deep under the surface of the slice, making diffusion of compounds more difficult. It is likely therefore that nifedipine would have only blocked a small proportion of TREK-1 channels. Thus, spadin should have still been able to produce a significant block if TREK-1 channels are present.

4.5.4 Are TREK-1 channels expressed exclusively in the AIS of PV cells?

Spadin does not alter the amplitude of TREK-1-isolated currents, nor does it increase the input resistance in PV cells. Spadin does however increase the firing of PV cells in response to given current injections. Minimal expression of TREK-1 channels around the somata of PV cells compared to other cellular compartments could explain the lack of effect of spadin on the input resistance and current-voltage relationship. Their blockade would not necessarily have been detected by the recording pipette which monitors changes in electrophysiological properties close to the soma. It was for this reason that the increase in excitability could be explained by an increase in TREK-1 channels predominantly in the AIS of PV cells.

The spatial composition of voltage-gated K^+ channels in cerebellar interneurons was recently investigated by analysing spiking output in response to the uncaging of voltage-gated K^+ channel blockers onto various regions of the AIS (Rowan et al. 2014). A similar approach was conducted in this thesis using puffing of a drug instead of photolysis of a caged compound. Pilot puffing experiments confirmed the efficacy of locally administering a drug to a specific subcellular location in pyramidal cells. Applying the same protocol with PV cells proved to be more challenging due to the morphological complexity of PV cell processes, which made it difficult to identify the axon from the dendrites in order to locate its AIS. Unlike layer IV pyramidal cells which have long and thin axons that usually point towards infragranular layers, PV cell axons were much less distinctive, and could point in any direction. Thus, it could be useful to conduct similar subcellular puffing experiments in a mouse line where the AIS can be visualised using fluorescent proteins tagged to structures specifically expressed in this region (as discussed previously).

4.5.5 TREK-1 channel expression in astrocytes

Although this thesis aims to specifically increase the excitability of PV cells, it is imperative to consider the effects blocking TREK-1 channels on other cells within the cortical network. It is possible that the effects observed on the RMP and firing

excitability could be mediated by the blockade of TREK-1 channels in a different population of cells that may influence the activity of PV cells indirectly.

Interestingly, astrocytes have been reported to express TREK-1 channels (Zhou et al. 2009). Astrocytes are the predominant housekeeping cells of the nervous system which act to remove neurotransmitter released during synaptic activity, modulate ion and water homeostasis and prevent excitotoxicity in surrounding cells (Takano et al. 2009). Astrocytes have also been shown to release glutamate which can alter the level of synaptic activity of neighbouring neurons (Parpura et al. 1994). The homeostatic mechanisms of glutamate uptake and K^+ buffering modulated by astrocytes rely on several electrogenic transporters which work much more effectively at negative resting potentials (Olsen & Sontheimer 2009). Although a large proportion of the astrocytic RMP is thought to be regulated by $K_{ir}4.1$ inward rectifying K^+ channels, recent studies have suggested that TREK-1 channels contribute significantly to the passive K^+ conductance (Djukic et al. 2007; Zhou et al. 2009).

Importantly, the blockade of $K_{ir}4.1$ channels was demonstrated to result in membrane depolarisation and inhibition of glutamate uptake from the extracellular space (Djukic et al. 2007). It is therefore possible that the effects of spadin and amlodipine on the RMP of PV cells could be due to the blockade of TREK-1 channels in astrocytes instead of PV cells. This would lead to a depolarisation of the RMP in astrocytes which could reduce the activity of glutamate transporters, resulting in a global increase in glutamate in the extracellular space. This could activate AMPA receptors in nearby cells which would result in PV cell depolarisation. The increase in extracellular glutamate could also bind to NMDA receptors which have a higher affinity for the neurotransmitter, although most NMDA receptors would be inactive at rest. Furthermore, the depolarisation of astrocytes upon TREK-1 blockade could promote glutamate release from astrocytes themselves, further escalating the concentration of glutamate in the extracellular space, and activating more AMPA receptors in PV cells. Nonetheless, the activation of glutamate receptors in PV cells

would concurrently reduce the input resistance and is therefore unlikely to be the mechanism for the observed 1 mV depolarisation of the RMP.

Several experiments could be implemented to test for the contribution of astrocytic TREK-1 blockade on PV cell activity. Firstly, whole-cell patch-clamp experiments on astrocytes in response to TREK-1 blockers would confirm the magnitude of TREK-1 blockade on the astrocytic RMP. Secondly, glutamate release from astrocytes could be pharmacologically or genetically inhibited during PV cell recordings to test whether the effect on the RMP and firing excitability persists. Astrocytes could be transfected to express archaerhodopsin in their plasma membrane which could be light-stimulated to hyperpolarise and therefore silence them during experiments. Although it is unlikely that astrocytes modulate the activity of PV cells via increases in extracellular glutamate, as the activation of glutamate receptors on PV cells would concurrently decrease their input resistance, these experiments would nonetheless help to distinguish any role that they may have on the effects observed in PV cells in response to TREK-1 blockade.

4.5.6 Summary

The aim of this chapter was to increase the intrinsic excitability of PV cells by blocking TREK-1 channels. As TREK-1 channels are believed to contribute to the background K^+ conductance, their blockade would have been expected to depolarise the cell and concurrently increase the input resistance, and thus, increase cell excitability. Indeed, TREK-1 channel blockade significantly depolarised the RMP and increased the firing excitability of PV cells in response to given current stimuli, however the measured input resistance remained unchanged. These data indicate a possibility that TREK-1 channels might not be uniformly distributed along the somatodendritic axis in PV cells, but instead form functional channels in the AIS. The observed depolarisation of the RMP in whole-cell patch-clamp recordings could indicate a larger magnitude of depolarisation at the AIS where TREK-1 channels might be expressed, thus propagating back to the soma where the membrane

potential was recorded. Additional experiments including specific subcellular targeting of TREK-1 would be required to validate this concept.

Chapter 5

Discussion

5.1 Discussion

Schizophrenia and autism may share common pathophysiological mechanisms emerging from imbalances in neuronal network activity (Gao & Penzes 2015). Animal models and human post-mortem studies of the two disorders indicate aberrant inhibitory signalling particularly at the level of PV cells and their synapses (Marín 2012). New pharmacological strategies aimed at specifically targeting and increasing the basal activity of the PV cell population could be used to mitigate some of the behavioural symptoms associated with these disorders that current treatments have so far failed to address. By connecting recent findings from molecular, genetic and electrophysiological studies in mice, a novel approach for increasing PV cell excitability through the blockade of TASK-1/3 and TREK-1 channels was investigated. Importantly, this was the first time that specific blockers were acutely applied to examine the true involvement of TASK-1/3 and TREK-1 channels in modulating PV cell activity. Although previous studies support the role of these two-pore channels in setting the membrane potential and membrane resistance, this thesis presents data that argue against the functional expression of TASK-1/3 in PV cells.

5.1.1 Overall goal

Although GABAergic interneurons represent a minority of the entire neuronal population, they nevertheless manage to reliably provide powerful and temporally precise inhibition, which is thought to be essential for regulating global network balance (Markram et al. 2004). Several studies have now indicated aberrant activity of PV cells as an underlying pathophysiological mechanism for the development of schizophrenia and autism (Marín 2012). As PV cells comprise almost half of all GABAergic interneurons in the mammalian cortex (Xu et al. 2010), it is therefore understandable that any malfunctioning property present in PV cells will have substantial consequences on the network circuitry. The fundamental aim of this thesis was to explore a method for increasing the excitability of cortical PV cells. This method of increasing neuronal excitability focused on exploiting the low input

resistance characteristic of PV cells, and increase it by targeting TASK-like currents using TASK-1/3 and TREK-1 blockers. If successful, a novel strategy aimed at targeting and elevating the intrinsic excitability of PV cells could one day be implemented to rectify part of the deficits in inhibitory signalling linked to schizophrenia and autism. As a result, a correction in the underlying network imbalance could lead to improvements in several behavioural symptoms associated with these disorders.

5.1.2 Overall outcome

This thesis represents the first study to incorporate the use of specific TASK-1/3 and TREK-1 channel blockers in brain slices to examine their acute effects on the intrinsic properties of PV cells. Previous studies analysing the molecular profile of PV cells established prominent mRNA expression of TASK-1/3, and to a lesser degree TREK-1, in relation to other background K+ channels. The electrophysiological data from this thesis however argue against the molecular findings in the PV-cell field suggesting that TASK-1/3 channels are either not functionally present, or present at extremely low levels in PV cells. Nonetheless, TREK-1 blockade significantly increased PV cell excitability. As TREK-1 blockade did not affect the somatic input resistance, it was hypothesised that TREK-1 channels are expressed particularly in the AIS of PV cells, although further experiments would need to confirm this theory. Furthermore, contrary to molecular findings, the electrophysiological data from this thesis support a possibility that TREK-1 channels are functionally present at higher levels than TASK-1/3 channels.

In summary, the results in this thesis demonstrate that the leak background conductance – which serves to regulate the RMP and intrinsic excitability – is not regulated by TASK-1/3 channels, as previously suggested, but involves other leak K^+ channels. The effects observed during TREK-1 blockade however indicate that the modulation of TREK-1 channels could still provide a useful method for increasing PV cell excitability, although more experiments would need to be performed to better

understand the role they play in this cell type. It could therefore be interesting to continue exploring the effects of TREK-1 blockade in PV cells on network function. Once more is known about the effects of blocking TREK-1 channels on network activity and behaviour, this channel could one day be employed as a mechanism for restoring network balance in schizophrenia and autism.

5.1.3 TASK

A conserved feature in PV cells is their unusually low input resistance compared to other neuronal populations (Doischer et al. 2008; Taverna et al. 2005). This allowed for the targeting of a large resting conductance for modulation. Previous studies using immunohistochemistry and microarrays from cortical PV cells in mice revealed high levels of TASK-1 and TASK-3 mRNA transcripts compared to many other K^+ channels that are believed to contribute to the passive background conductance (Goldberg et al. 2011; Okaty et al. 2009). TASK-1 and TASK-3 transcripts were shown to increase in expression during development (between P10 and P18), which was paralleled by a decrease in input resistance, hyperpolarisation of the RMP, a decrease in the membrane time constant and a reduction in the half-widths of action potentials (Goldberg et al. 2011). The magnitude of these developmental changes was extreme: The RMP was found to hyperpolarise by 6 mV on average, while the input resistance and membrane time constant were reported to decrease sixfold during development (Goldberg et al. 2011). Furthermore, mature fast-spiking cells in TASK-1/3 knockout mice displayed larger input resistances and membrane time constants, approaching values comparable to those observed in pyramidal cells (Goldberg et al. 2011). Finally, TASK-1 immunoreactivity in fast-spiking cells was increased almost twofold during development, indicating the presence of the channel protein (Okaty et al. 2009). In summary, microarray, immunohistochemical and genetic knockout studies on TASK channels all support the expression of TASK in cortical fast-spiking cells.

The electrophysiology of TASK-1/3 blockade on cortical PV cells in this thesis however do not support the functional presence of TASK-1/3 channels, as the RMP and input resistance – two key measures mediated by background K^+ currents - were unaffected in this neuronal population. Importantly, unlike previous studies on PV cells which investigated the role of TASK-like currents using generalised blockers (Goldberg et al. 2011; Okaty et al. 2009; Torborg et al. 2006), this was the first time that the functional effects of specific TASK-1/3 channel blockers were examined. Furthermore, three structurally distinct TASK-1/3 channel blockers yielded consistent results – one of which was confirmed to have a functional effect in HEK-293 cells. Fundamentally, this indicates a number of possibilities: The high expression levels of TASK-1/3 mRNA may not necessarily translate to a high density of functional TASK-1/3 channels in the PV cell membrane. This could be due to TASK-1/3 mRNAs not being translated, or that TASK-1/3 proteins are made but are not transported to the membrane. TASK-1/3 proteins may even congregate in intracellular pools or may be inactive due to specific post-translational modifications. Additionally, the effects reported in TASK-1/3 knockout mice may have been determined by the genetic strain.

The experiments conducted on PV cells in this thesis demonstrate acute pharmacological inhibition of specific K_{2P} channels. This is important because the acute effects of a drug on a channel can be used to analyse how a cell responds to various stimuli before, during and after pharmacological application. This can be especially useful for analysing the function of channels during development, where a drug can be tested in animals at different developmental time points. The effects observed from acute pharmacological inhibition of a channel can then be compared with other studies examining channel function to better understand the underlying physiology.

It is difficult to interpret why PV cells in TASK-1/3 knockout mice have larger input resistances and membrane time constants compared to wildtype mice (Goldberg et al. 2011), while the data in this thesis clearly demonstrate that acute pharmacological

inhibition of TASK-1/3 channels has no effect on the intrinsic membrane properties. This difference could be explained by the different brain regions that were used to sample PV cells between the two studies. Although both studies analysed PV cells from the mouse barrel cortex, Goldberg et al (2011) examined layer II/III PV cells, whereas experiments in this thesis examined layer IV PV cells. This small difference in brain region could result in a difference in the expression ratio of specific leak channels, thus effecting the function of background currents in PV cells. Another possibility for the discrepancy between the two studies may arise from different strains of mice used between the studies. This could also result in the expression of different proportions of specific leak channels. Finally, variations of protein-protein interactions between the mice used in this thesis and TASK-1/3 knockout mice may have impacted common TASK-1/3-binding proteins which could have affected the function of other leak channels.

In conclusion, the acute application of specific TASK-1/3 channel blockers demonstrates that TASK-1/3 channels are either not functionally expressed, or present at extremely low levels in PV cells. This suggests that despite previous molecular findings on TASK channels, the resting background conductance in PV cells is mediated by a population of background K^+ channels other than TASK-1/3. This therefore highlights a major challenge in the field for linking molecular composition to physiological function.

5.1.4 TREK

The blockade of TREK-1 channels significantly depolarised the RMP and increased the excitability of cortical PV cells. This is important because the overall goal of this thesis is to increase the excitability of PV cells. Unlike TASK-1/3 channel blockade, two independent TREK-1 inhibitors clearly modulate the RMP. However, the lack of effect of TREK-1 blockade on the input resistance suggests other possible mechanisms beyond the classic interpretation of blocking a leak K^+ channel. The discrepancy in the effect of TREK-1 blockade between RMP depolarisation and

input resistance is surprising considering that any modulation of the K^+ background conductance should have affected both parameters.

Spadin significantly increased PV cell excitability. It was therefore hypothesised that TREK-1 channels might be expressed in the AIS, where action potential generation originates 20 μm from the soma (Hu & Jonas 2014). This would correspond to the lack of effect observed with spadin on the somatic input resistance and somatic current-voltage relationship (assuming TREK-1 currents were not initially blocked by nifedipine). If this is the case, then the 1 mV depolarisation of the RMP detected in the somata of PV cells (as the patch-clamp configuration primarily measures changes in the membrane voltage near the recording electrode) could indicate a substantial local depolarisation in the AIS. Similarly, if TREK-1 channels are indeed expressed in the AIS, then the local increase in input resistance in this region could greatly influence the excitability of the cell. Two mechanisms would therefore take place during local inhibition of TREK-1 channels in the AIS: Firstly, the depolarisation of the RMP would bring the AIS closer to firing threshold; and secondly, the local increase in input resistance would make it easier for incoming inputs to summate and result in action potential firing. These mechanisms could therefore explain the robust effect that spadin had on increasing the number of action potentials generated in response to given current steps.

The effects of spadin on the RMP and action potential firing but not on the input resistance led to the hypothesis that TREK-1 channels are expressed predominantly in the AIS. If this is true, then the manner in which the cell integrates information would be altered very differently in comparison to a cell that expresses its ionic conductances uniformly. Cells typically receive multiple excitatory inputs onto their dendrites and multiple inhibitory inputs along their entire somatodendritic axis (Megías et al. 2001). Because of this, the integration of inputs will depend on the relative amplitudes and kinetics of EPSPs and IPSPs present at distinct subcellular locations within the cell (Pouille et al. 2013). An action potential is generated once the summation of inputs depolarises the cell sufficiently enough to bring the AIS to

firing threshold. The amplitude and duration of EPSPs in response to a change in membrane resistance at the soma will not only be affected by the change in resistance, but also by competing IPSCs – which will also reduce the local input resistance - mediated by other perisomatic PV cell terminals (Pouille et al. 2013). A conductance change in the AIS however will not be affected by further inputs, as chandelier cells – which preferentially target the AIS of their target cells – do not synapse with PV cells (DeFelipe et al. 1989). Thus, a very different effect on the integration of inputs will occur if TREK-1 channels are expressed predominantly in the AIS in comparison to a uniform distribution. While a uniform distribution of leak channels would influence the integration of all inputs by reducing the amplitude and duration and therefore the summation of EPSPs, a predominant distribution of TREK-1 channels in the AIS would not influence the summation of inputs until EPSPs reach the AIS. TREK-1 channels could therefore be functioning as a tonic inhibitory method in the AIS by reducing the input resistance and hyperpolarising the cell locally, in a critical subcellular location where inputs arrive before the generation of an action potential.

Several additional experiments would need to be performed to confirm whether TREK-1 channels are expressed predominantly in the AIS of PV cells. Firstly, analysing the activity of action potential firing during subcellular puffing of spadin onto the specific compartments in response to a given set of current steps would provide an initial understanding of the potentially non-uniform distribution of TREK-1 expression. Secondly, the effect of spadin on the RMP and input resistance from direct patch-clamp recordings at the AIS region of PV cells would confirm whether the depolarising effect observed from whole-cell recordings in this thesis was specifically mediated in the AIS: A larger effect of depolarisation (>1 mV) compared to the effect observed in somatic recordings would support this theory. Finally, immunostaining of TREK-1 and ankyrin-G, a well-established AIS marker, could be used to examine whether both proteins are coexpressed in this region. As K_{2P} antibodies can unfortunately be unreliable, a TREK-1 antibody would need to be characterised first, using TREK-1 knockout tissue. These experiments would

therefore help to elucidate whether TREK-1 is expressed exclusively in the AIS of PV cells.

Finally, the depolarisation of the RMP allows for further computational effects in response to network inputs. Although the depolarisation of PV cells by 1 mV may appear to be negligible (albeit the cells did increase in excitability), the effect on the output of cells in response to inputs could nevertheless be considerable. Weak inputs restricted to the lower range of a cell's input-output function can be enhanced by increases in tonic depolarisation or decreases in conductance (Chance et al. 2002), resulting in a reduction in rheobase. The addition of membrane potential variance – which is likely to occur *in vivo* – induces neurons to fire in a probabilistic fashion (Hô & Destexhe 2000). Thus, the depolarisation of a neuron by 1 mV could result in a small increase in activity at the lower end of a cell's input-output function – which was observed by a reduction in rheobase during TREK-1 blockade in this thesis - but when combined with barrages of synaptic potentials *in vivo*, the cell could increase in excitability significantly. A 1 mV change in RMP can therefore exert a substantial effect on the output of PV cells.

5.1.5 Other background K^+ channels

The data in this thesis have distinguished that PV cells do not express functional somatic TASK-1/3 and TREK-1 channels to a level where they function as main contributors to the K+ leak conductance. The effect of external acidification and bupivacaine conditions on the RMP and input resistance of PV cells however was substantial. This suggests that the presence of a large population of channels - at least in the soma – that mediates the background conductance responsible for their low resistivity remains to be targeted. Blockers for other bupivacaine- and acid-sensitive channels could therefore be explored in the same way as TASK and TREK to analyse their effects on the passive properties of PV cells. This would not only help to identify other suitable channels that could be modulated to increase cell

excitability, but also help to elucidate the relative composition of background channels in PV cells.

Unfortunately, little is known about the ion channels responsible for the acidification- and bupivacaine- sensitive currents. In the K_{2P} family, TWIK-1 and TASK-2 channels are sensitive to both conditions which could provide interesting targets for modulation. While TWIK-1 mRNA transcripts have been reported to be expressed in cortical PV cells (Goldberg et al. 2011), TASK-2 however is predominantly expressed in the spinal cord and therefore cannot contribute to the currents observed in this thesis. Finally, inwardly rectifying K^+ channels may contribute to the background conductance in PV cells. $Kir_{2.2}$ and $Kir_{2.3}$ mRNA subunits have been reported to increase during development, similar to TASK-1 and TASK-3 (Goldberg et al. 2011). These channels however do not respond to extracellular acidification and it is unclear whether they are sensitive to bupivacaine (Hibino et al. 2010; Sepulveda et al. 2015). Nonetheless, although these channels belong to an additional population that are not represented by the acidification- and bupivacaine-sensitive currents, they are however known to pass current at rest and could therefore be interesting targets. This highlights the complexity of characterising background K^+ currents in neurons.

5.1.6 Experimental approach

Although the aim of this thesis was to develop a method to increase the excitability of cortical PV cells, the primary benefit of a establishing a successful technique would have ultimately been applied to target PV cells in individuals with schizophrenia and autism. The experiments in this thesis however were performed on tissue slices from healthy mice, which may not have incorporated the aberrant network signalling characteristic to the diseased states. As a result, the experiments focused on elevating normal PV cell signalling instead of restoring the deficits that may have been found in the real disorders. The discrepancy between using a healthy and a diseased system may have had a significant effect on the outcome of the

experiments. Attempting to increase basal excitability of a population of cells in healthy tissue may have been restricted by compensatory mechanisms, whereas targeting a population of defunct cells in diseased tissue already low in excitability could have been more susceptible for modulation, thus restoring abnormalities in the underlying network imbalance. Finally, attempting to rectify network pathology in a diseased system rather than experimenting in healthy tissue would have directly addressed numerous deficits that could have been linked to the disease. These may have included alterations in specific protein-protein interactions at the cellular level, to changes in network activity, which might not have manifested in healthy tissue. Successfully implementing a novel strategy to correct the underlying network imbalance in a diseased slice could then have been used to test behaviour in a mouse with symptoms representing schizophrenia and autism.

Several approaches could have been employed to test the effects of two-pore channel blockers in disease conditions. Brain slices could have been pretreated with agents such as ketamine - which antagonise NMDA receptors – to mimic some of the pathophysiology in the brain tissue. Ketamine is known to produce acute psychotic states in normal individuals that resemble some of the symptoms of schizophrenia (Breier et al. 1997), and may induce the dysfunction of cortical PV cells (Behrens et al. 2007). Thus, the effects of two-pore channel blockade on the cellular and network function of PV cells could have therefore been analysed specifically in diseased tissue where ketamine would have been administered, in the attempt to directly rectify the pathophysiology. This would have provided a basis for which experiments could have been performed to reverse deficits in signalling from within a 'schizophrenic' slice which, if successful, could have then been applied to awake ketamine-administered mice to analyse behaviour. Performing similar *in vitro* and behavioural experiments on mice with the conditional deletion of ErbB4 in PV cells may have also provided interesting results. These mice have a reduced number of glutamatergic synapses onto PV cells paralleled by a reduction in the number of inhibitory synapses onto pyramidal cells (Fazzari et al. 2010) and exhibit schizophrenia-like phenotypes (Wen et al. 2010). Hence, two-pore blockers could

have been applied in the attempt to rectify cellular and network deficits in the diseased system.

5.1.7 Future directions for the treatment of Schizophrenia and autism

The experiments conducted in this thesis demonstrate TREK-1 as an interesting target for the modulation of PV cells. Although the effects of TREK-1 blockade may seem intricate, the overall goal of increasing the excitability of PV cells appears to have been achieved. The effect of spadin on increasing the excitability of PV cells in response to TREK-1 blockade was substantial. This suggests that targeting TREK-1 in this way could potentially be useful as a treatment for diseases linked to aberrant PV cell signalling, such schizophrenia and autism. TREK-1 channel blockade could therefore be used to increase the excitability of PV cells, and potentially restore part of the proposed network deficits associated with these disorders. The true molecular and functional profile of TREK-1 expression is evidently required before it can be identified as an appropriate target. First, a better understanding of the mechanism for which TREK-1 blockade exerts its effect is still required. Second, the relative expression of TREK-1 between PV cells and other cells types would need to be addressed, to prevent the effect of increasing neuronal excitability in multiple cell populations.

Developing a future therapy for the treatment of specific disorders by pharmacologically targeting a channel not only requires analysis of the effects on the target cell, but also the careful consideration that other cells may also be affected. Even if a drug is synthesised that is highly specific to a desired channel, other cells may express the same (or similar) channel which may result in the drug's effect on more populations that just the intended target group. Further experiments analysing the effects on other cell populations would therefore be required to ensure that the effects on their activity were minimal in comparison to the target group. These include analysing the effects on cellular and network functions. Moreover, this thesis examined a method to modulate PV cell excitability in the cortex - a region of the

brain where studies have uncovered abnormalities of this cell type in schizophrenia and autism. As such, the effects of a two-pore channel blocker would not only be restricted to cortical PV cells, but would also affect cells in other brain regions. Finally, target channels may also be present on cells in other organs outside the brain. Several two-pore channels including TREK-1 have been reported to contribute to electrical activity in the heart (Xian et al. 2006). This global action of a TREK-1 blocker would therefore need to be considered to prevent unwanted effects in other organs as well as in healthy brain areas.

The pathological complexity of neuropsychiatric disorders unfortunately makes them difficult to treat with a single drug (Donegan & Lodge 2016; Young & Findling 2015). These neurodevelopmental disorders have multiple genetic aetiologies which result in complex behavioural phenotypes, suggesting that the cause manifests from a wide spectrum of pathological abnormalities (Owen et al. 2016; Levy et al. 2009). In schizophrenia for example, antipsychotics appear to be effective for treating positive symptoms, such as hallucinations and delusions, but seem to be poor in treating negative symptoms, including social withdrawal and apathy, as well as cognitive deficits (Miyamoto et al. 2012). It is therefore worth considering that one drug designed to rectify aberrant function in a specific biological pathway linked to the progression of a disease is unlikely to compensate entirely for deficits associated with other pathways. For example, antipsychotics which block dopamine D2 receptors (Meltzer 1989) might alleviate the positive symptoms of schizophrenia because the underlying pathology that contributes to positive symptoms are perhaps linked to D2 receptors. Thus, other pathological mechanisms are likely to contribute to the negative and cognitive symptoms associated with schizophrenia. In particular, cognitive symptoms have been linked to impairments in the synchronisation of oscillatory activity (Marín 2012). As PV cells are known to maintain fast network synchrony (Bartos et al. 2007), future treatments aimed at increasing PV cell activity - such as TREK-1 modulation – could therefore be extremely useful for alleviating the cognitive symptoms. It is therefore important to understand the functional pathology in order to elucidate novel targets for treatments of neuropsychiatric disorders. Moreover, several treatments each designed to rectify distinct

neuropathological deficits could then be used in conjunction to alleviate a wider scope of symptoms.

References

Agmon, A. & Connors, B.W., 1991. Thalamocortical responses of mouse somatosensory (barrel) cortex in vitro. *Neuroscience*, 41(2–3), pp.365–379.

Akbarian, S. et al., 1995. Gene expression for glutamic acid decarboxylase is reduced without loss of neurons in prefrontal cortex of schizophrenics. *Archives of General Psychiatry*, 52(4), pp.258–266.

Ascoli, G. a et al., 2008. Petilla terminology: nomenclature of features of GABAergic interneurons of the cerebral cortex. *Nature Reviews Neuroscience*, 9(7), pp.557–568.

Atallah, B. V. & Scanziani, M., 2009. Instantaneous modulation of gamma oscillation frequency by balancing excitation with inhibition. *Neuron*, 62(4), pp.566–577.

Azouz, R., 2005. Dynamic spatiotemporal synaptic integration in cortical neurons: neuronal gain, revisited. *Journal of Neurophysiology*, 94(4), pp.2785–2796.

Azouz, R. & Gray, C.M., 2000. Dynamic spike threshold reveals a mechanism for synaptic coincidence detection in cortical neurons in vivo. *Proceedings of the National Academy of Sciences of the United States of America*, 97(14), pp.8110–8115.

Bacci, A., Huguenard, J.R. & Prince, D. a, 2003. Functional autaptic neurotransmission in fast-spiking interneurons: a novel form of feedback inhibition in the neocortex. *The Journal of Neuroscience*, 23(3), pp.859–866.

Barbato, A., 1998. Psychiatry in transition: outcomes of mental health policy shift in Italy. *Australian & New Zealand Journal of Psychiatry*, 32(5), pp.673–679.

Bartos, M. et al., 2002. Fast synaptic inhibition promotes synchronized gamma oscillations in hippocampal interneuron networks. *Proceedings of the National Academy of Sciences of the United States of America*, 99(20), pp.13222–13227.

Bartos, M., Vida, I. & Jonas, P., 2007. Synaptic mechanisms of synchronized gamma oscillations in inhibitory interneuron networks. *Nature Reviews Neuroscience*, 8(1), pp.45–56.

Behrens, M.M. et al., 2007. Ketamine-induced loss of phenotype of fast-spiking interneurons is mediated by NADPH-oxidase. *Science*, 318(5856), pp.1645–1647.

Belforte, J.E. et al., 2010. Postnatal NMDA receptor ablation in corticolimbic interneurons confers schizophrenia-like phenotypes. *Nature Neuroscience*, 13(1), pp.76–83.

Benes, F.M., Vincent, S.L. & Todtenkopf, M., 2001. The density of pyramidal and

nonpyramidal neurons in anterior cingulate cortex of schizophrenic and bipolar subjects. *Biological Psychiatry*, 50(6), pp.395–406.

Binzegger, T., Douglas, R.J. & Martin, K.A.C., 2004. A quantitative map of the circuit of cat primary visual cortex. *Journal of Neuroscience*, 24(39), pp.8441–8453.

Breier, A. et al., 1997. Association of ketamine-induced psychosis with focal activation of the prefrontal cortex in healthy volunteers. *American Journal of Psychiatry*, 154(6), pp.805–811.

Brooks-Kayal, A., 2010. Epilepsy and autism spectrum disorders: Are there common developmental mechanisms? *Brain and Development*, 32(9), pp.731–738.

Bucurenciu, I. et al., 2008. Nanodomain coupling between Ca2+ channels and Ca2+ sensors promotes fast and efficient transmitter release at a cortical GABAergic synapse. *Neuron*, 57(4), pp.536–545.

Bucurenciu, I., Bischofberger, J. & Jonas, P., 2010. A small number of open Ca2+ channels trigger transmitter release at a central GABAergic synapse. *Nature Neuroscience*, 13(1), pp.19–21.

Buzsaki, G. & Draguhn, A., 2004. Neuronal oscillations in cortical networks. *Science*, 304(5679), pp.1926–1929.

Buzsáki, G. & Schomburg, E.W., 2015. What does gamma coherence tell us about inter-regional neural communication? *Nature Neuroscience*, 18(4), pp.484–489.

Buzsáki, G. & Wang, X.-J., 2012. Mechanisms of gamma oscillations. *Annual Review of Neuroscience*, 35, pp.203–225.

Campbell, D.B. et al., 2008. Genetic evidence implicating multiple genes in the met receptor tyrosine kinase pathway in autism spectrum disorder. *Autism Research*, 1(3), pp.159–168.

Cardin, J. a et al., 2009. Driving fast-spiking cells induces gamma rhythm and controls sensory responses. *Nature*, 459(7247), pp.663–667.

Chance, F.S., Abbott, L.F. & Reyes, A.D., 2002. Gain modulation from background synaptic input. *Neuron*, 35(4), pp.773–782.

Chatelain, F.C. et al., 2012. TWIK1, a unique background channel with variable ion selectivity. *Proceedings of the National Academy of Sciences of the United States of America*, 109(14), pp.5499–5504.

Chattopadhyaya, B. et al., 2007. GAD67-mediated GABA synthesis and signaling regulate inhibitory synaptic innervation in the visual cortex. *Neuron*, 54(6),

pp.889–903.

Chattopadhyaya, B. & Di Cristo, G., 2012. GABAergic circuit dysfunctions in neurodevelopmental disorders. *Frontiers in Psychiatry*, 3(51), pp.1–9.

Chesney, E., Goodwin, G.M. & Fazel, S., 2014. Risks of all-cause and suicide mortality in mental disorders: A meta-review. *World Psychiatry*, 13(2), pp.153–160.

Cheung, C. et al., 2010. Autistic disorders and schizophrenia: Related or remote? An anatomical likelihood estimation. *PLoS ONE*, 5(8).

Chih, B., Engelman, H. & Scheiffele, P., 2005. Control of excitatory and inhibitory synapse formation by neuroligins. *Science*, 307(5713), pp.1324–1328.

Cho, R.Y., Konecky, R.O. & Carter, C.S., 2006. Impairments in frontal cortical synchrony and cognitive control in schizophrenia. *Proceedings of the National Academy of Sciences*, 103(52), pp.19878–19883.

Cline, H., 2005. Synaptogenesis: A balancing act between excitation and inhibition. *Current Biology*, 2(6), pp.203–205.

Cobb, S.R. et al., 1995. Synchronization of neuronal activity in hippocampus by individual GABAergic interneurons. *Nature*, 378(6552), pp.75–78.

Coburn, C.A. et al., 2012. Discovery of a pharmacologically active antagonist of the two-pore-domain potassium channel K 2P9.1 (TASK-3). *ChemMedChem*, 7(1), pp.123–133.

Conti, F., Minelli, A. & Melone, M., 2004. GABA transporters in the mammalian cerebral cortex: Localization, development and pathological implications. *Brain Research Reviews*, 45(3), pp.196–212.

Courchesne, E., Redcay, E. & Kennedy, D.P., 2004. The autistic brain: birth through adulthood. *Current Opinion in Neurology*, 17(4), pp.489–496.

Cross-Disorder Group of the Psychiatric Genomics Consortium et al., 2013. Genetic relationship between five psychiatric disorders estimated from genome-wide SNPs. *Nature Genetics*, 45(9), pp.984–994.

Cruikshank, S.J. et al., 2010. Pathway-specific feedforward circuits between thalamus and neocortex revealed by selective optical stimulation of axons. *Neuron*, 65(2), pp.230–245.

Cruikshank, S.J. et al., 2004. Potent block of Cx36 and Cx50 gap junction channels by mefloquine. *Proceedings of the National Academy of Sciences*, 101(33), pp.12364–12369.

Cruikshank, S.J., Lewis, T.J. & Connors, B.W., 2007. Synaptic basis for intense thalamocortical activation of feedforward inhibitory cells in neocortex. *Nature Neuroscience*, 10(4), pp.462–468.

Curley, A.A. et al., 2011. Cortical deficits of glutamic acid decarboxylase 67 expression in schizophrenia: clinical, protein, and cell type-specific features. *American Journal of Psychiatry*, 168(9), pp.921–929.

Daw, M.I., Ashby, M.C. & Isaac, J.T.R., 2007. Coordinated developmental recruitment of latent fast spiking interneurons in layer IV barrel cortex. *Nature Neuroscience*, 10(4), pp.453–461.

Deans, M.R. et al., 2001. Synchronous activity of inhibitory networks in neocortex requires electrical synapses containing connexin36. *Neuron*, 31(3), pp.477–485.

DeBoer, E.M. & Anderson, S.A., 2016. Fate determination of cerebral cortical GABAergic interneurons and their derivation from stem cells. *Brain Research*, 1655, pp.277–282.

Decher, N. et al., 2011. Knock-out of the potassium channel TASK-1 leads to a prolonged qt interval and a disturbed QRS complex. *Cellular Physiology and Biochemistry*, 28(1), pp.77–86.

Defelipe, J. et al., 2013. New insights into the classification and nomenclature of cortical GABAergic interneurons. *Nature Reviews Neuroscience*, 14(3), pp.202-216.

DeFelipe, J., Hendry, S.H. & Jones, E.G., 1989. Visualization of chandelier cell axons by parvalbumin immunoreactivity in monkey cerebral cortex. *Proceedings of the National Academy of Sciences of the United States of America*, 86(6), pp.2093–2097.

DeVries, S.H., 2001. Exocytosed protons feedback to suppress the Ca2+ current in mammalian cone photoreceptors. *Neuron*, 32(6), pp.1107–1117.

Dichter, M.A. & Ayala, G.F., 1987. Cellular mechanisms of epilepsy: a status report. *Science*, 237(4811), pp.157–64.

Djukic, B. et al., 2007. Conditional knock-out of Kir4.1 leads to glial membrane depolarization, inhibition of potassium and glutamate uptake, and enhanced short-term synaptic potentiation. *Journal of Neuroscience*, 27(42), pp.11354–11365.

Doischer, D. et al., 2008. Postnatal differentiation of basket cells from slow to fast signaling devices. *Journal of Neuroscience*, 28(48), pp.12956–12968.

Donegan, J.J. & Lodge, D.J., 2016. Cell-based therapies for the treatment of

schizophrenia. *Brain Research*, 1655, pp.262–269.

Dror, V. et al., 1999. hKCa3/KCNN3 potassium channel gene: association of longer CAG repeats with schizophrenia in Israeli Ashkenazi Jews, expression in human tissues and localization to chromosome 1q21. *Molecular Psychiatry*, 4(3), pp.254-260

Du, J. et al., 1996. Developmental expression and functional characterization of the potassium-channel subunit Kv3.1b in parvalbumin-containing interneurons of the rat hippocampus. *Journal of Neuroscience*, 16(2), pp.506–518.

Dunning, D.D. et al., 1999. GABAA receptor-mediated miniature postsynaptic currents and à-subunit expression in developing cortical neurons. *Journal of Neurophysiology*, 82(6), pp.3286–3297.

Duprat, F. et al., 1997. TASK, a human background K+ channel to sense external pH variations near physiological pH. *EMBO Journal*, 16(17), pp.5464–5471.

Ehninger, D. et al., 2008. Reversing neurodevelopmental disorders in adults. *Neuron*, 60(6), pp.950–960.

Elvevåg, B. & Goldberg, T.E., 2000. Cognitive impairment in schizophrenia is the core of the disorder. *Critical reviews in neurobiology*, 14(1), pp.1–21.

Engel, A.K., Fries, P. & Singer, W., 2001. Dynamic predictions: oscillations and synchrony in top-down processing. *Nature Reviews Neuroscience*, 2(10), pp.704–716.

Erisir, A. et al., 1999. Function of specific K(+) channels in sustained high-frequency firing of fast-spiking neocortical interneurons. *Journal of Neurophysiology*, 82(5), pp.2476–2489.

Fagiolini, M. et al., 2004. Specific GABAA circuits for visual cortical plasticity. *Science*, 303(5664), pp.1681–1683.

Fatemi, S.H. et al., 2002. Glutamic acid decarboxylase 65 and 67 kDa proteins are reduced in autistic parietal and cerebellar cortices. *Biological Psychiatry*, 52(8), pp.805–810.

Fatemi, S.H. et al., 2010. mRNA and protein levels for GABAAα4, α5, β1 and GABABR1 receptors are altered in brains from subjects with autism. *Journal of Autism and Developmental Disorders*, 40(6), pp.743–750.

Fazzari, P. et al., 2010. Control of cortical GABA circuitry development by Nrg1 and ErbB4 signalling. *Nature*, 464(7293), pp.1376–1380.

Feliciangeli, S. et al., 2014. The family of K2P channels: salient structural and

functional properties. *Journal of Physiology*, 593(12), pp.2587–2603.

Fell, J. et al., 2001. Human memory formation is accompanied by rhinal-hippocampal coupling and decoupling. *Nature Neuroscience*, 4(12), pp.1259–1264.

Fink, M. et al., 1996. Cloning, functional expression and brain localization of a novel unconventional outward rectifier K+ channel. *EMBO Journal*, 15(24), pp.6854–6862.

Flames, N. et al., 2004. Short- and long-range attraction of cortical GABAergic interneurons by neuregulin-1. *Neuron*, 44(2), pp.251–561.

Fox, K., 2002. Anatomical pathways and molecular mechanisms for plasticity in the barrel cortex. *Neuroscience*, 111(4), pp.799–814.

Friedrich, G. & Soriano, P., 1991. Promoter traps in embryonic stem cells: a genetic screen to identify and mutant developmental genes in mice. *Genes and Development*, 5, pp.1513–1523.

Fries, P., 2005. A mechanism for cognitive dynamics: neuronal communication through neuronal coherence. *Trends in Cognitive Sciences*, 9(10), pp.474–480.

Furukawa, T. et al., 1997. Voltage and pH dependent block of cloned N-type Ca2+ channels by amlodipine. *British Journal of Pharmacology*, 121(6), pp.1136–1140.

Furutani, K. et al., 2010. Bupivacaine inhibits glutamatergic transmission in spinal dorsal horn neurons. *Anesthesiology*, 112(1), pp.138–143.

Gabernet, L. et al., 2005. Somatosensory integration controlled by dynamic thalamocortical feed-forward inhibition. *Neuron*, 48(2), pp.315–327.

Galarreta, M. & Hestrin, S., 1999. A network of fast-spiking cells in the neocortex connected by electrical synapses. *Nature*, 402(6757), pp.72–75.

Galarreta, M. & Hestrin, S., 2002. Electrical and chemical synapses among parvalbumin fast-spiking GABAergic interneurons in adult mouse neocortex. *Proceedings of the National Academy of Sciences of the United States of America*, 99(19), pp.12438–12443.

Galarreta, M. & Hestrin, S., 2001. Spike transmission and synchrony detection in networks of GABAergic interneurons. *Science*, 292(5525), pp.2295–2299.

Gao, R. & Penzes, P., 2015. Common mechanisms of excitatory and inhibitory imbalance in schizophrenia and autism spectrum disorders. *Current Molecular Medicine*, 15(2), pp.146–167.

Geiger, J.R.P. et al., 1995. Relative abundance of subunit mRNAs determines gating and Ca2+ permeability of AMPA receptors in principal neurons and interneurons in rat CNS. *Neuron*, 15(1), pp.193–204.

Geiger, J.R.P. et al., 1997. Submillisecond AMPA receptor-mediated signaling at a principal neuron- interneuron synapse. *Neuron*, 18(6), pp.1009–1023.

Gelman, D.M. & Marín, O., 2010. Generation of interneuron diversity in the mouse cerebral cortex. *European Journal of Neuroscience*, 31(12), pp.2136–2141.

Gibson, J.R., Beierlein, M. & Connors, B.W., 1999. Two networks of electrically coupled inhibitory neurons in neocortex. *Nature*, 402(6757), pp.75–79.

Gillberg, C. & Billstedt, E., 2000. Autism and asperger syndrome: coexistence with other clinical disorders. *Acta Psychiatrica Scandinavica*, 102(5), pp.321–330.

Glantz, L. & Lewis, D., 2000. Decreased dendritic spine density on prefrontal cortical pyramidal neurons in schizophrenia. *Archives of General Psychiatry*, 57(1), pp.65–73.

Glausier, J.R. & Lewis, D.A., 2013. Dendritic spine pathology in schizophrenia. *Neuroscience*, 251, pp.90–107.

Glausier, J.R. & Lewis, D.A., 2011. Selective pyramidal cell reduction of GABA(A) receptor α1 subunit messenger RNA expression in schizophrenia. *Neuropsychopharmacology*, 36(10), pp.2103–2110.

Glickfeld, L.L. et al., 2009. Interneurons hyperpolarize pyramidal cells along their entire somatodendritic axis. *Nature Neuroscience*, 12(1), pp.21–23.

Gogolla, N. et al., 2009. Common circuit defect of excitatory-inhibitory balance in mouse models of autism. *Journal of Neurodevelopmental Disorders*, 1(2), pp.172–181.

Goldberg, E.M. et al., 2008. K+ channels at the axon initial segment dampen near-threshold excitability of neocortical fast-spiking GABAergic interneurons. *Neuron*, 58(3), pp.387–400.

Goldberg, E.M. et al., 2011. Rapid developmental maturation of neocortical FS cell intrinsic excitability. *Cerebral Cortex*, 21(3), pp.666–682.

Goldberg, E.M. et al., 2005. Specific functions of synaptically localized potassium channels in synaptic transmission at the neocortical GABAergic fast-spiking cell synapse. *Journal of Neuroscience*, 25(21), pp.5230–5535.

Goldstein, S. a N. et al., 2005. International Union of Pharmacology. LV. Nomenclature and molecular relationships of two-P potassium channels.

Pharmacological Reviews, 57(4), pp.527–540.

Grützner, C. et al., 2013. Deficits in high- (>60 Hz) gamma-band oscillations during visual processing in schizophrenia. *Frontiers in Human Neuroscience*, 7(88).

Guidotti, A. et al., 2000. Decrease in reelin and glutamic acid decarboxylase 67 (GAD 67) expression in schizophrenia and bipolar disorder. *Archives of General Psychiatry*, 57(11), pp.1061–1069.

Gulyá, A.I. et al., 1999. Total number and ratio of excitatory and inhibitory synapses converging onto single interneurons of different types in the CA1 area of the rat hippocampus. *Journal of Neuroscience*, 19(22), pp.10082–10097.

Gupta, A. et al., 2007. Organizing principles for a diversity of GABAergic interneurons and synapses in the neocortex. *Science*, 287(5451), pp.273–278.

Gutman, G.A. et al., 2005. International Union of Pharmacology. LIII. Nomenclature and molecular relationships of voltage-gated potassium channels. *Pharmacological Reviews*, 57(4), pp.473–508.

Haider, B. et al., 2006. Neocortical network activity in vivo is generated through a dynamic balance of excitation and inhibition. *Journal of Neuroscience*, 26(17), pp.4535–4545.

Haider, B. & McCormick, D.A., 2009. Rapid neocortical dynamics: cellular and network mechanisms. *Neuron*, 62(2), pp.171–189.

Hájos, N. et al., 2009. Maintaining network activity in submerged hippocampal slices: importance of oxygen supply. *European Journal of Neuroscience*, 29(2), pp.319–327.

Happé, F. & Frith, U., 2006. The weak coherence account: detail-focused cognitive style in autism spectrum disorders. *Journal of Autism and Developmental Disorders*, 36(1), pp.5–25.

Harrison, P.J. & Law, A.J., 2006. Neuregulin 1 and schizophrenia: genetics, gene expression, and neurobiology. *Biological Psychiatry*, 60(2), pp.132–140.

Harrison, P.J. & Weinberger, D.R., 2005. Schizophrenia genes, gene expression, and neuropathology: on the matter of their convergence. *Molecular Psychiatry*, 10(8), pp.804–804.

Hashimoto, T. et al., 2003. Gene expression deficits in a subclass of GABA neurons in the prefrontal cortex of subjects with schizophrenia. *Journal of Neuroscience*, 23(15), pp.6315–6326.

Hestrin, S. & Armstrong, W.E., 1996. Morphology and physiology of cortical

neurons in layer I. *Journal of neuroscience,* 16(17), pp.5290–5300.

Heurteaux, C. et al., 2006. Deletion of the background potassium channel TREK-1 results in a depression-resistant phenotype. *Nature Neuroscience*, 9(9), pp.1134–1141.

Hibino, H. et al., 2010. Inwardly rectifying potassium channels: their structure, function, and physiological roles. *Physiological Reviews*, 90(1), pp.291–366.

Hikida, T. et al., 2007. Dominant-negative DISC1 transgenic mice display schizophrenia-associated phenotypes detected by measures translatable to humans. *Proceedings of the National Academy of Sciences of the United States of America*, 104(36), pp.14501–14506.

Hioki, H. et al., 2013. Cell type-specific inhibitory inputs to dendritic and somatic compartments of parvalbumin-expressing neocortical interneuron. *Journal of Neuroscience*, 33(2), pp.544–555.

Hippenmeyer, S. et al., 2005. A developmental switch in the response of DRG neurons to ETS transcription factor signaling. *PLoS Biology*, 3(5).

Hô, N. & Destexhe, a, 2000. Synaptic background activity enhances the responsiveness of neocortical pyramidal neurons. *Journal of Neurophysiology*, 84(3), pp.1488–1496.

Homayoun, H. & Moghaddam, B., 2007. NMDA receptor hypofunction produces opposite effects on prefrontal cortex interneurons and pyramidal neurons. *Journal of Neuroscience*, 27(43), pp.11496–11500.

Hu, H., Gan, J. & Jonas, P., 2014. Interneurons. Fast-spiking, parvalbumin^{+} GABAergic interneurons: from cellular design to microcircuit function. *Science*, 345(6196).

Hu, H. & Jonas, P., 2014. A supercritical density of Na+ channels ensures fast signaling in GABAergic interneuron axons. *Nature Neuroscience*, 17(5), pp.686–693.

Hu, H., Martina, M. & Jonas, P., 2010. Dendritic mechanisms underlying rapid synaptic activation of fast-spiking hippocampal interneurons. *Science*, 327(5961), pp.52–58.

Hull, C., Isaacson, J.S. & Scanziani, M., 2009. Postsynaptic mechanisms govern the differential excitation of cortical neurons by thalamic inputs. *Journal of neuroscience*, 29(28), pp.9127–9136.

Hutsler, J.J. & Zhang, H., 2010. Increased dendritic spine densities on cortical projection neurons in autism spectrum disorders. *Brain Research*, 1309, pp.83–

94.

Isaacson, J.S. & Scanziani, M., 2011. How inhibition shapes cortical activity. *Neuron*, 72(2), pp.231–243.

Ito, S., 2016. GABA and glycine in the developing brain. *Journal of Physiological Sciences*, 66(5), pp.375–379.

Jentsch, T.J. et al., 2002. Molecular structure and physiological function of chloride channels. *Physiological Reviews*, 82(2), pp.503–568.

Ji, Y. et al., 2009. Role of dysbindin in dopamine receptor trafficking and cortical GABA function. *Proceedings of the National Academy of Sciences of the United States of America,* 106(46), pp.19593-19598

Johnson, M.E. et al., 2002. Effect of local anesthetic on neuronal cytoplasmic calcium and plasma membrane lysis (necrosis) in a cell culture model. *Anesthesiology*, 97(6), pp.1466–1476.

Joho, R.H. et al., 1999. Increased gamma- and decreased delta-oscillations in a mouse deficient for a potassium channel expressed in fast-spiking interneurons. *Journal of Neurophysiology*, 82(4), pp.1855-1864

Joshi, D. et al., 2012. Higher gamma-aminobutyric acid neuron density in the white matter of orbital frontal cortex in schizophrenia. *Biological Psychiatry*, 72(9), pp.725–733.

Kang, D. & Kim, D., 2004. Single-channel properties and pH sensitivity of two-pore domain K + channels of the TALK family. *Biochemical and Biophysical Research Communications*, 315(4), pp.836–844.

Kapfer, C. et al., 2007. Supralinear increase of recurrent inhibition during sparse activity in the somatosensory cortex. *Nature Neuroscience*, 10(6), pp.743–753.

Karube, F., Kubota, Y. & Kawaguchi, Y., 2004. Axon branching and synaptic bouton phenotypes in GABAergic nonpyramidal cell subtypes. *Journal of Neuroscience*, 24(12), pp.2853–2865.

Kass, R.S., Arena, J.P. & Chin, S., 1989. Cellular electrophysiology of amlodipine: Probing the cardiac L-type calcium channel. *American Journal of Cardiology*, 64(17), pp.35–42.

Kaupmann, K. et al., 1998. GABA(B)-receptor subtypes assemble into functional heteromeric complexes. *Nature*, 396(6712), pp.683–687.

Kawaguchi, Y., 2001. Distinct firing patterns of neuronal subtypes in cortical synchronized activities. *Journal of Neuroscience*, 21(18), pp.7261–7272.

Kawaguchi, Y. & Kubota, Y., 1997. GABAergic cell subtypes and their synaptic connections in rat frontal cortex. *Cerebral Cortex*, 7(6), pp.476–486.

Keane, T.M. et al., 2011. Mouse genomic variation and its effect on phenotypes and gene regulation. *Nature*, 477(7364), pp.289–294.

Kennard, L.E. et al., 2005. Inhibition of the human two-pore domain potassium channel, TREK-1, by fluoxetine and its metabolite norfluoxetine. *British Journal of Pharmacology*, 144(6), pp.821–829.

Kerr, A.M., Reisinger, E. & Jonas, P., 2008. Differential dependence of phasic transmitter release on synaptotagmin 1 at GABAergic and glutamatergic hippocampal synapses. *Proceedings of the National Academy of Sciences of the United States of America*, 105(40), pp.15581–15586.

Kestler, L.P., Walker, E. & Vega, E.M., 2001. Dopamine receptors in the brains of schizophrenia patients: a meta-analysis of the findings. *Behavioural Pharmacology*, 12(5), pp.355–371.

Kindler, C.H., Yost, C.S. & Gray, A.T., 1999. Local anesthetic inhibition of baseline potassium channels with two pore domains in tandem. *Anesthesiology*, 90(4), p.1092-1102.

Kinney, J.W. et al., 2006. A specific role for NR2A-containing NMDA receptors in the maintenance of parvalbumin and GAD67 immunoreactivity in cultured interneurons. *Journal of Neuroscience*, 26(5), pp.1604–1615.

Kirov, G. et al., 2014. The penetrance of copy number variations for schizophrenia and developmental delay. *Biological Psychiatry*, 75(5), pp.378–385.

Klausberger, T. et al., 2003. Brain-state- and cell-type-specific firing of hippocampal interneurons in vivo. *Nature*, 421(6925), pp.844–848.

Klausberger, T., Roberts, J.D.B. & Somogyi, P., 2002. Cell type- and input-specific differences in the number and subtypes of synaptic GABA(A) receptors in the hippocampus. *Journal of neuroscience*, 22(7), pp.2513–2521.

Klausberger, T. & Somogyi, P., 2008. Neuronal diversity and temporal dynamics: the unity of hippocampal circuit operations, *Science*, 321(5885), pp.53–57.

Ko, Y. et al., 2013. Cell type-specific genes show striking and distinct patterns of spatial expression in the mouse brain. *Proceedings of the National Academy of Sciences*, 110(8), pp.3095–3100.

Kole, M.H.P. et al., 2008. Action potential generation requires a high sodium channel density in the axon initial segment. *Nature Neuroscience*, 11(2), pp.178–186.

Korostynski, M. et al., 2006. Gene expression profiling in the striatum of inbred mouse strains with distinct opioid-related phenotypes. *BMC Genomics*, 7(146).

Krishnan, G.P. et al., 2005. Steady state visual evoked potential abnormalities in schizophrenia. *Clinical Neurophysiology*, 116(3), pp.614–624.

Krystal, J.H. et al., 2003. NMDA receptor antagonist effects, cortical glutamatergic function, and schizophrenia: toward a paradigm shift in medication development. *Psychopharmacology*, 169(3–4), pp.215–233.

Kubo, Y. et al., 2005. International Union of Pharmacology. LIV. Nomenclature and molecular relationships of inwardly rectifying potassium channels. *Pharmacological Reviews*, 57(4), pp.509–526.

Kulik, A. et al., 2003. Subcellular localization of metabotropic GABA(B) receptor subunits GABA(B1a/b) and GABA(B2) in the rat hippocampus. *Journal of neuroscience*, 23(35), pp.11026–11035.

Kwon, J.S. et al., 1999. Gamma frequency-range abnormalities to auditory stimulation in schizophrenia. *Archives of General Psychiatry*, 56(11), pp.1001–1005.

Lau, D. et al., 2000. Impaired fast-spiking, suppressed cortical inhibition, and increased susceptibility to seizures in mice lacking Kv3.2 K+ channel proteins. *Journal of Neuroscience*, 20(24), pp9071-9085

Laurie, D.J., Wisden, W. & Seeburg, P.H., 1992. The distribution of thirteen GABAA receptor subunit mRNAs in the rat brain. III. Embryonic and postnatal development. *Journal of neuroscience*, 12(11), pp.4151–4172.

Lee, S. et al., 2010. The largest group of superficial neocortical GABAergic interneurons expresses ionotropic serotonin receptors. *Journal of Neuroscience*, 30(50), pp.16796–16808.

Léger, J.-F. et al., 2005. Synaptic integration in rat frontal cortex shaped by network activity. *Journal of Neurophysiology*, 93(1), pp.281–293.

Leonoudakis, D. et al., 1998. An open rectifier potassium channel with two pore domains in tandem cloned from rat cerebellum. *Journal of Neuroscience*, 18(3), pp.868–877.

Lesage, F., 2003. Pharmacology of neuronal background potassium channels. *Neuropharmacology*, 44(1), pp.1–7.

Lesage, F. et al., 1996. TWIK-1, a ubiquitous human weakly inward rectifying K+ channel with a novel structure. *EMBO journal*, 15(5), pp.1004–1011.

Levy, S., Mandell, D. & Schultz, R., 2009. Autism. *Lancet*, 374(9701), pp.1627–1638.

Lewis, D.A. et al., 2012. Cortical parvalbumin interneurons and cognitive dysfunction in schizophrenia. *Trends in Neurosciences*, 35(1), pp.57–67.

Lewis, D.A. et al., 2001. Lamina-specific deficits in parvalbumin-immunoreactive varicosities in the prefrontal cortex of subjects with schizophrenia: Evidence for fewer projections from the thalamus. *American Journal of Psychiatry*, 158(9), pp.1411–1422.

Li, L., Bischofberger, J. & Jonas, P., 2007. Differential gating and recruitment of P/Q-, N-, and R-type Ca2+ channels in hippocampal mossy fiber boutons. *Journal of Neuroscience*, 27(49), pp.13420–13429.

Liu, B.G. et al., 2001. Effects of bupivacaine and ropivacaine on high-voltage-activated calcium currents of the dorsal horn neurons in newborn rats. *Anesthesiology*, 95(1), p.139-143.

Liu, H., Enyeart, J. a & Enyeart, J.J., 2007. Potent inhibition of native TREK-1 K+ channels by selected dihydropyridine Ca2+ channel antagonists. *Journal of Pharmacology and Experimental Therapeutics*, 323(1), pp.39–48.

Lorincz, A. & Nusser, Z., 2008. Cell-type-dependent molecular composition of the axon initial segment. *Journal of Neuroscience*, 28(53), pp.14329–40.

Ma, T. et al., 2013. Subcortical origins of human and monkey neocortical interneurons. *Nature Neuroscience*, 16(11), pp.1588–1597.

Ma, Y. et al., 2011. Expression of gap junction protein connexin36 in multiple subtypes of gabaergic neurons in adult rat somatosensory cortex. *Cerebral Cortex*, 21(11), pp.2639–2649.

Maffei, A. et al., 2006. Potentiation of cortical inhibition by visual deprivation. *Nature*, 443(7107), pp.81–84.

Le Magueresse, C. & Monyer, H., 2013. GABAergic interneurons shape the functional maturation of the cortex. *Neuron*, 77(3), pp.388–405.

Mainen, Z.F. & Sejnowski, T.J., 1996. Influence of dendritic structure on firing pattern in model neocortical neurons. *Nature*, 382(6589), pp.363–366.

Marín, O., 2013. Cellular and molecular mechanisms controlling the migration of neocortical interneurons. *European Journal of Neuroscience*, 38(1), pp.2019–2029.

Marín, O., 2012. Interneuron dysfunction in psychiatric disorders. *Nature Reviews*

Neuroscience, 13(2), pp.107–120.

Markram, H. et al., 2004. Interneurons of the neocortical inhibitory system. *Nature Reviews Neuroscience*, 5(10), pp.793–807.

Martina, M. & Jonas, P., 1997. Functional differences in Na+ channel gating between fast-spiking interneurones and principal neurones of rat hippocampus. *Journal of Physiology*, 505(3), pp.593–603.

Mazella, J. et al., 2010. Spadin, a sortilin-derived peptide, targeting rodent TREK-1 channels: A new concept in the antidepressant drug design. *PLoS Biology*, 8(4).

McCall, B., 2017. UK failing to meet the needs of people with autism. *The Lancet*, 389(10067), p.351.

McMahon, L.L., Williams, J.H. & Kauer, J. a, 1998. Functionally distinct groups of interneurons identified during rhythmic carbachol oscillations in hippocampus in vitro. *Journal of Neuroscience*, 18(15), pp.5640–5651.

McNaughton, N.C.L. et al., 2000. Inhibition of recombinant low-voltage-activated Ca2+ channels by the neuroprotective agent BW619C89 (Sipatrigine). *Neuropharmacology*, 39(7), pp.1247–1253.

Meadows, H.J. et al., 2000. Cloning, localisation and functional expression of the human orthologue of the TREK-1 potassium channel. *Pflügers Archiv European Journal of Physiology*, 439(6), pp.714–722.

Meadows, H.J. et al., 2001. The neuroprotective agent sipatrigine (BW619C89) potently inhibits the human tandem pore-domain K+ channels TREK-1 and TRAAK. *Brain Research*, 892(1), pp.94–101.

Megías, M. et al., 2001. Total number and distribution of inhibitory and excitatory synapses on hippocampal CA1 pyramidal cells. *Neuroscience*, 102(3), pp.527–540.

Meltzer, H.Y., 1989. Clinical studies on the mechanism of action of clozapine: the dopamine-serotonin hypothesis of schizophrenia. *Psychopharmacology (Berl)*, 99(Suppl), pp.S18–S27.

Meltzer, H.Y., 2013. Update on typical and atypical antipsychotic drugs. *Annual Review of Medicine*, 64(1), pp.393–406.

Meyer, H.S. et al., 2011. Inhibitory interneurons in a cortical column form hot zones of inhibition in layers 2 and 5A. *Proceedings of the National Academy of Sciences*, 108(40), pp.16807–16812.

Miles, R. et al., 1996. Differences between somatic and dendritic inhibition in the

hippocampus. *Neuron*, 16(4), pp.815–823.

Milne, E. et al., 2009. Independent component analysis reveals atypical electroencephalographic activity during visual perception in individuals with autism. *Biological Psychiatry*, 65(1), pp.22–30.

Miyamoto, S. et al., 2012. Pharmacological treatment of schizophrenia: a critical review of the pharmacology and clinical effects of current and future therapeutic agents. *Molecular Psychiatry*, 17(12), pp.1206–1227.

Modabbernia, A., Velthorst, E. & Reichenberg, A., 2017. Environmental risk factors for autism: an evidence-based review of systematic reviews and meta-analyses. *Molecular Autism*, 8(1), p.13.

Mohn, A.R. et al., 1999. Mice with reduced NMDA receptor expression display behaviors related to schizophrenia. *Cell*, 98(4), pp.427–436.

Morton, M.J. et al., 2003. Determinants of pH sensing in the two-pore domain K(+) channels TASK-1 and -2. *Pflügers Archiv European journal of physiology*, 445(5), pp.577–583.

Mouridsen, S.E., Rich, B. & Isager, T., 2008. Psychiatric disorders in adults diagnosed as children with atypical autism. A case control study. *Journal of Neural Transmission*, 115(1), pp.135–138.

Niemeyer, M.I. et al., 2007. Neutralization of a single arginine residue gates open a two-pore domain, alkali-activated K+ channel. *Proceedings of the National Academy of Sciences of the United States of America*, 104(2), pp.666–671.

Nörenberg, A. et al., 2010. Distinct nonuniform cable properties optimize rapid and efficient activation of fast-spiking GABAergic interneurons. *Proceedings of the National Academy of Sciences of the United States of America*, 107(2), pp.894–899.

Novarino, G. et al., 2004. Involvement of the intracellular ion channel CLIC1 in microglia-mediated beta-amyloid-induced neurotoxicity. *Journal of Neuroscience*, 24(23), pp.5322–5330.

Ogiwara, I. et al., 2007. Nav1.1 localizes to axons of parvalbumin-positive inhibitory interneurons: a circuit basis for epileptic seizures in mice carrying an Scn1a gene mutation. *Journal of Neuroscience*, 27(22), pp.5903–5914.

Okaty, B.W. et al., 2009. Transcriptional and electrophysiological maturation of neocortical fast-spiking GABAergic interneurons. *Journal of neuroscience*, 29(21), pp.7040–7052.

Oláh, S. et al., 2009. Regulation of cortical microcircuits by unitary GABA-mediated

volume transmission. *Nature*, 461(7268), pp.1278–1281.

Olschewski, A. et al., 1998. Blockade of Na+ and K+ Currents by Local Anesthetics in the Dorsal Horn Neurons of the Spinal Cord. *Anesthesiology*, 88(1), pp.172–179.

Olsen, M.L. & Sontheimer, H., 2009. Functional implications for Kir4.1 channels in glial biology: from K+ buffering to cell differentiation. *Journal of Neurochemistry*, 107(3), pp.589–601.

van Os, J., Kenis, G. & Rutten, B.P.F., 2010. The environment and schizophrenia. *Nature*, 468(7321), pp.203–212.

Owen, M.J., Sawa, A. & Mortensen, P.B., 2016. Schizophrenia. *The Lancet*, 388(10039), pp.86–97.

Owen, M.J., Williams, N.M. & O'Donovan, M.C., 2004. The molecular genetics of schizophrenia: new findings promise new insights. *Molecular Psychiatry*, 9(1), pp.14–27.

Parpura, V. et al., 1994. Glutamate-mediated astrocyte–neuron signalling. *Nature*, 369(6483), pp.744–747.

Patel, A.J. & Honoré, E., 2001. Properties and modulation of mammalian 2P domain K+ channels. *Trends in Neurosciences*, 24(6), pp.339–346.

Pfeffer, C.K. et al., 2013. Inhibition of inhibition in visual cortex: the logic of connections between molecularly distinct interneurons. *Nature Neuroscience*, 16(8), pp.1068–1076.

Pi, H.-J. et al., 2013. Cortical interneurons that specialize in disinhibitory control. *Nature*, 503(7477), pp.521–524.

Pierri, J.N. et al., 1999. Alterations in chandelier neuron axon terminals in the prefrontal cortex of schizophrenic subjects. *American Journal of Psychiatry*, 156(11), pp.1709–1719.

Pina-Camacho, L., Parellada, M. & Kyriakopoulos, M., 2016. Autism spectrum disorder and schizophrenia: boundaries and uncertainties. *British Journal of Psychiatry Advances*, 22(5), pp.316–324.

Van den Pol, a N. & Gorcs, T., 1988. Glycine and glycine receptor immunoreactivity in brain and spinal cord. *Journal of Neuroscience*, 8(2), pp.472–492.

Poo, C. & Isaacson, J.S., 2009. Odor representations in olfactory cortex: "sparse" coding, global inhibition, and oscillations. *Neuron*, 62(6), pp.850–861.

Porcello, D.M. et al., 2002. Resilient RTN fast spiking in Kv3.1 null mice suggests redundancy in the action potential repolarization mechanism. *Journal of Neurophysiology*, 87(3), pp1303-1310

Pouille, F. et al., 2013. The contribution of synaptic location to inhibitory gain control in pyramidal cells. *Physiological Reports*, 1(5)

Powell, E.M. et al., 2003. Genetic disruption of cortical interneuron development causes region- and GABA cell type-specific deficits, epilepsy, and behavioral dysfunction. *Journal of Neuroscience*, 23(2), pp.622–631.

Putzke, C. et al., 2007. The acid-sensitive potassium channel TASK-1 in rat cardiac muscle. *Cardiovascular Research*, 75(1), pp.59–68.

Rajan, S. et al., 2005. Sumoylation silences the plasma membrane leak K+ channel K2P1. *Cell*, 121(1), pp.37–47.

Rajan, S. et al., 2001. THIK-1 and THIK-2, a novel subfamily of tandem pore domain K+ channels. *Journal of Biological Chemistry*, 276(10), pp.7302–7311.

Rapin, I. & Tuchman, R.F., 2008. Autism: definition, neurobiology, screening, diagnosis. *Pediatric Clinics of North America*, 55(5), pp.1129–1146.

Raymond, G. V., Bauman, M.L. & Kemper, T.L., 1995. Hippocampus in autism: a Golgi analysis. *Acta Neuropathologica*, 91(1), pp.117–119.

Rees, E. et al., 2014. CNV analysis in a large schizophrenia sample implicates deletions at 16p12.1 and SLC1A1 and duplications at 1p36.33 and CGNL1. *Human Molecular Genetics*, 23(6), pp.1669–1676.

Ripke, S. et al., 2014. Biological insights from 108 schizophrenia-associated genetic loci. *Nature*, 511(7510), pp.421–427.

Rivera, C., Voipio, J. & Payne, J.A., 1999. The K+/Cl- co-transporter KCC2 renders GABA hyperpolarizing during neuronal maturation. *Nature*, 397(6716), pp.251–255.

Rotaru, D.C., Lewis, D.A. & Gonzalez-Burgos, G., 2012. The role of glutamatergic inputs onto parvalbumin-positive interneurons: relevance for schizophrenia. *Reviews in the Neurosciences*, 23(1), pp.97–109.

Roux, L. & Buzsáki, G., 2015. Tasks for inhibitory interneurons in intact brain circuits. *Neuropharmacology*, 88, pp.10–23.

Rowan, M.J.M., Tranquil, E. & Christie, J.M., 2014. Distinct Kv channel subtypes contribute to differences in spike signaling properties in the axon initial segment and presynaptic boutons of cerebellar interneurons. *Journal of Neuroscience*,

34(19), pp.6611–6623.

Rudy, B. et al., 1999. Contributions of Kv3 channels to neuronal excitability. *Annals of the New York Academy of Sciences*, 868, pp.304–343.

Rudy, B. et al., 2011. Three groups of interneurons account for nearly 100% of neocortical GABAergic neurons. *Developmental Neurobiology*, 71(1), pp.45–61.

Rudy, B. & McBain, C.J., 2001. Kv3 channels: Voltage-gated K+ channels designed for high-frequency repetitive firing. *Trends in Neurosciences*, 24(9), pp.517–526.

Sandoz, G. et al., 2009. Extracellular acidification exerts opposite actions on TREK1 and TREK2 potassium channels via a single conserved histidine residue. *Proceedings of the National Academy of Sciences of the United States of America*, 106(34), pp.14628–14633.

Schizophrenia Commission, 2012. The abandoned illness: a report from the schizophrenia commission. *Rethink Mental Illness*, (online) Available at: https://www.rethink.org/about-us/the-schizophrenia-commission. (Accessed 1 June 2017).

Schoffelen, J.-M., Oostenveld, R. & Fries, P., 2005. Neuronal coherence as a mechanism of effective corticospinal interaction. *Science*, 308(5718), pp.111–113.

Selby, L., Zhang, C. & Sun, Q.Q., 2007. Major defects in neocortical GABAergic inhibitory circuits in mice lacking the fragile X mental retardation protein. *Neuroscience Letters*, 412(3), pp.227–232.

Sepulveda, F. V. et al., 2015. Molecular aspects of structure, gating, and physiology of pH-sensitive background K2P and Kir K+-transport channels. *Physiological Reviews*, 95(1), pp.179–217.

Shattuck, P.T., 2006. The Contribution of diagnostic substitution to the growing administrative prevalence of autism in US special education. *Pediatrics*, 117(4), pp.1028–1037.

Shu, Y., Hasenstaub, A. & McCormick, D.A., 2003. Turning on and off recurrent balanced cortical activity. *Nature*, 423(6937), pp.288–293.

Sik, A. et al., 1995. Hippocampal CA1 interneurons: an in vivo intracellular labeling study. *Journal of neuroscience*, 15(10), pp.6651–6665.

Silver, R.A., 2010. Neuronal arithmetic. *Nature reviews. Neuroscience*, 11(7), pp.474–489.

Sharma, K. et al., 2015. Cell type– and brain region–resolved mouse brain proteome. *Nature Neuroscience*, 18(12), pp.1819–1831.

Soghomonian, J.J. & Martin, D.L., 1998. Two isoforms of glutamate decarboxylase: Why? *Trends in Pharmacological Sciences*, 19(12), pp.500–505.

Sommeijer, J.P. & Levelt, C.N., 2012. Synaptotagmin-2 is a reliable marker for parvalbumin positive inhibitory boutons in the mouse visual cortex. *PLoS ONE*, 7(4), pp.1–12.

Spencer, C.M. et al., 2005. Altered anxiety-related and social behaviors in the Fmr1 knockout mouse model of fragile X syndrome. *Genes Brain Behavior*, 4(7), pp.420–430.

Spencer, K.M. et al., 2003. Abnormal neural synchrony in schizophrenia. *Journal of Neuroscience*, 23(19), pp.7407–7411.

Srinivas, S. et al., 2001. Cre reporter strains produced by targeted insertion of EYFP and ECFP into the ROSA26 locus. *BMC Developmental Biology*, 1(4).

Stahlberg, O. et al., 2004. Bipolar disorder, schizophrenia, and other psychotic disorders in adults with childhood onset AD/HD and/or autism spectrum disorders. *Journal of Neural Transmission*, 111(7), pp.891–902.

Staiger, J.F. et al., 2015. What types of neocortical GABAergic neurons do really exist? *e-Neuroforum*, 6(2), pp.49–56.

Stefánsson, H. et al., 2003. Neuregulin 1 in schizophrenia: out of Iceland. *Molecular psychiatry*, 8(7), pp.639–40.

Steinecke, a. et al., 2012. Disrupted-in-schizophrenia 1 (DISC1) Is necessary for the correct migration of cortical interneurons. *Journal of Neuroscience*, 32(2), pp.738–745.

Stephan, K.E., Friston, K.J. & Frith, C.D., 2009. Dysconnection in Schizophrenia: From abnormal synaptic plasticity to failures of self-monitoring. *Schizophrenia Bulletin*, 35(3), pp.509–527.

Streit, A.K. et al., 2011. A specific two-pore domain potassium channel blocker defines the structure of the TASK-1 open pore. *Journal of biological chemistry*, 286(16), pp.13977–13984.

Sullivan, E. V et al., 1996. Cognitive and motor impairments are related to gray matter volume deficits in schizophrenia. *Biological Psychiatry*, 39(4), pp.234–240.

Swadlow, H.A., 2002. Thalamocortical control of feed-forward inhibition in awake

somatosensory “barrel” cortex. *Philosophical transactions of the Royal Society of London. Series B, Biological Sciences*, 357(1428), pp.1717–1727.

Swanson, G.T., Kamboj, S.K. & Cull-Candy, S.G., 1997. Single-channel properties of recombinant AMPA receptors depend on RNA editing, splice variation, and subunit composition. *Journal of neuroscience*, 17(1), pp.58–69.

Sweet, R.A. et al., 2009. Reduced dendritic spine density in auditory cortex of subjects with schizophrenia. *Neuropsychopharmacology*, 34(2), pp.374–389.

Szabadics, J. et al., 2006. Excitatory effect of GABAergic axo-axonic cells in cortical microcircuits. *Science*, 311(5758), pp.233–5.

Tabuchi, K. et al., 2007. A neuroligin-3 mutation implicated in autism increases inhibitory synaptic transmission in mice. *Science*, 318(5847), pp.71–76.

Takano, T. et al., 2009. Astrocytes and ischemic injury. *Stroke*, 40(3 Suppl), pp.S8–S12.

Talley, E.M. et al., 2001. Cns distribution of members of the two-pore-domain (KCNK) potassium channel family. *Journal of neuroscience*, 21(19), pp.7491–7505.

Tamagnini, F. et al., 2014. Low concentrations of the solvent dimethyl sulphoxide alter intrinsic excitability properties of cortical and hippocampal pyramidal cells. *PLoS ONE*, 9(3).

Tamás, G. et al., 2003. Identified sources and targets of slow inhibition in the neocortex. *Science*, 299(5614), pp.1902–1905.

Tamás, G. et al., 2000. Proximally targeted GABAergic synapses and gap junctions synchronize cortical interneurons. *Nature Neuroscience*, 3(4), pp.366–371.

Tang, C.M., Dichter, M. & Morad, M., 1990. Modulation of the N-methyl-D-aspartate channel by extracellular H+. *Proceedings of the National Academy of Sciences of the United States of America*, 87(16), pp.6445–6449.

Taniguchi, H. et al., 2011. NeuroResource A Resource of Cre Driver Lines for Genetic Targeting of GABAergic Neurons in Cerebral Cortex. *Neuron*, 72(6), pp.995–1013.

Taverna, S. et al., 2005. Differential expression of TASK channels between horizontal interneurons and pyramidal cells of rat hippocampus. *Journal of Neuroscience*, 25(40), pp.9162–9170.

Tiesinga, P. & Sejnowski, T.J., 2009. Cortical enlightenment: are attentional gamma oscillations driven by ING or PING? *Neuron*, 63(6), pp.727–732.

Toal, F. et al., 2009. Psychosis and autism: magnetic resonance imaging study of brain anatomy. *British Journal of Psychiatry*, 194(5), pp.418–425.

Torborg, C.L. et al., 2006. TASK-like conductances are present within hippocampal CA1 stratum oriens interneuron subpopulations. *Journal of Neuroscience*, 26(28), pp.7362–7367.

Toro, R. et al., 2010. Key role for gene dosage and synaptic homeostasis in autism spectrum disorders. *Trends in Genetics*, 26(8), pp.363–372.

Traub, R.D. et al., 1996. A mechanism for generation of long-range synchronous fast oscillations in the cortex. *Nature*, 383(6601), pp.621–624.

Tremblay, R., Lee, S. & Rudy, B., 2016. GABAergic interneurons in the neocortex: from cellular properties to circuits. *Neuron*, 91(2), pp.260–292.

Tsai, M.T. et al., 1999. Genetic association study of a polymorphic CAG repeats array of calcium-activated potassium channel (KCNN3) gene and schizophrenia among the Chinese population from Taiwan. *Molecular Psychiatry*, 4(3), pp.271-3.

Tuchman, R. & Rapin, I., 2002. Epilepsy in autism. *Lancet Neurology*, 1(6), pp.352–358.

Tukker, J.J. et al., 2013. Distinct dendritic arborization and in vivo firing patterns of parvalbumin-expressing basket cells in the hippocampal area CA3. *Journal of neuroscience*, 33(16), pp.6809–25.

Uhlhaas, P.J. et al., 2006. Dysfunctional long-range coordination of neural activity during Gestalt perception in schizophrenia. *Journal of neuroscience*, 26(31), pp.8168–8175.

Uhlhaas, P.J. & Silverstein, S.M., 2005. Perceptual organization in schizophrenia spectrum disorders: empirical research and theoretical implications. *Psychological Bulletin*, 131(4), pp.618–632.

Uhlhaas, P.J. & Singer, W., 2007. What do disturbances in neural synchrony tell us about autism? *Biological Psychiatry*, 62(3), pp.190–191.

Vervaeke, K. et al., 2012. Gap junctions compensate for sublinear dendritic Integration in an inhibitory network. *Science*, 335(6076), pp.1624–1628.

Vida, I., Bartos, M. & Jonas, P., 2006. Shunting inhibition improves robustness of gamma oscillations in hippocampal interneuron networks by homogenizing firing rates. *Neuron*, 49(1), pp.107–117.

Vogels, T.P. & Abbott, L.F., 2009. Gating multiple signals through detailed balance

of excitation and inhibition in spiking networks. *Nature Neuroscience*, 12(4), pp.483–491.

Volk, D.W. et al., 2002. Reciprocal alterations in pre- and postsynaptic inhibitory markers at chandelier cell inputs to pyramidal neurons in schizophrenia. *Cerebral Cortex*, 12(10), pp.1063–1070.

Van Vreeswijk, C., Abbott, L.F. & Bard Ermentrout, G., 1994. When inhibition not excitation synchronizes neural firing. *Journal of Computational Neuroscience*, 1(4), pp.313–321.

Waldmann, R. et al., 1997. A proton-gated cation channel involved in acid-sensing. *Nature*, 386(6621), pp.173–177.

Wang, H.X. & Gao, W.J., 2009. Cell type-specific development of NMDA receptors in the interneurons of rat prefrontal cortex. *Neuropsychopharmacology*, 34(8), pp.2028–2040.

Wang, Y. et al., 2004. Anatomical, physiological and molecular properties of Martinotti cells in the somatosensory cortex of the juvenile rat. *Journal of Physiology*, 561(1), pp.65–90.

Wang, Y.-Z. & Xu, T.-L., 2011. Acidosis, acid-sensing ion channels, and neuronal cell death. *Molecular Neurobiology*, 44(3), pp.350–358.

Wass, S., 2011. Distortions and disconnections: disrupted brain connectivity in autism. *Brain and Cognition*, 75(1), pp.18–28.

Wehr, M.S. & Zador, A.M., 2003. Balanced inhibition underlies tuning and sharpens spike timing in auditory cortex. *Nature*, 426(6965), pp.442–446.

Wei, A.D. et al., 2005. International Union of Pharmacology. LII. Nomenclature and molecular relationships of calcium-activated potassium channels. *Pharmacological Reviews*, 57(4), pp.463–472.

Wen, L. et al., 2010. Neuregulin 1 regulates pyramidal neuron activity via ErbB4 in parvalbumin-positive interneurons. *Proceedings of the National Academy of Sciences of the United States of America*, 107(3), pp.1211–1216.

Whittington, M. a, Traub, R.D. & Jefferys, J.G.R., 1995. Synchronized oscillation in interneuron networks driven by metabotropic glutamate receptor activation. *Nature*, 373(6515), pp.612–615.

Wilson, T.W. et al., 2007. Children and adolescents with autism exhibit reduced MEG steady-state gamma responses. *Biological Psychiatry*, 62(3), pp.192–197.

Woo, T.-U. et al., 1998. A subclass of prefrontal gamma-aminobutyric acid axon

terminals are selectively altered in schizophrenia. *Proceedings of the National Academy of Sciences USA*, 95(9), pp.5341–5346.

Xian, T.L. et al., 2006. The stretch-activated potassium channel TREK-1 in rat cardiac ventricular muscle. *Cardiovascular Research*, 69(1), pp.86-97.

Xie, X.M. & Garthwaite, J., 1996. State-dependent inhibition of Na+ currents by the neuroprotective agent 619C89 in rat hippocampal neurons and in a mammalian cell line expressing rat brain type IIA Na+ channels. *Neuroscience*, 73(4), pp.951–962.

Xu, J., Mashimo, T. & Südhof, T.C., 2007. Synaptotagmin-1, -2, and -9: Ca2+ Sensors for Fast Release that Specify Distinct Presynaptic Properties in Subsets of Neurons. *Neuron*, 54(4), pp.567–581.

Xu, X. & Callaway, E.M., 2009. Laminar specificity of functional input to distinct types of inhibitory cortical neurons. *Journal of Neuroscience*, 29(1), pp.70–85.

Xu, X., Roby, K.D. & Callaway, E.M., 2010. Immunochemical characterization of inhibitory mouse cortical neurons: Three chemically distinct classes of inhibitory cells. *Journal of Comparative Neurology*, 518(3), pp.389–404.

Yanagi, M. et al., 2014. Kv3.1-containing K+ channels are reduced in untreated schizophrenia and normalized with antipsychotic drugs. *Molecular Psychiatry*, 19(5), pp.573-579.

Yanagidate, F. & Strichartz, G.R., 2006. Bupivacaine inhibits activation of neuronal spinal extracellular receptor-activated kinase through selective effects on ionotropic receptors. *Anesthesiology*, 104(4), pp.805–814.

Yangmi Kim, Hyoweon Bang, and D.K., 2000. TASK-3, a new member of the tandem pore K+ channel Family. *Journal of Biological Chemistry*, 275(13), pp.9340–9347.

Yizhar, O. et al., 2011. Neocortical excitation/inhibition balance in information processing and social dysfunction. *Nature*, 477(7363), pp.171–178.

Young, N. & Findling, R.L., 2015. An update on pharmacotherapy for autism spectrum disorder in children and adolescents. *Current Opinion in Psychiatry*, 28(2), 91-101.

Zaitsev, A. & Povysheva, N., 2007. P/Q-type, but not N-type, calcium channels mediate GABA release from fast-spiking interneurons to pyramidal cells in rat prefrontal cortex. *Journal of neurophysiology*, 97(5), pp.3567–3573.

Zeisel, a. et al., 2015. Cell types in the mouse cortex and hippocampus revealed by single-cell RNA-seq. *Science*, 347(6226), pp.1138–1142.

Zhang, H. et al., 2014. Voltage-dependent blockade by bupivacaine of cardiac sodium channels expressed in Xenopus oocytes. *Neuroscience Bulletin*, 30(4), pp.697–710.

Zhang, L. et al., 2006. Possible role of potassium channel, big K in etiology of schizophrenia. *Medical Hypotheses*, 67(1), pp41-43

Zhang, Z., Jiao, Y.Y. & Sun, Q.Q., 2011. Developmental maturation of excitation and inhibition balance in principal neurons across four layers of somatosensory cortex. *Neuroscience*, 174, pp.10–25.

Zhou, D. et al., 1998. Ankyrin(G) is required for clustering of voltage-gated Na channels at axon initial segments and for normal action potential firing. *Journal of Cell Biology*, 143(5), pp.1295–1304.

Zhou, M. et al., 2009. TWIK-1 and TREK-1 Are potassium channels contributing significantly to astrocyte passive conductance in rat hippocampal slices. *Journal of Neuroscience*, 29(26), pp.8551–8564.

Zikopoulos, B. & Barbas, H., 2013. Altered neural connectivity in excitatory and inhibitory cortical circuits in autism. *Frontiers in human neuroscience*, 7(609).